Thermophysical Properties and Performance Evaluation of a Mechanical Vapor Compression Cycle with Next Generation Refrigerants

Perera, Amoda Colombatantirige Uthpala
九州大学大学院総合理工学府環境エネルギー工学専攻

Thermophysical Properties and Performance Evaluation of a Mechanical Vapor Compression Cycle with Next Generation Refrigerants

COLOMBATANTIRIGE UTHPALA AMODA PERERA

KYUSHU UNIVERSITY

interdisciplinary Graduate School of Engineering Sciences IGSES Kyushu University

Department of Energy and Environmental Engineering
INTERDISCIPLINARY GRADUATE SCHOOL OF ENGINEERING SCIENCES | GREEN ASIA

KYUSHU UNIVERSITY | JAPAN

Thermophysical Properties and Performance Evaluation of a Mechanical Vapor Compression Cycle with Next Generation Refrigerants

DECLARATION

I hereby declare that this work, which is being presented in the thesis entitled "Thermophysical Properties and Performance Evaluation of a Mechanical Vapor Compression Cycle with Next Generation Refrigerants" is submitted in partial fulfillment of the requirements for the award of the degree of Master of Engineering (M.Eng.), Interdisciplinary Graduate School of Sciences, Kyushu University, Japan, is an authentic record of my own research work.

The research work presented in this thesis has not been submitted by me for the award of any degree in this or any other university.

Colombatantirige Uthpala Amoda Perera

August 2019

ACKNOWLEDGEMENT

The opportunity to pursue a Master of Engineering at Kyushu University in Japan would not have been possible without the guidance, encouragement and vision of my supervisor Prof. Kyaw Thu. I am deeply indebted to the opportunity that you have provided me and for also continuously training me for my future. I strongly believe in your wisdom in guiding me along this path towards the pinnacle and I hope to continuously learn along the way and strive to do my utmost. I would also like to thank Prof. Takahiko Miyazaki for giving me the opportunity to continue my research in the field of thermodynamics and heat transfer under his laboratory, which has produced and continues to produce important work in these fields. I am also greatly honored to have the opportunity to work with Prof. Yukihiro Higashi who is at the forefront of his field in expertise and knowledge regarding thermophysical property measurements of refrigerants. This was a once in a million opportunity which I will forever be grateful for and I hope to continue learning under your guidance and work towards developing Next Generation Refrigerants. I would also like to thank Prof. Giovanni Di Nicola of UNIVPM, for being a wonderful host for my stay in Italy and for introducing me to Sebastiano Tomassetti, who has made an immense contribution towards my growing understanding of my field. I also wish to thank Prof. Naoya Sakoda for giving me chance to widen my experimental knowhow.

I would also like to thank Dr. Nobuo Takata, for his ever ready availability of any components and instrument information for the experimental setups. I am also greatly thankful for all the staff at Kyushu University, especially the staff at the Green Asia Office, who were always there to make sure that I was doing okay, and to the staff of the EEE department as well as the staff at NEXT-RP for their constant light heartedness.

I also express my gratitude to the government and people of Japan for the support they have given through the Program for Leading Graduate Schools, Advanced Graduate Program in Global Strategy for Green Asia.

I would also like to thank all the lab members of Miyazaki (TECS) Lab and a special thank you goes to Takezato san, Kawakami san, Oishi san, Sakuma san, Nakauchi san, Senba san and Abirham san. I would also like to thank all my friends at KU including Kiro san and family, Ujin san, Akira san, Ishibashi san, Aira san and the new friends I have made along the way, as well as the rest of my friends from Sri Lanka, Singapore and

all over the world. A heartfelt thank you also goes out to Mizuguchi sensei for being my Japanese grandmother and making me feel welcome here in Japan.

Lastly I owe all my achievements to my family, my loving parents who have nurtured me since a young age and are a constant source of love, kind words, encouragement and hope and to my sister whom I value, trust and together will strive to be kinder to the world as our parents have raised us. Lastly, I am grateful for the opportunity to be alive in this miracle of a planet, to be able to experience the wonders of the world, the beauty of art, the peace of nature and the endlessness of the stars. I hope to strive to be a kinder and better version of myself and to continue to work toward environmental conservation.

TABLE OF CONTENTS

LIST OF FIGURES

LIST OF TABLES

CHAPTER 1
GENERAL INTRODUCTION

Humanity has progressed a great deal since our humble beginnings dating back to more than 2.8 million years, where the Homo habilis started making primitive tools out of sticks and stones [1]. Through the progress of time, we passed from the stone age to the iron age and then to the industrial revolution which took place in the 18th century, which created a vast leap for humanity's development [2]. However, the massive growth in industries, the creation of cities and the concept of urban dwelling were followed with several negative externalities which would come to haunt the future generations. The use of coal for production of energy resulted in large amounts of 'Black Smoke' or carbon particulate matter emissions in many of the industrialized areas, causing higher mortality rates as a direct cause of the pollution [3], there was also the encompassed release of massive amounts of Carbon dioxide (CO_2) into our atmosphere [4], [5]. Though the immediate effects of industrialization were endured by the people living in the 18th century, an almost 'domino effect' like consequence is being experienced by us, living in modern day times. This is mainly caused by the massive amounts of CO2 that were released and are still being released today, accumulating in our atmosphere, resulting in the global phenomena of 'Global Warming' [6], [7]. What began from the industrial revolution, has been further worsened by the heightened release of CO_2 [4], [7] and other greenhouse gases, due to an increased production of electricity and energy consumption through fossil fuel burning, to cater to an ever increasing population which will hit 9 billion by 2050 [8].

As mentioned before, the many benefits that resulted from mankind's progression is undoubtedly acceptable and seen around us today, in the form of technology such as smartphones and social media, to transport services from personal mobility devices to large aircraft, to the exploration of the depths of the ocean, to satellites and space exploration, to the increased life span and living standards of people around the world, and the ability to control the conditions of the rooms and buildings we live in to storing food and medicines in refrigerators. The latter, where cooling and heating can be provided, was a concept visibly dating back to the Chinese and Roman civilizations, where the use of ice from mountains or the use of a mechanically rotating fan were utilized to create favorable

and comfortable conditions for survival [9]. This has since then progressed to a very large global industry, collectively known as the Heating, Ventilation, Air Conditioning and Refrigeration or HVAC&R industry. The HVAC&R industry has massively progressed since its early days and now impact the lives of many. From the initial beginnings of using wet cloths and evaporation for cooling, the industry progressed on to exploring the possible use of volatile liquids such as alcohol to attain freezing by Benjamin Franklin [9], which led to the beginnings of modern day Air Conditioner which was invented by Willis Haviland Carrier around 1902, to solve a problem related to high humidity in a printing factory [9]. Based on these initial inventions, the modern day Air Conditioner and other HVAC&R systems have now become a staple seen in houses, schools and offices. Our dependency on these HVAC&R equipment, has resulted in many consequences, especially on the environment. According to the UN, 20% of domestic electricity use in warm regions is used for cooling purposes [10], and the stock of global air conditioners is expected to rise from 660 million to 1.5 billion units by just 2030 [10]. In the European Union (EU), the energy used for the heating and cooling in both domestic and commercial sectors, accounts for 50% of the EU's total energy consumption [11]. The production of energy for these purposes is still highly dependent on fossil fuels which accounts for 84%, whilst renewables only supply 16% [11]. Hence, there is a clear problem related to the HVAC&R industry, with the predicted increasing energy consumption caused by an increasing demand, which will eventually result in more emissions, contributing to a further worsening climate crisis. These changes in the climate will continue to fuel that increase in demand, which will then result in an almost cyclic battle between climatic issues and the HVAC&R industry. Thus there is major space and an urgent need for improving the status quo of the HVAC&R industry, in order to tackle climatic problems through the reduction of greenhouse gas emissions and reduced consumption of energy.

1.1 Air Conditioners and Heat Pumps

HVAC&R systems can be used for a wide array of needs such as providing cooling, heating and for maintaining certain conditions such as relative humidity and even air quality and particulate matter concentrations.

In our day to day lives, we know how a hot cup of coffee if placed in the room, will slowly cool down and lose its heat till it reaches room temperature, whilst a cold ice cream will melt as it gains heat from the room, again reaching room temperature. However, the reverse process where a cold ice cream suddenly becomes colder, or a hot coffee, continue to heat up is never experienced. These processes however can be achieved with the aid of the refrigeration cycle.

Shown in Figure 1.1 1(a) is the typical flow of energy in the form of heat and electrical power input for a refrigerator. As seen in Figure 1.1 1(a) in order to remove heat Q_L from the cold space, it necessary to put in work ($W_{net,in}$), and a certain amount of heat Q_H must be then rejected to the warmer environment. This process of heat gain, power input and heat rejection is required to maintain an energy balance, such that no energy is destroyed. This is a fundamental concept which shows the conservation of energy, or is often referred to as the first law of thermodynamics.

$$Q_L + W_{Net,in} = Q_H \qquad (1.1\text{-}1)$$

This process of removing heat from a space, and rejecting it to the environment is often achieved through a device such as an air-conditioner / chiller, or a refrigerator.

The opposite process can also occur, and is often referred to as a Heat Pump (See Figure 1.1-1(b)) [12].

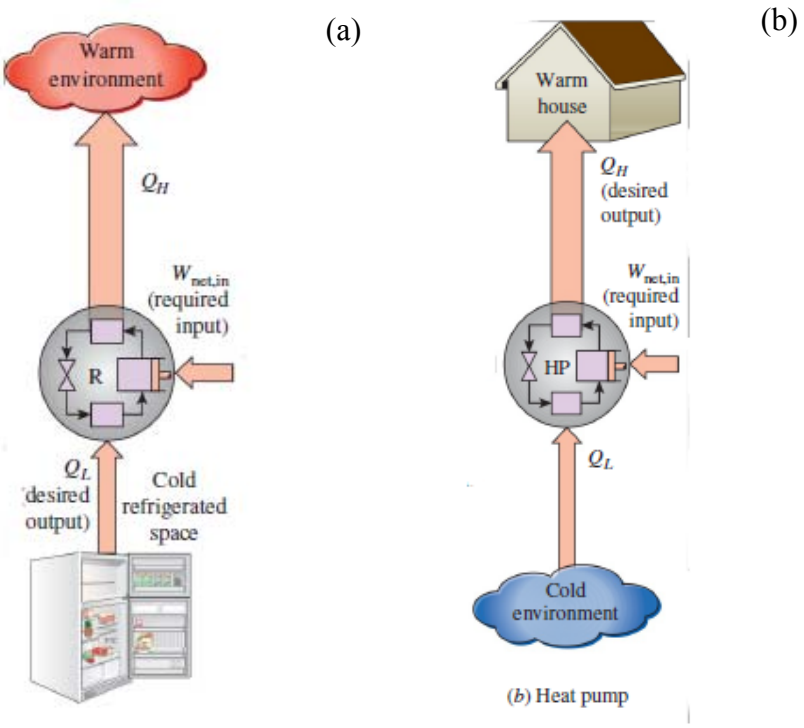

Figure 1.1-1(a) The energy flow of a typical refrigeration cycle; (b) The energy flow of a typical air conditioner operating on heat mode as a heat pump [12]

In both of these cases, the same 'refrigeration' cycle is used, however, the main purpose is different, where the former provides cooling by removing heat, whilst the latter focuses on the heat rejection for heating. A more detailed explanation of refrigeration cycles will be provided in the following sections.

1.2 Performance Indicators

The performance or efficiency of HVAC&R equipment are commonly measured with what is known as the Coefficient of Performance or COP, which gives the ratio between what is desired, over what must be input into the system.

For the refrigeration process, the COP_R represents the efficiency, whilst the heat pump is presented by COP_{HP}

$$COP_R = \frac{\text{DesiredOutput}}{\text{RequiredInput}} = \frac{Q_L}{W_{net,in}} \quad (1.2\text{-}1)$$

$$COP_{HP} = \frac{\text{DesiredOutput}}{\text{RequiredInput}} = \frac{Q_H}{W_{net,in}} \quad (1.2\text{-}2)$$

Using an energy balance equation (Equation 1.1-1) for any such system, it is possible to see that, the input energy should equal the output.

This allows the following relation to be derived,

$$COP_{HP} = COP_R + 1 \quad (1.2\text{-}3)$$

Since the values for COP_R and COP_{HP}, can both be larger than 1, provided that Q_L or Q_H are larger than $W_{net,\,in}$, it also mentionable that for a given system, COP_{HP} will always be larger than one, since COP_R, will always be a positive value.

In the industry, it also common to use what is known as the Energy Efficiency Ratio (EER)[13], instead of the COP.

$$EER\,(BTU/Wh) = \frac{\text{Output Cooling Energy (BTU)}}{\text{Input Electrical Energy (Wh)}} \quad (1.2\text{-}4)$$

Which measures the amount of cooling provided in BTU (1 BTU = 1055.06 J) [13].

$$EER(BTU/Wh) = COP \times 3.41 \quad (1.2\text{-}5)$$

Kilo-watt per Ton, is also used in order to determine the efficiency, which measures the amount of electricity consumption to provide 1 ton of cooling [14], [15].

$$Efficiency\ \text{(kW/ton)} = \frac{\text{Input Electricit y Energy (kW)}}{\left(\frac{\text{Output Cooling Energy (kW)}}{3.517\,(kW\,/\,ton)}\right)} = \frac{3.517}{COP_R} \qquad (1.2\text{-}6)$$

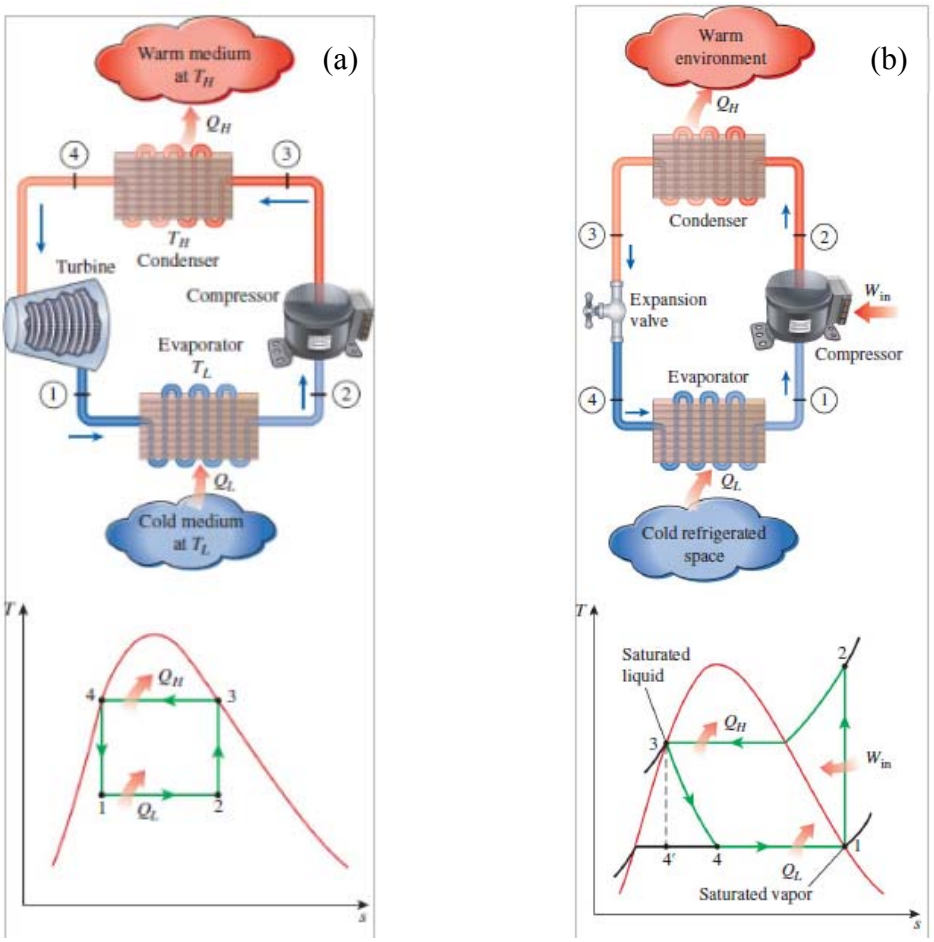

Figure 1.2-1 (a) The Reveres Carnot Cycle on a T-s diagram together with the components of the cycle; (b) The Ideal Refrigeration Cycle on a T-s diagram together with the cycle components [12]

1.3 Reversed Carnot Cycle

In order to represent the behavior of a refrigeration cycle, the Carnot Cycle can be used as a starting point (Figure 1.2-1(a)) [12].

Here the cycle consists of 4 main components, the Compressor, 2 Heat exchangers in the form of the Evaporator and Condenser and the Turbine. The T-s diagram represents the 4 reversible paths (2 isothermal and 2 isentropic), which are followed in counter-clockwise direction, making it the 'Reverse' Carnot Cycle.

$$COP_{R,Carnot} = \frac{1}{\left(\frac{T_H}{T_L} - 1\right)} \qquad (1.3\text{-}1)$$

$$COP_{HP,Carnot} = \frac{1}{\left(1 - \frac{T_L}{T_H}\right)} \qquad (1.3\text{-}2)$$

The Reversed Carnot Cycle represents the most efficient possible refrigeration cycle that can operate between two temperature T_L and T_H. Though this provides the best efficiency, it also possesses many impracticalities, which make it difficult to implement in reality.

Impracticalities of the Reversed Carnot Cycle

1. The exact quality of the inlet and outlet conditions from the heat exchangers are difficult to maintain, especially within the evaporator (1,2)
2. Also the compressions process from 2 → 3, is difficult to conduct when there is the presence of 2-phase liquid and vapor. Since in most cases, the presence of liquid can damage a compressor.
3. The expansion process from 4 → 1, is again difficult to carry out since, there will a very low quality, or high amount of liquid present at point 4, making it difficult to expand using a turbine.

Hence, this led to the study of the Ideal Vapor Compression Cycle

1.4 Ideal Vapor Compression Cycle

The Ideal Vapor Compression Cycle, allows to overcome some of the problems associated with the Reversed Carnot Cycle.

1. The Outlet conditions of the Evaporator are now easier to maintain, since they reach the Saturation Vapor line with a quality of 1 (as seen in Figure 1.2-1(b)) [12]
2. The compression process 2 → 3, is now possible to conduct, since the refrigerant is in the vapor phase and will reach the superheated vapor region
3. For the expansion process from 4 →1, instead of a turbine, and expansion valve can be used, making it an isenthalpic process, instead of an isentropic process

In order to calculate the COP, it is beneficial to use a p-h diagram shown in Figure 1.4-1 [12],

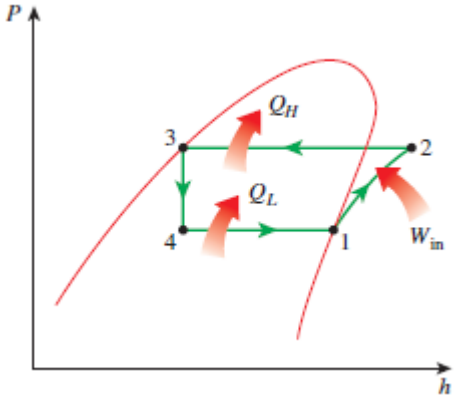

Figure 1.4-1 Pressure – Enthalpy (p-h) diagram for an Ideal Vapor Compression Cycle [12]

The heat transfer and work inputs can be calculated based on the enthalpy, h.

$$COP_R = \frac{q_L}{w_{net,in}} = \frac{h_1 - h_4}{h_2 - h_1} \qquad (1.4\text{-}1)$$

$$COP_H = \frac{q_H}{w_{net,in}} = \frac{h_2 - h_3}{h_2 - h_1} \qquad (1.4\text{-}2)$$

Where q_L, q_H and $w_{net,in}$, represent the specific cooling, specific heating and specific power input (per kg or refrigerant).

1.5 Actual Vapor Compression Cycle

Moving on from the Ideal Vapor Compression Cycle, represented in Figure 1.5-1 [12] is an Actual Vapor Compression Cycle.

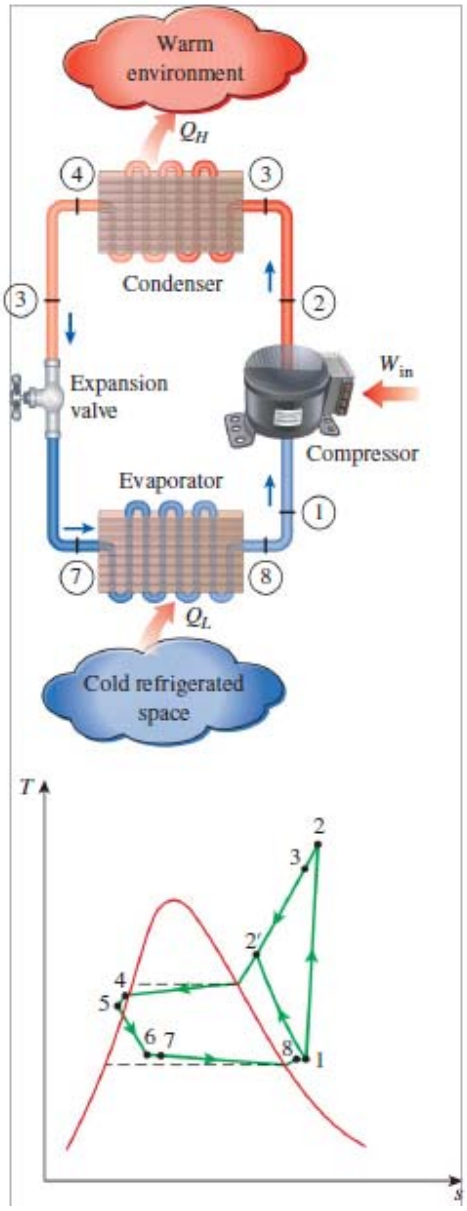

Figure 1.5-1 The Ideal Vapor Compression Cycle represented on a T-s diagram together with the cycle components [12]

The main differences between the Ideal and Actual Cycles are given below,

1. The outlet conditions from the heat exchangers are not limited to the saturation curves, but will go to point 1 in the superheated region for the evaporator and point 5 in the subcooled region for the condenser
2. The heat exchange process within the 2 phase region will also no longer be isothermal, due to pressure drops within the heat exchangers
3. The expansion process will also no longer be isenthalpic due to expansion losses
4. The compression process will also deviate slightly from the isentropic conditions, due to losses within the compressor

1.6 Diversity of HVAC&R Systems

The types of HVAC&R equipment vary considerably based on the purpose as well as capacity. A brief overview of the types of systems are given below.

1.6.1 Split Type Air Conditioners / Heat Pump

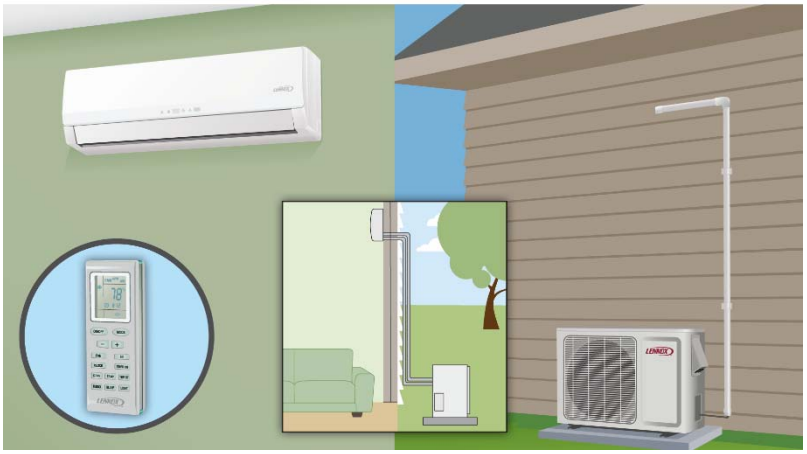

Figure 1.6-1 The typical layout of a Split Type Air Conditioning Unit, with the condensing unit placed outside, whilst the evaporative unit is placed within the conditioned space [16]

(Figure 1.6-1 [16]) Commonly seen in households, uses the vaporization of refrigerant to cool air, or the condensation to heat air. The main heat exchanger (cooling mode → evaporator, heating mode → condenser) is located within the room, whilst the expansion device, compressor and secondary heat exchanger are located outside the room.

1.6.2 Chillers

Figure 1.6-2 The typical structure of a large scale chiller, where the two major components which are visible are the Shell-in-tube type Heat Exchangers for the Evaporator and Condenser [17]

These can vary in size from small capacity 10 tons to large capacity 2000 tons for cooling industrial or commercial buildings. These systems cool chilled water and pump this water to required spaces, instead of directly pumping large amounts of refrigerant across a space. Typically, Mechanical Vapor Compression cycle is used, but can also be Absorption systems. (Figure 1.6-2 [17])

1.6.3 Absorption Chillers

Instead of using the typical Mechanical Vapor Compression (MVC), these chillers use a refrigerant and absorbent, together with a waste heat source to provide a pressure lift. They are considered more environmentally friendly, but still lack the performance capabilities of the MVC systems (Figure 1.6-3[18]).

1.6.4 District Cooling / Heating

Essentially these are very large scale chillers, which can cater to may buildings within a given area. They will again pump chilled water, hot water or even steam across large areas or cities for cooling, heating or providing hot water (Figure 1.6-4 [19]).

Figure 1.6-4 An Absorption Chiller, which can look similar to a conventional vapour compression chiller, but a marked difference in the Heat Exchangers, which are more cuboidal due to the presence of packed adsorbent materials [18]

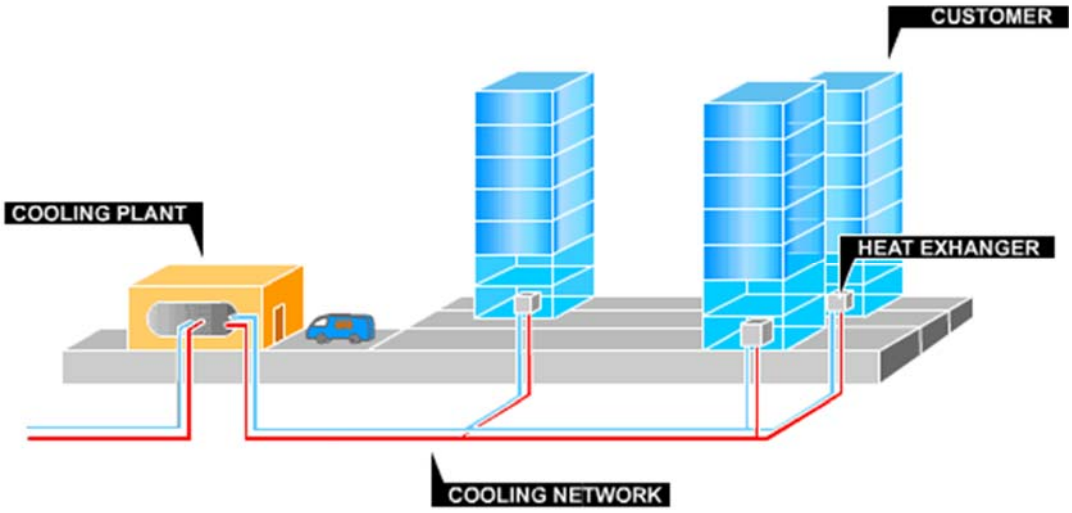

Figure 1.6-3 The typical layout of a District Cooling System, where the chilled thermofluid is pumped from the main cooling plant to several buildings, where users can utilize Heat Exchangers to produce require cooling [19]

1.6.5 Refrigerators / Coolers / Cold Rooms

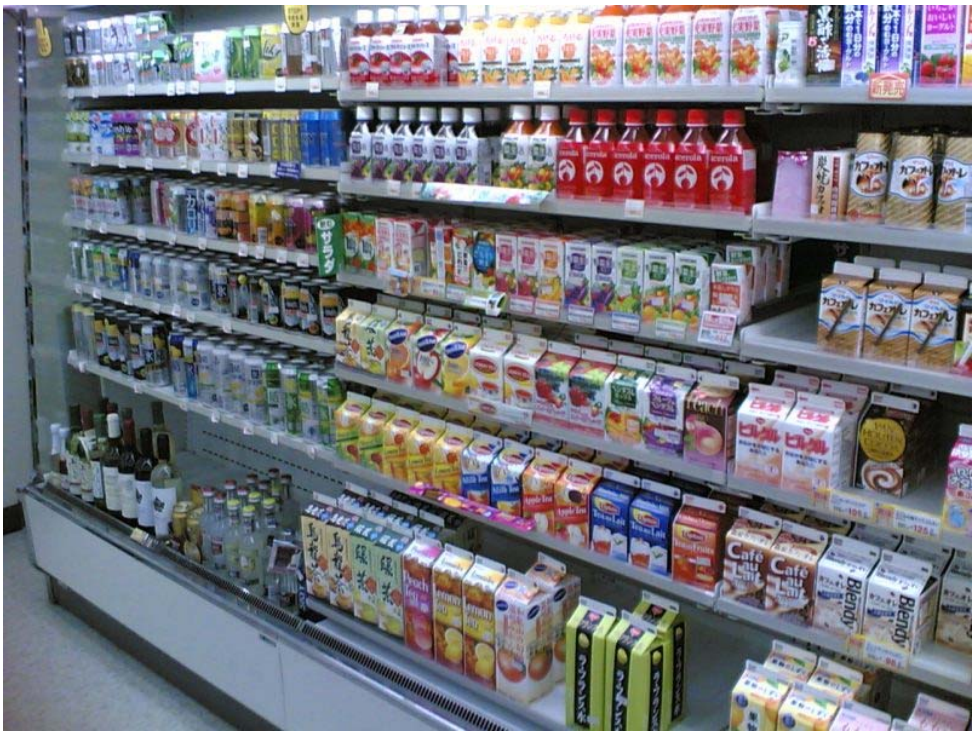

Figure 1.6-5 (a) A typical domestic refrigerator [20] ; (b) The cold cabinets often seen at convenience stores widely in Japan [21]

Again seen commonly in both domestic and commercial settings. These systems can provide a cool space for storing and preserving food, medical or other items. Large scale systems are used in commercial settings and are an essential part in many food and agriculture industries. (Figure 16.5(a)[20]; (b)[21])

Described in this section are just a few of the main systems which are in use. There are several other systems, sub-systems and even hybrid systems combining several applications in order to improve efficiency and make the HVAC&R industry more sustainable and even more useful.

1.7 Refrigerant History

According to the historical review work carried out by J. M. Calm [22], the refrigerant timeline can be separated into 5 distinct generations which are represented in graphical form in Figure 1.7-1 [22].

The first generation of refrigerants lacked any regulations on safety regarding flammability and toxicity. It is mentioned in the review work that accidents were common, due to either toxic gas leaks and the flammability of refrigerants. However, towards the end of these 100 years, small changes in safety were seen as refrigerants such as carbon tetrachloride were not promoted for use due to their toxicity.

The second generation saw the introduction of fluorochemicals, which were highlighted for their safety and durability due to low reactivity. During this period, Thomas Midgley Jr., Albert L. Henne and Robert R. McNary conducted investigations on possible alternative refrigerants through the use of the periodic table. They were able to conclude that that the flammability and toxicity of the refrigerants would vary with the limited elements they proposed, and also discovered the possible use of fluorine, which helped develop many other refrigerants to come [23].

Following this breakthrough, the production and use of Chlorofluorocarbons (CFC) and Hydro chlorofluorocarbons (HCFC) increased. These fluorinated refrigerants were promoted as non-toxic, inflammable and non-reactive refrigerants [24]. This allowed an increase in use of these chemicals, which were later on in 1985 verified to cause Ozone

depletion as predicted by the research work of Molina and Rowland [25]. With this breakthrough, the Montreal Protocol was adopted to prevent the further possible implications of such harmful chemicals.

This led to the third generation , where Ozone friendly refrigerants such as Hydrofluorocarbons (HFCs), Perfluorocarbons (PFCs) and Sulphur hexafluoride (SF_6) were promoted [24]. There was also a revival of the use of many of the natural refrigerants which has been reduced, such as CO_2, NH_3 and Water [22]. With the shift in refrigerant use, it was slowly reported that the ozone layer was finally healing [26], [27]. However, towards the fourth generation another climatic issue was discovered, caused by the HFCs which had been used as alternatives. These chemicals seemed to possess high Global Warming Potentials (GWPs), which was resulting in the greenhouse effect within the atmosphere to heighten and lead to the rise of global temperatures. Thus in the fourth generation, the world has been working towards reducing this impact by increasing the search for alternative refrigerants to be classified as Next Generation Refrigerants, which will help prevent the anthropogenic effects on the environment.

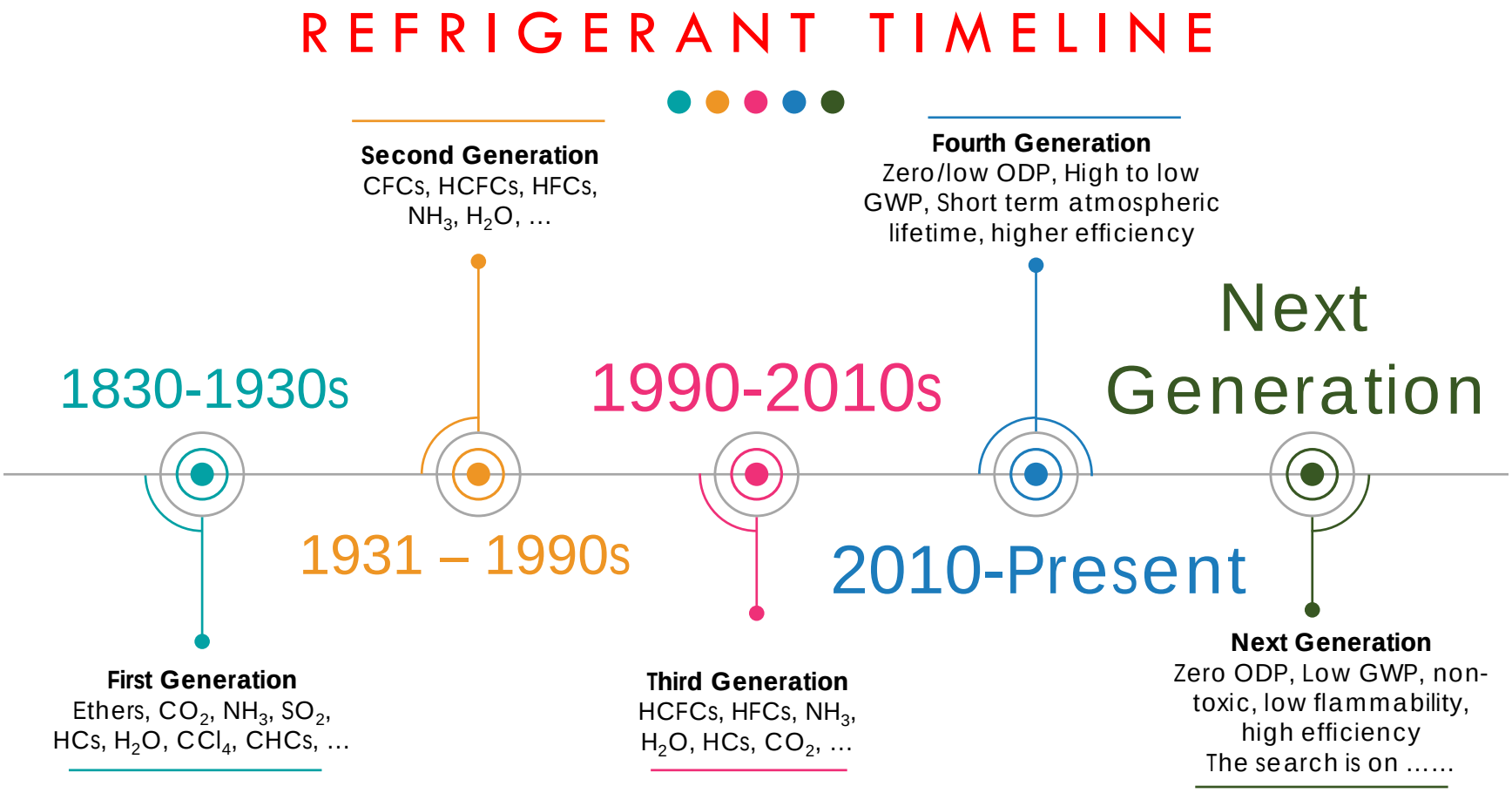

Figure 1.7-1 Refrigerant Timeline from the 1st Generation to the current 4th Generation and the future Next Generation of Refrigerants [22]

1.8 Environmental Impacts and Issues

The environmental issues related to the Heating, Ventilation, Air Conditioning and Refrigeration (HVAC&R) industry have been mentioned in brief before. These are contributing to the overall change in the climate [28]. This section will give on a more detailed insight of two of the environmental impacts caused by the HVAC&R industry.

1.8.1 Ozone Issues

The Ozone layer is a protective casing around the earth. It is made up of oxygen atoms which are combined in triplets to make Ozone or O_3. The ozone layer acts as a shield in deflecting much of the sun's harmful ultraviolet radiation (UV) [29]. The layer is located around 20 – 30 km above the earth's surface [29]. Its main capability is to absorb UV-B rays, which are often very harmful to humans, plants and animals and can cause skin cancer and cataracts. There is also a very large impact on the oceans which contain vast amounts of micro-organisms such as algae [29], and can absorb up most of the CO_2 in the atmosphere. The UV rays can penetrate deep into the ocean causing an impact on oceanic life, which eventually threaten a key part of the food chain essential for supplying sustenance to humanity [29]. The agriculture industry is also affected, together with the world's forests since the plant growth will be impeded by UV rays [29]. Besides these factors, there will be several other effects on many of the cycles that govern out planets, such as the carbon dioxide cycle which will be heavily affected due to the impact on the ocean [29].

Overall, the ozone layer it vital for our survival and humanity has understood this and have initiated a worldwide effort beginning from the Vienna Convention, to adopt the Montreal Protocol, to combat ozone depletion [30], [31].

1.8.2 Greenhouse Gasses and Global Warming

The ability to inhabit Earth is due to a combination of many factors, such as the presence of oxygen, the availability of land masses for habitation, the abundance of greenery and food as well as the suitable temperatures and weather conditions. The average temperature of the world is such that habitation by mankind is possible. This is achieved mainly by the 'greenhouse' effect, which helps trap soar radiation within the atmosphere, in a similar

fashion to that of a greenhouse trapping heat in winter. Though this phenomenon is essential for survival, human actions have resulted in additional warming of the planet, called 'Global Warming' [32]. Since the industrial revolution, the increased emission of CO_2 through the burning of fossil fuels has caused more heat to be trapped in the atmosphere, which has created unpredictable and devastating climatic effects such as sea level rise, melting of polar ice caps, extreme weather events such as increased and stringer storms to the lack of water in severe droughts [28]. These have mainly been a result of the global greenhouse gas emissions, not just including CO_2 from the production of energy, but due to the more harmful refrigerants such as HFCs, which are capable of causing several thousand times the effect of 1 molecule of CO_2, due their high Global Warming Potentials (GWPs).

"Climate change is running faster than we are - and we are running out of time" as put to words by the Secretary General of the UN [33], reiterates the immense threat these climatic issues pose and sounds the alarm on the need for immediate action to prevent further catastrophes.

1.9 International and National Climate Action

1.9.1.1 Montreal Protocol (Ozone)

The first treaty related to the HVAC&R industry in a global scale was the Montreal Protocol under the Vienna Convention on Climate Change [30], [31]. This was considered to be the most successful international treaty to date due to its global ratification by all 197 UN Member States in 1987 and also due to its success in controlling more than a 100 chemical substance [34] that were contributing to the ozone hole which was forming over the Antarctic [27], [35].

1.9.1.2 Kyoto Protocol (Global Warming)

The second international treaty which was adopted in Kyoto, Japan was the Kyoto protocol which hoped to tackle the increasing greenhouse gas emissions which were contributing

towards global warming and climate change. This was formulated by the United nations Framework Convention on Climate Change and entered into force in 2005 [36].

1.9.1.3 Paris Agreement

In 2015, there was a landmark proposal brought forth to the world which highlighted the dangers to come due to climate change and that immediate action was necessary. The Paris Agreement prompted nations to make efforts to limit the global temperatures rise to below 1.5°C [37][38] This is planned to be achieved through Nationally Determined Contributions (NDCs), which are handed in by most nations in the late 2016 [37]–[39].

1.9.1.4 Kigali Amendment (addition to Montreal Protocol)

One of the latest additions to the global initiative to fight global warming came into force earlier this year (2019), as the Kigali Amendment to the highly successful Montreal Protocol [40]. This amendment has a mammoth task ahead since it hopes to phase out many of the harmful Hydrofluoro carbons (HFCs) by 2047, which are causing global warming. Doing so will hope to reduce the global temperature rise by 0.4 – 0.5°C [40], [41].

1.9.1.5 National Policies

There has also been the individual action of nations through their governments and legislative bodies towards making contributions towards climate change.

The European Union (EU) has proposed and implemented many F-gas or Fluorinated-gas regulations since 2006 [42]. One of the significant policies was known as the MAC directive [43], which brought forth regulations to prohibit the use of R134a for passenger car air conditioning systems for the vehicles which will be introduced after 2011 [44]. This was an landmark contribution by the EU and has since then prompted the development and use of alternative refrigerants such as R1234yf to keep the Global Warming Potential (GWP) below 150 [44]. The latest addition to the EU F-gas policies is the Regulation 517/2014 introduced in 2014 [45].

Japan as a nation which is highly dependent on HVAC&R systems has also been taking many steps towards committing to a greener future [46], [47]. Under the Ministry of Environment Japan introduced a revised F-gas law in 2015, which took into account the need for measuring and proper tabulations of F-gasses in all aspects of the HVAC&R lifecycle and also proposed GWP targets which have prompted the study and development of new refrigerants and mixtures to reduce GWP levels to 150 in automotive air conditioners and to below 750 in domestic air conditioners [48].

1.10 Solutions for the HVAC&R Industry's Environmental Impact

Solving these climatic issue related to the HVAC&R industry requires a multi-dimensional approach, specifically focusing on every step of the HVAC&R life cycle. Some of the key steps involved in this life cycle are the selection of suitable chemicals for use as refrigerants, the design of equipment, the consumer life span of equipment and finally the retrofit and update of existing systems.

In order to initiate a change from the first step, there is a need for the exploration of new refrigerants or refrigerant mixture to be used as environmentally friendly alternatives to the more harmful ones being currently used. Typically, environmentally friendly refrigerants should possess zero Ozone Depletion Potential (ODP) (according to the Montreal Protocol), and low Global Warming Potential (GWP) (according to the multitude of local and international treaties and policies such as the Kigali Amendment and F-gas policies of Japan and EU [31], [42], [48]–[50].

Once possible alternatives are identified, their thermophysical properties of these refrigerants need to be tested, and reliable Equations of State (EOSs) need to be derived to represent their behavior, so that design of new systems can be catered to these refrigerants and the possibilities of using these refrigerants and their mixtures in pre-existing systems as either retrofits (with changes to the system), or 'drop-in' (without any adjustments to the system) can be identified.

The new refrigerants or mixtures should also be practically tested using HVAC&R systems such as heat pumps or chillers and refrigerators in order to verify their performance and characteristics. Finally, this information should be available at an international level for

researchers and the industry, in order to help policy making and to push the industry further towards a more sustainable future.

Two of the steps mentioned above, will be further explored in this work. Chapter 2 will deal with the possibilities of using ‘drop-in’ refrigerants for a Mechanical Vapor Compression Cycle, in order to replace high GWP refrigerants, with low GWP alternatives.

Chapter 3 on the other hand will focus on the thermophysical properties of a new low GWP refrigerant, which is hoped to be utilized as a Next Generation Refrigerant to help meet Japan’s national F-Gas policies as well as help Japan to contribute to international treaties such as the Kigali Amendment to the Montreal Protocol [31], [50], [51].

CHAPTER 2 VAPOR COMPRESSION CYCLE

In Chapter 2 my research carried out at Thermal Energy Conservation Systems (TECS) Lab, Chikushi Campus, IGSES, is presented. One area of focus at the TECS lab is to test refrigerants and mixtures as 'drop-in' refrigerants in a Mechanical Vapor Compression cycle. 'Drop-in' refers to the introduction of a different refrigerant to a pre-existing system, without the need for modifications in components, which allow great cost savings and easier changeovers, since new components do not need to be introduced. The refrigerants which are tested, fall under consideration as low Global Warming Potential (GWP) alternatives or Next Generation Refrigerants, which are being extensively tested and developed in the hopes of replacing the current refrigerants used in the global markets. Some of the common refrigerants used in Japan as well as in the world include R404a, R410a and R134a for domestic refrigerators, R134a for vehicles, R410a and R32 for domestic air-conditioners and R245fa and R134a for large scale commercial buildings [46], [52]–[54]. Out of these refrigerants, the focus of this research was on R410a, due to its wide use as an alternative to R22 under the Montreal Protocol in many parts of the world [55], [56] ranging from USA [57], to the EU [58] ,and Japan [46] and since it is currently being considered for phase out in Japan and other parts of the world due to its high GWP [46], [54].

The first step towards replacing R410a with alternative 'drop-in' refrigerants is to carry out a baseline test, which can then be used as a standard for comparing alternative refrigerants. Hence, a standard performance analysis of a chiller using R410a is proposed. Since this analysis will be used to compare other 'drop-in' refrigerants using the same chiller, the experimental procedure was carried out under Air Conditioning, Heating and Refrigeration Institute (AHRI) Standard 551/591 (SI) [59]. The analysis of the chiller cycle was carried out using the first law analysis and was extended to the second law analysis in order to provide a deeper understanding into the occurrence of irreversibilities and losses at each respective component within the system. The second law analysis of the system

consisted of the exergy destroyed within each individual component as well as the exergetic efficiency of the chiller.

2.1 Introduction

As established in the Chapter 1, the Heating, Ventilation, Air Conditioning and Refrigeration (HVAC&R) industry has a major impact on the energy use of nations as well as the contribution towards climatic issues such as Global Warming. The global demand for the HVAC&R industry is set to reach 5.6 billion Air Conditioner units by 2050, which will also increase the energy demands of the sector by an amount equal to the current electricity capacity of USA, Japan and the EU combined [60]. Hence there is a huge potential to combat climate issues by combating the emissions of the HVAC&R industry. This will assist in maintaining the global temperature rise below 1.5°C as per the Paris Agreement [37], [61].

The climatic impact of the industry as mentioned before is caused both through direct emissions of refrigerants which act as greenhouse gases and through the indirect emissions of Carbon dioxide (CO_2) for the production of electricity and power for the operation of HVAC&R equipment. Hence, the solutions for reducing the climatic impact should be focused on reducing both the direct and indirect contributions by the industry. The reduction of the direct impact of refrigerants is related to the Global Warming Potential (GWP) of the refrigerants whilst the indirect emissions through fossil fuel and natural gas burning is related mainly to the performance of the equipment, since better performance will help reduce the electricity consumption and power use and also the amount of emissions.

Both these aspects have been either examined individually or are often combined in the research carried out on the multitude of HVAC&R systems available ranging from heatpumps, chillers and air-conditioners to other devices such as refrigerators, cold rooms, hot water units and ice makers [62]–[66].

Since the amount of research carried out regarding HVAC&R systems is immense, a non-exhaustive list of some of these works is presented in Table 2.1-1

Table 2.1-1 Literature review on some of the research carried out on HVAC&R Systems between 1979 - 2019

Year	Authors	Summary	Notes
1979	R Jakobs, H Kruse[67]	The possibility of using non-azeotropic or zeotropic mixtures in commercial refrigeration units is presented.	The study was done on a heat pump system. The floating temperature in HXs helped improve the performance and allowed capacity control. For the experiments mixtures of R12/R114 were compared with pure R12. The COP showed improves of up to 16%.
1987	M.O McLinden, R. Radermacher[68]	A theoretical approach to analysis the use of potential refrigerant mixtures is proposed	2 Models for predicting the behavior of pure and mixtures of refrigerants is presented. The COP and heating capacity for a vapor compression cycle is found for binary mixtures of R22/R11 and their pure forms. The temperature glides were considered to be crucial since difference between the HX temperature and the temperature glides will result in changes in COP. The highest COP increase was achieved with larger temperature glides, which caused larger temperature changes within the HXs. The counter flow arrangement is vital for the HXs to utilize the temperature glide. The heat exchanger area takes a flat form at the optimum, which makes slight deviations negligible.
1988	G. Lorentzen[69]	A review on Ammonia which has been already in use for more than a 100 years, and how it can be still used in large scale industries with proper precautions	Ammonia is often viewed as a toxic and harmful refrigerant that should not be used, however, with CFC restrictions, an increase in use will be prompted especially in the industrial sector. The thermophysical properties of ammonia make it a very good alternative to use in vapor compression cycles, but the mentioned precautions in design and safety measures need to be taken.
1989	Adrian Bejan[70]	An investigation of the second law efficiency to deal with refrigeration and liquefaction plants. The second law efficiency decrease as the load temperature decreases. Two possible reasons provided.	The second law efficiency of refrigeration and liquefaction plants which use cold temperatures is said to be nondependent on load temperature. Instead 2 possible reasons, caused by the internal heat transfer irreversibility and another which includes not only this, but also due to external temperature differences between ambient and the plant as well as the load temperature is proposed. The use of a simple model is emphasized for easier applications, and also highlight the thermodynamic irreversibilities of such plants.

Year	Authors	Summary	Notes
1992	A.Henatsch, P.Zeller[71]	An analysis on the possible use of the cold air refrigeration was carried out via a developed model.	The possible analysis of using cold air refrigeration to overcome the use of alternative refrigerants was carried out via a model. The possibility to achieve COPs larger than 1 are shown.
1993	Gustav Lorentzen, Jostein Pettersen[72]	The re-use of CO2 is proposed for Car Air-conditioning systems, instead of the use of chemical compounds such as HFCs.	Since the use of fluorocarbons is still considered to provide the best solution for air conditioning especially in the automotive industry, the author purposes through the use of a practical setup, the possibility to use CO2 in vehicles. A comparison with R12 was conducted.
1995	N.E.Wijeysundera[73]	Irreversibilities caused due to heat transfer are examined through a model for an absorption refrigeration cycle.	The efficiency changes are presented with respect to the developed model, which includes heat transfer irreversibilities. The model is based on the temperatures of the heat reservoirs. The predicted values are larger than those available in literature, possible due to the presence of larger irreversibilities.
1997	K.C.Ng, H.T.Chua, W.Ong, S.S.Lee, J.M.Gordon[74]	A simple analytical diagnostic model for reciprocating chillers was developed, based on the previous work by the authors. This model also can help determine the optimal operation of these chillers.	The comparison with actual data is used to validate the developed model, for diagnostics as well as optimization of performance of reciprocating chillers. The model can predict with accuracy the COP as well as take into account external and internal dissipative heat losses at a 50:50 basis.
1997	Lingen Chen, Chih Wu, Fengrui Sun[75]	The optimal performance of a combined refrigeration cycle is determined through the use of a model and the inclusion of a bypass heat leak.	The performance of the refrigeration cycle with heat leak was compared to the endoreversible model, and the behavior was different. Hence there is an importance of focusing on heat leaks for design and use.

Year	Authors	Summary	Notes
1997	S.B.Riffat, C.F.Afonso, A.C.Oliveira, D.A.Reay[76]	A review of the use of natural refrigerants in place of CFCs.	There is still a wide scope to research into the use of natural refrigerants such as water, HCs for practical application for refrigeration and air-conditioning. These natural refrigerants are more environmentally friendly and can be applied to different cycles including vapor compression, absorption and transcritical cycles.
1997	R.Ayala, C.L.Heard, F.A.Holland[77]	The use of ammonia / lithium nitrate for absorption refrigeration providing a 10% increase in efficiency for a hybrid system.	The use of the recommended refrigerant pair for a combined system of absorption and mechanical vapor compression has shown a 10% increase in efficiency for retrofits. Though these efficiency show promise for hybrid systems, they are very much dependent on the quality of waste heat and also are affected by temperature fluctuations.
1997	Yau-Ming Chen, Chung-Yung Sun[78]	Using steam ejector refrigeration as an alternative to vapor compression refrigeration.	A performance review of using steam ejector refrigeration instead of traditional MVC chillers is presented. The use of moderate Mach numbers such as 4.35 at the primary nozzle are considered adequate. With the use of two-stage ejector, the utilization of low grade heat can also be achieved. However, there still needs to be more detailed analysis especially on the flow characteristics, since steam leads to the formation of droplets.
1997	F.Meunier, F.Poyelle, M.D.LeVan[79]	The role of thermal coupling in entropy production for an Adsorption refrigeration cycle is analyzed.	The absorption cycle is compared to the Carnot cycle. The entropy production or second law analysis is carried out for an adsorption cycle pertaining to the heat reservoir thermal coupling. The cycle times also are said to affect both the internal and external entropy generation.
1998	Lingen Chen, Chih Wu, Fengrui Sun[80]	Cooling load and performance of an air refrigeration cycle.	The cooling load vs. COP is examined for an air refrigeration cycle. This is also analyzed with the pressure ratio and the cooling effect and COP. The Irreversibilities due to the resistance heat losses in between the hot and cold heat exchangers and the compression and expansion process is also presented.

Year	Authors	Summary	Notes
1998	Lingen Chen, Fengrui Sun, Ning Ni, Chih Wu[81]	Determining the optimal COP for variation of cycle time, heat leak and adsorbed heat for a two heat reservoir cycle.	Adsorption refrigeration and the measurement of COP through a theoretical approach. The reservoir effects on the COP are analyzed with the inclusion of heat leaks, finite heat capacity, and low and high temperatures. The ability to determine the optimal COP for practical heat reservoirs with finite size and heat leaks is obtained. The heat leak seems to only affect the COP and not the configuration. The finite heat capacity seems to affect the configuration as opposed to the heat leak.
1998	Robert Tozer, Ron W. James[82]	Use of absorption refrigeration systems for combined heating and power (CHP).	The CHP using Absorption refrigeration is compared to traditional MVC system, through exergy and cost analysis. Both systems are said to require the same amount of exergy. However, with the use of the absorption system, the annual capital cost difference is offset by the running cost savings.
1998	S.Wu, I.W.Eames [83]	A novel ejector boosted absorption refrigeration system is presented.	A novel absorption refrigeration system is proposed and experimental data is provided, to show the benefits of using an ejector boosted single effect absorption cycle, where the generators are replaced with a steam generator, ejector and concentrator. The initial cost will be much lower than a double effect absorption system, and the maintenance will be much lower as well due to the limited mechanical components.
2000	Hiroyuki Fukui, Ken-ichi Sanechika, Masanori Ikeda[84]	The proposed use of new lubricants for HFC refrigerants	The practicality of using these new lubricants is presented with the use of fluorinated alkyl aryl ethers, which help eliminate performance issues related to poor stability and high moisture absorption. These lubricants are also easily miscible with HFCs and will allow excellent performance. They can also be retrofitted to system which were operating on R12 and R22.

Year	Authors	Summary	Notes
2000	Selahattin Göktun, Hasbi Yavuz[85]	The effects of irreversibilities regarding the performance of a combined MVC and Brayton Power cycle were examined.	For cryogenic refrigeration which requires very low temperature for long periods of time, the performance of the two systems, one based on a four stage vapor compression cycle and the other a solar driven combiner Brayton power and refrigeration cycle were compared and showed almost identical behavior. The theoretical approach employed the inclusion of thermal resistance of the HXs, internal dissipations, pressure drops and component efficiencies. The COPs tabulated were found to be lower than the data available on practical systems, which makes the model more realistic and can be employed as a potential standard. Though at some points the combined VC cycle showed disadvantages with energy consumption.
2000	Y.S Chang, M.S Kim, S.T Ro[86]	Use of HC refrigerants for a heat pump.	The performance of some HC in both single pure form and binary mixtures of propane/isobutane/butane and propylene were compared to that of R22, for both cooling and heating. The compressor speeds are also varied to show part load conditions and the temperature levels of the cooling fluid are also changed. Though some HCs showed similar performance to R22, they often suffered from heat transfer degradation due to composition variation in the mixture form. Some empirical correlations and heat transfer coefficients are also developed and presented. The HCs seemed to show higher thermal conductivity and lower viscosity than liquid R22, which allows better heat exchange at the evaporator and condenser. However, the flammability of the HCs need to be also considered.
2001	T.F.Qu, R.Z.Wang, W.Wang[87]	Adsorption air-conditioning with heat and mass recovery.	The performance of using heat and mass recovery were tested for an adsorption system. The COP was affected either positively or negatively by mass recovery depending on the operating conditions of the system. When favorable operating conditions permit, the COP can be increased by 20%. The cycle times are also shortened, and hence the mass/heat recovery systems show better performance for particular conditions.

Year	Authors	Summary	Notes
2001	Adnan Sözen[88]	The heat exchangers and its effects on an absorption refrigeration cycle.	The HX and its effect on the absorption cycle were examined. The 3 different configurations where both HXs are included and individual omission of either the refrigerant HX or the mixture HX are studied. The different component exergy analysis shows the importance of developing the performance of certain parts in order to reduce the exergy losses. The refrigerant HX seemed to show the highest importance in increasing performance, rather than the mixture HX.
2002	Y.S Lee, C.C Su[89]	An investigation on the performance of a domestic VC refrigeration system using Isobutane.	The performance of the VC system was analyzed for different component conditions and test conditions using R600a. For a configuration of capillary tubes, parallel ones performed better for cold storage and air conditioning applications, whilst single tubes were better for freezing applications. The refrigeration capacity with changes in cooling temperature, capillary tube lengths, capillary tube diameter as well as the configurations are tested and presented.
2006	Fu Wing Yu, Kwoktai Chan, Hoyin Chu [90]	A thermodynamic chiller model for an air cooled chiller is used to improve the possible performance of the system.	The use of variable speed condenser fans can help increase the efficiency of an air cooled MVC system. A model is developed which includes the set point required for the condenser, which then tabulates the required cooling fan speed for any operating conditions. The inclusion of the cooling fan power, will not enable the increase of the COP even though the condensing temperature can be reduced. With the correct control of the cooling fan speed, the COP can be increased between 1.7 - 84.8% .
2012	Shigeru KOYAMA, Yukihiro HIGASHI, Akio MIYARA, Ryo AKASAKA[91]	The progress of research under the NEDO project for the search and practical use of low GWP refrigerants in Japan is presented.	The thermophysical properties and behavior characteristics of the R1234ze(Z) and the binary mixture R1234ze(Z)/R32 as well as other mixtures of R1234ze(E)/R32/CO2 are evaluated. The use of R1234ze(Z) is enabled with the newly derived and calculated thermophysical properties. Whilst the mixtures and their behavior in a VC cycle will also be analyzed as future work.

Year	Authors	Summary	Notes
2013	Yitai Maa, Zhongyan Liu a, Hua Tian[92]	A review on transcritical CO2 heat pump research	A review regarding the research carried out on improving the performance of transcritical CO2 heat pumps is presented. This involves literature published since the 1990s, and progresses to the latest developments including cycle improvements and even lubricant changes to achieve optimum performance. CO2 cycles seem to be able to still provide adequate performance for vehicle use, hot water production and some commercial refrigeration systems. The use of internal heat exchangers, expansion work recovery etc. have helped boost the performance and practicality of the CO2 cycle.
2015	J.M.Belman-Flores, J.M.Barroso-Maldonado, A.P.Rodríguez-Muñoz, G.Camacho-Vázquez[62]	Review on the research regarding refrigeration with the greatest impact on this part of the industry. Presents a trend which is expected in this area.	The refrigerator is deemed to be an essential household appliance. Most refrigerators have high energy use due to their technology and cause environmental deterioration due the working fluids used. 30% of world energy consumption in developed nations is caused by Vapor Compression cycles. The general trend in domestic refrigeration research is focused on theoretical aspects, with models being used in 40% of the work and there is a gap in the development of hybrid refrigerators which can especially be used for developing nations.
2015	Adrián Mota-Babiloni, Joaquín Navarro-Esbrí, Ángel Barragán-Cervera, Francisco Molés, Bernardo Peris, Gumersindo Verdú[63]	Commercial refrigeration including supermarkets, cold rooms, food freezing and their latest trends, energy improvements, emission reductions and phase out of certain refrigerants and the potential use of Hydrocarbons and CO2 is presented.	High impact of commercial refrigeration is evident from the fact that supermarkets use half of their energy consumption for the refrigeration equipment. Globally around 15% of all electricity used worldwide is used for refrigeration. However, these climate issues are being tackled by policies and the development of efficient equipment, but there is still a lack of a substantial improvement to the whole sector.

Year	Authors	Summary	Notes
2015	Chieko Kondou, Fumiya Mishima & Shigeru Koyama[93]	The heat transfer characteristics of the low GWP mixture are reported.	Heat transfer characteristics of the low GWP Mixture R744/R32/R1234ze (E) in horizontal microfin tubes were investigated. The temperature glides between 8-18K at 40C operating conditions were achieved at different compositions. Whilst the condensation heat transfer coefficient was somewhat lower for the 9/29/62 mass% mixture, in comparison to the other tested mixtures. At 10C operating conditions the temperature glides changed between 9-22K. The heat transfer coefficients seem to exhibit a similar behavior to that at 40C. These mixtures are at GWP values between 200 - 300. A comparison with R32 showed that R1234ze (E) had some lower heat transfer characteristics (HTC). However, the HTC of the mixtures were much lower than both pure components.
2015	F.W.Yu, K.T.Chan, R.K.Y.Sit, J.Yang[94]	Improving the central air-conditioning system of a building through the use of oil free chillers.	Oil free chillers used to replace water-cooled centrifugal chillers of a building, showed the increase in performance, with energy savings up by 9.6%. The technical efficiency was reported to be 0.6. The main reason for this was the COP of the 3 oil-free chillers was much higher at lower capacities. With further chilled water temperature control and even load distribution, better COP values could also be achieved.
2016	Honghyun Cho, Chasik Park[95]	The exergetic performance of R1234yf in an automotive air-conditioner is presented at variable compressor speeds.	The comparison of R1234yf for a vehicle air-conditioning system with the use of an Internal HX and variable compressor speeds for load variation is presented. With a comparison to R134a, the yf system showed a smaller cooling capacity of around 4-7% less than the current system. The COP was also lower at around 3.6-4.5%. The inclusion of the IHX however, helped increase the cooling capacity to current levels and the COP difference was reduced to between 0.3-2.9%. The exergy destruction of the components were higher than the compressor at lower compressor speeds, but the compressor showed dominant exergy destruction at higher speeds. To avoid the IHX was able to help reduce the compressor exergy destruction by around 1.5-4.6% for the yf system. Thus the IHX was considered to be an important component for the implementation of alternative refrigerants such as R1234yf.

Year	Authors	Summary	Notes
2017	Zhaohong He, Yu Bai, Hongyu Huang, Jun Li, Huhetaoli, Noriyuki Kobayashi, Yugo Osaka, Lisheng Deng[96]	Adsorption refrigeration in compact form through the use of vacuum valve for automotive implementation	Adsorption chillers often suffer in size issues, which make them difficult to implement in cases such as automotive uses. Hence, the performance of a 40L adsorption chiller for vehicular use was analyzed and is presented, with efficiencies at different operating conditions. With the aid of vacuum valves, 1.5 kW output was achieved with a driving heat source at 368K and a cycle time of 3 minutes. The COP was recorded at 0.31, such that a 37.7W/L chiller could be placed in an automotive cooling cabinet.
2017	A.E.Kabeel, Y.A.F.El-Samadony, M.H.Khiera[97]	Using a novel cold mist evaporative cooler for a chiller to increase performance.	Cooling ambient air below its wet bulb temperature, through this novel method to achieve improved system performance in comparison to traditional evaporative cooled chillers is presented. The use of cold mist water to achieve better heat exchange at the condenser allowed the increase in COP of 91% in comparison to traditional air cooled chillers, whilst the evaporative cooled chiller had a CPO better than 82% of an air cooled chiller.
2018	Zhaofeng Meng, Hua Zhang, Mingjing Lei, Yanbin Qin, Jinyou Qiu[98]	Replacing R134a in Automotive Air-conditioning systems, through R1234yf mixtures.	Based on their previous work, a R134a/R1234yf mixture was proposed to be used for automotive vapor compression cycles. The GWP was maintained below 150. The use of a micro-channel HX was proposed which allowed similar cooling and heating capacities, but the COP of the mixture was lower by 4-9% for cooling and 4-16% for heating. This mixture could possibly be used for new automotive regulations of the EU.
2018	Faraz Afshari, Omer Comakli, Sendogan Karagoz, Hadi Ghasemi Zavaragh[99]	The steady state behavior of a heat pump and the variable behavior of a refrigerator are analyzed using different refrigerants	The variations in operation times and charge amounts were analyzed for a refrigeration and heat pump system due to their fundamental difference in operating requirement but identical cycle foundations. An existing heat pump with varied refrigerants R134a, R407c, R22 and R404a are used, then converted to a refrigeration unit for the second stage of experiments. The heat pump required a constant consumption of power, whilst the refrigerator for freezing purposes showed a decrease in power consumption over time. Due to the thermal restrictions the COP of the refrigerator was smaller than the HP. The cooling COP would also tend towards 0, when the operation time is increased. The optimum charge amounts for the freezer were also determined to be 15-25% lower than the HP requirement.

Year	Authors	Summary	Notes
2018	Michael Olbricht, Federico Lonardi, Andrea Luke[100]	Absorption chiller performance increase through additives, a numerical approach.	A numerical model is proposed to identify the effects of using additives on the overall performance of the absorption chiller. The use of surfactants helped increase the COP and cooling capacity pf the absorption system by around 83%.
2018	F.W.Yu, W.T.Ho[101]	The practical variations in chiller conditions during operation and its effects on COP for a large scale chiller plant.	The real life demand and conditions of a building are used to determine the performance variations of a chiller. The system consisted of 4 large chillers and 2 small scale chiller, with chilled water circuits and variable speeds pumps as well as evaporative cooled cooling water towers. The pair up operation of the chillers still allowed higher COP values even at higher wet bulb temperatures.
2019	S.Salehi, M.Yari, M.A.Rosen[102]	the Exergy and Economic analysis for a solar assisted absorption heat pump, solar heater and gas boiler system for district heating as a practical case study in Iran is presented.	The heating loads for the absorption system are analyzed between 50-2MW, with the assistance of geothermal reservoirs present in the town of Sarein. The production cost is said to decrease with increased hot spring temperatures and irradiation, whilst an ambient temperature increase will result in larger unit costs. A LiBr/H2O system is said to provide better performance than a NH3/H2O system.
2019	George Kosmadakis, Panagiotis Neofytou[103]	The use of nanoparticles for increasing heat transfer in Vapor Compression heat pumps.	The possibility of using nano particles to increase the heat transfer for VC heat pumps is presented. The refrigerants R134a and R1234yf are tested with Cu, Al2)3 and CuO nanoparticles. The use of nanoparticles at mass fractions from 0-5%, showed increase in COP of 5-6% in both heating and cooling modes. The load was almost constant, whilst the compressor power input decreased.

Year	Authors	Summary	Notes
2019	Paul Byrne, Redouane Ghoubali[104]	Prototype for air-source heat pump providing simultaneous cooling and heating,	The exergy analysis helped develop the 2 porotype's and identify their positives and weaknesses for an air source heat pump which can operate in both heating and cooling modes simultaneously. The heating mode allows the hot water production, whilst the cooling mode produced cold water. Two prototypes working on R407c and R290 were tested under the European Standard EN 14,511. The design of the system and the refrigerant choice affected the performance of the two. The lack of an exergy analysis is also highlighted and will be tackled in the future work.
2019	Dariusz Mikielewicz, Jan Wajs[105]	High temperature heat pump with low GWP refrigerant, with ethanol and multi stage, an analysis.	Single and multi-stage cycles are analyzed for high temperature applications based on an array of possible refrigerants. Ethanol was identified as the best fluid for operating single stage compression systems. The cascade systems were lacking in efficiency. Other fluids which were considered such as pentane and R365mfc offer good COP values as well. However, they are either flammable or have a very high cost.
2019	Miquel Pitarch, Estefanía Hervas-Blasco, Emilio Navarro-Peris, José M.Corberán[106]	The exergy analysis for individual components of the heat pump cycle for non-constant heat source and sink temperatures is presented.	For subcritical refrigeration cycles, the performance is often dependent on the temperature lift between the heat sink and source. The possibility to improve performance through subcool and superheat control are presented and analyzed using exergy on individual components. The condenser and expansion valve contributed the most with increased subcool, by showing reduced exergy destroyed. When the secondary fluid enters at a low temperature and is subjected to a high temperature lift at the condenser, the exergy destruction was higher for the compressor and condenser. In the opposite scenario, the compressor still showed large exergy destruction, but was followed by the expansion valve. Hence the control of subcool and superheat are shown to be very influential in the overall performance of the VC cycle.

Year	Authors	Summary	Notes
2019	F.W.Yu, W.T.Ho[107]	The performance of different combinations for real life chillers are studied and predicted using a developed model.	The diverse possibilities of chiller system configuration and its impacts on performance are presented. A combination of 51 component types was analyzed with the use of models. 5 chillers were analyzed, at 2 different capacities. The optimized system could operate at COP values of 3.34 for 58% of the time, while the average COP was 3.15 for no -pair -up combinations. The use of general linear models, network analysis and survival analysis are presented here as key ways of predicting COP behavior and finding optimized configurations.

The research mentioned in Table 2.1-1 focuses on a variety of ways to contribute to the development of the HVAC&R industry, which includes research carried out by Jakobs et. al. [67] who focused on the possibility of using non-azeotropic refrigerant mixtures with temperature glides to improve Vapor Compression (VC) cycle performance, work by Lorentzen [69] and Riffat et. al.[76], highlight the re-emergence of natural refrigerants in the hope of replacing CFC and HCFC which were coming under scrutiny due to their ozone depleting behavior. There was also the focus on non VC cycles such as absorption systems by Ayala et. al.[77], who were proposing the use of combined systems which could show a 10% increase in performance. There was also a focus shifting from just thermodynamic analysis to exergetic and economic aspects of HVAC&R systems such as the work done by Tozer et. al. in 1998 [82] on absorption systems and their exergetic behavior and cost analysis and the research by Pitarch et. al. in 2019 [106] on the VC cycle and its exergy analysis. There has also been a focus on not just the systems, but increasing component performance by focusing specifically on certain lubricants to improve the compressor performance by Fukui et. al. [84], to the use of nanoparticles to increase heat transfer coefficients in absorption systems by Kosmadakis et. al. [103]. The theoretical approaches to performance of such systems has also evolved from Ng. et. al. [74] who focused on diagnostic models and optimization to some of the latest work by Yu et. al. [107] which can compare up to 51 combinations of components to determine optimum systems.

Hence, the research relating to this industry has been very diverse and also has been developing continuously. One of the particular drivers contributing to the HVAC&R industry growth has been global and local policies. With the implementation and introduction of international treaties [36], [49], [50] and other national policies [53], [108], there has been an increasing need for replacing some of the harmful refrigerants which possess either high ODP or GWP.

Some of the research seen in Table 2.1-1…, show how researchers have been focusing on finding alternatives or even testing alternative refrigerants and mixtures in HVAC&R systems such as the work by McLinden et. al. [68], which shows a theoretical approach to comparing potential behavior of refrigerant mixtures in 1987, to the work by Meng et. al.[98] on automotive refrigerant replacements with low GWP mixtures in 2018.

A specific research approach which was also prompted by these treaties and policies was catered to the industry's needs of exploring suitable refrigerants which can be easily incorporated into existing equipment, rather than requiring the design, manufacturing and supply of new equipment. This cost effective way of using the already existing systems with different and more suitable refrigerants is collectively known as 'drop-in' replacements. 'Drop-in' signifies the ability for a new refrigerant to be introduced to an existing system without involving major changes. Before commercialization of such refrigerants, the performance of existing systems using these 'drop-in' replacements must be verified and this created the path for many research works. Since the research is again very extensive, some of these are presented in Table 2.1-2, with the relevant refrigerants and systems used for the 'drop-in' tests.

Table 2.1-2 Literature review on 'drop-in' tests carried out on several types of refrigerants and HVAC&R systems

Year	Authors	Summary	Notes	Refrigerants	System	Approach
2001	Cecilia Gabrielii, Lennart Vamling[109]	For a large scale cooling facility the possibility of replacing R22, with potential mixtures which meet safety requirements include R134a, R125, R32 and R143a.	A multitude of criteria and performance statistics are used to evaluate over 2000 possible mixtures to replace R22 in district heating facilities. The possible mixtures of R134a and the behavior of heating capacity and COP are explored with the use of a developed model for the heating system.	R22 to R134a, R125, R32 and R143a	District Heating	Experimental, Theoretical
2008	K.Mani, V.Selladurai[110]	Drop in investigations for a VC Chiller to replace R12, R134a using R290/R600a mixture.	Better performance was provided with the use of the new mixture, which makes it a possible drop in replacement for R12 or R134a. This included increased capacity and COP at ranges between 19.9 - 50% and 3.9 - 25.1% respectively.	R12, R134a to R290/R600a Mixture	Vapor Compression Cycle	Experimental
2009	D.J.Clelanda, R.W.Keedwell, S.R.Adams[111]	R22 replacement for a dairy farm using a propane and ethane mixture, via drop in.	The mixture proved to be a good replacement for this scenario with low retrofit costs and similar cooling capacity and better efficiency. The propane/ethane mixture reduced energy consumption by 6-8%, with similar cooling capacities. The pure propane system did reduce energy intake by 5%, but the cooling capacity was 9% lower.	R22 to Propane, Ethane and HCs	Commercial Refrigeration	Experimental

Year	Authors	Summary	Notes	Refrigerants	System	Approach
2012	R.Llopis, E.Torrell, R.Cabello, D.Sánchez[112]	For a low temperature system, the possible alternatives to R22 in the form of drop in R422A R417B and a retrofit R404a are explored	The drop in show larger mass flow rates and reduced capacity as well as COP with comparison to R22. The drops in COP were also greater than theoretically predicted.	R22 to R422A, R417B	Commercial Refrigeration	Experimental, Theoretical
2013	J.Navarro-Esbrí, J.M.Mendoza-Miranda, A.Mota-Babiloni, A.Barragán-Cervera, J.M.Belman-Flores[113]	The possibility to replace R134a with R1234yf is explored for a VC system.	Though R1234yf showed lower performance than R134a at around 9% lower cooling capacity and 19% lower COP, this effect can be reduced through the use of an IHX	R134a to R1234yf	Vapor Compression Cycle	Experimental, Theoretical
2013	R.Cabello, E.Torrella, R.Llopis, D.Sánchez, J.A.Larumbe[114]	The use of IHX in drop in replacements for R22 in a refrigeration plant were explored for chlorine free refrigerants R417B R422A R404A	Though the COP reduced without the IHX, the amount can be reduced with the introduction of an IHX	R22 to R404A, R417B, R422A	Commercial Refrigeration	Experimental, Theoretical

Year	Authors	Summary	Notes	Refrigerants	System	Approach
2014	Adrián Mota-Babiloni, Joaquín Navarro-Esbrí, Ángel Barragán, Francisco Molés, Bernardo Peris[115]	Two alterative refrigerants R1234yf and R1234ze(E) are tested as drop in replacements for a R134a Vapor Compression System. An IHX is also introduced to see the increase in performance.	Again, the use of the IHX is shown to reduce the performance decrease due to the introduction of the new Low GWP refrigerants. The cooling capacities initially dropped at an average of 9% and 30% for the individual refrigerants, causing a drop in COP to 3% and 11%, but with the IHX, the drops in COP were only at 2% and 8%.	R134a to R1234yf, R1234ze(E)	Vapor Compression Cycle	Experimental
2015	Zvonimir Janković, Jaime Sieres Atienzaa, José Antonio Martínez Suáreza[116]	Two alterative refrigerants R1234yf and R1234ze(E) are tested as drop in replacements for a R134a small power refrigeration system. A model is used for behavior prediction then compared with experimental data.	Even though the COP is lower for the drop in replacements, small changes to the compressor can allow an adequate performance. R1234yf seemed to be an easier drop-in replacement for R134a, whilst ze(E) can actually perform better, with an overridden compressor can match the cooling capacity. yf showed higher cooling capacities but at lower COPs, whilst, ze(E) showed lower cooling capacities at higher COPs.	R134a to R1234yf, R1234ze(E)	Domestic Refrigeration	Experimental, Theoretical

Year	Authors	Summary	Notes	Refrigerants	System	Approach
2015	Mohamed El-Morsi[117]	The theoretical approach to use HCs to replace a refrigeration system which runs on R134a. An energy and exergetic analysis.	The energy and exergetic analysis show that the R600 can perform better than R134a but requires the change of the compressor, whilst the LPG which is cheaper shows a lower performance than R134a by 10% and can be used as a drop in.	R134a to R600, LPG	Domestic Refrigeration	Theoretical
2015	Adrián Mota-Babiloni, Joaquín Navarro-Esbrí, Ángel Barragán-Cervera, Francisco Molés, Bernardo Peris[118]	The drop in replacement for R134a, with R1234ze(E)/R134a mixture for an Air-Conditioning system.	The Cooling capacity dropped by 6% with the use of the new mixture, however there was a 1% increase in COP. The use on an IHX can help as predicted in other cases, with the performance.	R134a to R1234ze(E)/R134a (R450A) Mixture	Domestic Air-Conditioning	Experimental
2016	Ciro Aprea, Adriana Greco, Angelo Maiorino, Claudia Masselli, Antonio Metallo[119]	R1234ze(E) is used as a drop in for a domestic refrigeration unit operating on R134a, with a focus on the environmental impact.	The lower environmental impact of the alternative refrigerant is highlighted. HFO1234ze as a refrigerant under sub-tropical conditions is analyzed to replace R134a. The direct GWP impact of the new refrigerant is much lower, but the indirect impact is almost the same.	R134a to R1234ze(E)	Domestic Refrigeration	Experimental

Year	Authors	Summary	Notes	Refrigerants	System	Approach
2016	Ciro Aprea, Adriana Greco, Angelo Maiorino[120]	Drop in experiments for a domestic refrigeration unit for replacing R134a. A slight energy saving is also reported with an improved cooling capacity.	Drop in experiments in a domestic refrigeration circuit with R1234yf to replace R134a, show that the new refrigerant will increase the condensation pressure, and cause a higher compression ratio, but with 24 hours of operation, it still shows a 3% lower energy demand. The refrigerant can also be easily used as a drop-in.	R134a to R123yf	Domestic Refrigeration	Experimental
2017	Pavel Makhnatch, Adrián Mota-Babiloni, Rahmatollah Khodabandeh[121]	The performance of a drop in R450a for a R134a refrigeration unit is evaluated.	The performance was not able to reach or exceed that of R134a, however similar thermophysical characteristics make it an ideal refrigerant where the drop in Cooling Capacity is acceptable.	R134a to R450a	Domestic Refrigeration	Experimental
2017	R.Cabello, D.Sánchez, R.Llopis, J.Catalán, L.Nebot-Andrés, E.Torrella[122]	The energetic analysis of a drop in replacement for R134a for a large scale cascade refrigeration plant, with the use of R152a.	The use of R152a to replace R134a in this scenario showed little energy improvements. At lower temperature differences between the hot and cold sides, R134a showed better performance. But technologically it is still feasible.	R134a to R152a	Commercial Refrigeration	Experimental

Year	Authors	Summary	Notes	Refrigerants	System	Approach
2017	Yu Fang, Sergio Croquer, Sébastien Poncet, Zine Aidoun, Yann Bartosiewicz[123]	The possibility to replace R134a for a supersonic ejector, with the use of drop in R1234yf r R1234ze(E) is studied using a numerical model.	The possibility of replace R134a in an ejector heat driven refrigeration cycle is explored. The reductions in COP and cooling capacity for the use of ze(E) is 4.2% and 26.6%, whilst yf showed a 9.6% and 19.8% reduction.	R134a to R1234yf, R1234ze(E)	Ejector Heat Driven Refrigeration, Absorption Cycle	Theoretical
2017	Rodrigo Llopis, Daniel Sánchez, Ramón Cabello, Laura Nebot-Andrés, Jesús Catalán-Gil[124]	For a low temperature direct expansion type refrigeration system, which operates on R404a, the drop in alternative R407H in order to reduce the GWP was studied.	Though there was a reduction in energy use of 4.0% in the system, the overall temperature increase was larger with the use of the new refrigerant.	R404a to R407H	Commercial Refrigeration	Experimental
2017	Ciro Aprea, Adriana Greco, Angelo Maiorino[125]	The drop in capabilities for a domestic refrigeration unit to replace R134a with R1234ze binary mixtures with R134a were tested.	A 14% energy savings for the mixture and 8.92% savings for the pure HFO together with the reduction in GWP were reported.	R134a to R1234ze/R134a Mixture	Domestic Refrigeration	Experimental

Year	Authors	Summary	Notes	Refrigerants	System	Approach
2018	J.M.Mendoza-Miranda, C.Salazar-Hernández, R.Carrera-Cerritos, J.J.Ramírez-Minguel M.Salazar-Hernández, J.Navarro-Esbrí, A.Mota-Babiloni[126]	A model was developed to analyze the performance of a variable speed liquid chiller with a drop in replacement for R134a, with R1234yf.	A 2-11% reduction in COP was reported with the use R1234yf, and similar emissions including energy sources were also reported.	R134a to R134yf	Chiller	Theoretical
2018	Juan Garcia, Thiago Ali, Willian Moreira Duarte. Ali Khosravi, Luiz Machado[127]	The transient response of an evaporator model for replacing R134a with drop in R1234yf for a refrigeration unit were studied.	The model results were validated with experimental results, showing a good agreements at ±1°C. The correlations describing the two phase flow and heat transfer coefficients as well as pressure drops were also within good agreement. The yf refrigerant also required less mass flow.	R134a to R1234yf	Water Refrigeration	Experimental, Theoretical
2018	Adrián Mota-Babiloni, Jorge Haro-Ortuño, Joaquín Navarro-Esbrí, Ángel Barragán-Cervera[128]	The use of R454C and R455A to replace R404A in high temperature climates was explored with the addition of an IHX.	The cooling capacities were unable to meet those of R404A, however an improvement in COP was reported. The use of the IHX in this high temperature case was not recommended due to low benefits.	R404A to R454C, R455A	High Temperature Chiller	Experimental

Year	Authors	Summary	Notes	Refrigerants	System	Approach
2018	C.Aprea, A.Greco, A.Maiorino[129]	The drop in possibilities of several HFO mixtures to replace R134a HFC in a refrigeration unit in a domestic setting is explored.	Pure HFO1234yf, HFO1234yf/HFC134a,HFO1234ze (E),HFO1234ze (E)/HFC134a mixtures were evaluated, with the ability to achieve the required temperatures within the cooling cabinet and freezer, whilst also showing lower environmental impact with Life Cycle Climate performance.	R134a to R1234yf, R1234ze(E)	Domestic Refrigeration	Experimental
2018	C.Aprea, A.Greco, A.Maiorino, C.Masselli[130]	The use of R1234ze to replace R134a as a Drop In in a domestic refrigeration unit is presented.	An energy saving of 9% is reported with the use of the new refrigerant.	R134a to R1234ze	Domestic Refrigeration	Experimental

Year	Authors	Summary	Notes	Refrigerants	System	Approach
2019	V.H.Rangel-Hernández, J.M.Belman-Flores, D.A.Rodríguez-Valderrama, D.Pardo-Cely, A.P.Rodríguez-Muñoz, J.J.Ramírez-Minguela[131]	The domestic refrigeration system with drop in replacement of R134a with R1234yf at various operating conditions is presented.	R134a was still performing better than R1234yf with respect to both an energy, exergy and cost outlook. The Unit exergy cost, exergoeconomic factor are used to compare with R134a. For the unit exergy cost R134a showed better performance. Whilst it also showed higher values for the exergoeconomic factor, which signifies the less exergy destruction within the system. Optimizing the system, will allow an energy saving of 9% with R134a and 6.5% with yf.	R134a to R1234yf	Domestic Refrigeration	Experimental, Theoretical

From the drop-in research carried out over the years, Table 2.1-3 further presents the research work regarding drop-in research with a particular focus on the replacement of R410a, or the use of R410a as a 'drop-in' in a multitude of HVAC&R systems.

Table 2.1-3 The literature review on R410a related 'drop-in' experiments on various HVAC&R systems

Year	Authors	Summary	Notes	Refrigerants	System	Method
2003	Richard E. Cawley[132]	A mixture of R32 and R134a is proposed as an environmentally friendly alternative to R410a as a drop-in substitute.	~	R410a to R32/R134a Mixture	All	Invention
2004	Mark W Spatz, Samuel, F. Yana Motta[133]	The possibility of replacing R22, with alternatives such as R410a for medium temperature applications	Through theoretical analysis and the use of a model, the behavior and performance of alternatives to R22 were predicted and compared with experimental results. R410a is chosen as the optimum solution for replacing R22.	R22 to R410a, R404a, R290	Refrigeration	Experimental, Theoretical
2008	W.Chen[134]	The comparison of R410a vs R22 is 4 domestic split type air conditioners	The performance analysis of split type air conditioners was carried out according to ISO Standard. The efficiency off R410a was around 3% and 12% higher in the different systems. The transport properties and working pressure are better for R410a than R22.	R22 to R410a	Residential Air Conditioning	Theoretical
2010	Shigeru Koyama, Nobuo Takata, Sho Fukuda[135]	Drop-in experiments were carried out for a heat pump operating on heating mode, to replace R410a with R1234ze(E), R1234ze(E)/R32 Mixtures	The sub cooling was affected slightly by using the mixture, however, the COP values remained the same, which make the mixture a suitable alternative to heat pump applications instead of R410a.	R410a to R1234ze(E), R1234ze(E)/R32 Mixture	Heat Pump	Experimental

Year	Authors	Summary	Notes	Refrigerants	System	Method
2011	Shigeharu TAIRA, Takeshi YAMAKAWA, Akinori NAKAI, Ryuuzaburou YAJIMA [136]	The suitable substitutes based on currently available refrigerants is proposed for a diverse range of applications and climatic conditions, to reduce the Global Warming Impact.	R32 has been proposed as a good alternative, in different climatic conditions. However, it is not an all-encompassing solution. Possible alternatives for specific applications are given in form of a 'refrigerant map'.	R410a, R134a, R407C, CO2 to R32, R1234yf, CO2	All	Experimental, Theoretical
2012	Hung Pham, Rajan Rajendran[137]	A status of global technical information and policies for replacing R410a with R32 are presented in this work.	An experimental analysis is performed to compare the possibility of using R32 and HFO blends as a drop-in for R410a replacement in Unitary Split Type Air-conditioning for cooling and heating according to AHRI standards 540. R32 shows the best efficiency and cost analysis to use as an alternative. Hoverer, lower GWP HFOs will be required to replace pure R32 systems in the future, but still lack lower costs. The natural refrigerants CO2 and R290 face efficiency issues even though their GWP is ultra-low.	R410a to R32, HFOs and Natural Refrigerants	Split Type Domestic Air Conditioner	Experimental

Year	Authors	Summary	Notes	Refrigerants	System	Method
2012	Ken Shultz, Steve Kujak[138]	Several mixtures of R32 and pure R32 are tested as drop-in replacements for an Air-Cooled Water Chiller	The ambient air conditions were used according to the AHRI Standard 550/590-2011. R32 showed a similar performance with respect to the R410a within the evaporator, whilst the other mixtures due to temperature glides showed larger or smaller entering and leaving temperatures. The pressure drops were often lower for the alternative refrigerants. These were also compared with predicted values.	R410a to R32 and mixtures	Air-Cooled Chiller	Experimental / Theoretical
2013	L.Cremaschi, X.Wu, A.Biswas, P.Deokar[139]	The behaviour of 2 compressors (Residential and Commercial) for replacing R410a with R32, R1234yf and 2 new refrigerants	The Compressor performance with respect to discharge temperatures and pressures and volumetric efficiencies were presented.	R410a to R32, R1234yf	Residential Refrigeration, Commercial Refrigeration	Experimental
2013	Xing Xu, Yunho Hwang, Reinhard Radermacher[140]	The performance difference of a vapor-injection heat pump for residential use is explored, with R32 as an alternative drop-in to R410a.	The COP increase using R32 was reported to be between 9-10%, coupled with the reduction of GWP as well.	R410a to R32	Domestic Air-Conditioning	Experimental

Year	Authors	Summary	Notes	Refrigerants	System	Method
2014	Bachir BELLA, Norbert KAEMMER, Riccardo BRIGNOLI, Claudio ZILIO[141]	A simulation model was developed for an air cooled water chiller, to predict the performance of R410a and R32.	With the simulation data, and optimized performance for each individual refrigerant, R32 was determined to be a potential substitute for R410a. Seasonal Energy Efficiency Ratio is also calculated according to European Standard EN 14825 for water chillers. R32 had higher cooling capacities by 5.7% at 35C ambient conditions. Though the EER was almost the same for both refrigerants R32 again showed a better SEER at 2-3% higher values.	R410a to R32	Air Cooled Water Chiller	Theoretical

Year	Authors	Summary	Notes	Refrigerants	System	Method
2014	Sho Fukuda , Chieko Kondou , Nobuo Takata , Shigeru Koyama[142]	The possibility of using R1234ze(Z) and R1234ze(E) for replacing R410a in high temperature heat pumps are explored using a simple simulation model as well as validated through experimental results.	The simulated values for COP and irreversible losses fell with 18% and 20% of the experimental values at the condensation temperature of 75°C. The p-h diagrams for the cycles were also used to validate their behaviour. The COP behaviour of R1234ze(Z) became much lower than ze(E) with larger heating loads above 1.5 kW. ze(Z) also showed simulated irreversibilities larger than ze(E) at 1.8 kW, which was again validated with the experimental behaviour. The increasing temperature differences between the HXs for the ze(Z) results in larger losses.	R410a to R1234ze(Z) and R1234ze(E)	High Temperature Heat Pump	Theoretical / Experimental

Year	Authors	Summary	Notes	Refrigerants	System	Method
2015	Qiqi Tian, Dehua Cai, Liang Ren, Weier Tang, Yuanfei Xie, Guogeng He, FengLiu[143]	A refrigerant mixture of R32/R290 is used as a drop in replacement for R410a for a domestic split type units.	The ODP is 22% lower than R410a. The charge amount is also 30-35% lower. The power consumption increased by 14-23.7%. The cooling capacity improved by 6.4 - 16.4%, and the COP was 6-7% lower than R410a. The use of a micro finned HX will allow the Cooling capacity and COP to increase by 6.4% and 6.8%.	R410a to R32/R290	Domestic Air-Conditioning	Experimental

Year	Authors	Summary	Notes	Refrigerants	System	Method
2016	Sho Fukuda ,Hideki Kojima, Chieko Kondou, Nobuo Takata & Shigeru Koyama[144]	The drop in experiments for a heat pump using refrigerant mixtures for both cooling and heating to replace R410a or R32 is presented.	Presents the alternatives TF300, YF200, ZE300 and ZE200, which are ternary mixtures of CO2/R32/R1234yf and R1234ze(E) as drop-in replacements for R410a. The irreversible losses within the cycle are analyzed and presented. The smaller volumetric capacity of YF200 and ZE200 lead to significantly higher irreversible losses within the cycle. These are mainly caused by pressure drops which increase with heat load. The COPs of YF200 and ZE200 are also lower than those of R410a and R32 at the rated heat load. ZE200, exhibits a temperature glide due to its non-azeotropic behavior of around 22K. This temperature glide then results in the increased irreversible losses as well, especially within the 2 HXs and expansion valve. Due to the presence of a temperature glide larger than 20K, it said that the air conditioning applications are impractical. YF300 and ZE300 were presented as alternatives to R410a and R32.	R410A, R32 to YF300, YF200, ZE300, ZE200	Air Conditioning	Experimental

Year	Authors	Summary	Notes	Refrigerants	System	Method
2016	Sho Fukuda ,Hideki Kojima, Chieko Kondou, Nobuo Takata & Shigeru Koyama[145]	The heating mode performance for the ternary and binary mixture of CO2/R32/R1234yf and R32/R1234yf with GWP of 300 and 200 are explored.	The ternary 300 and binary 300 mixtures show comparable performance to that of R410a. The mixtures behave in a zeotropic manner, resulting in a temperature glide, which however does not reduce the irreversibilities. This suggests the lower heat transfer performance of the HXs. The COP could be improved within the system if the compressor is modified ad the diameter of the connecting pipes and HX are increased to provide better mass flows and heat exchange.	R410a to CO2/R32/R1234ze(E) and R32/R1234ze(E)	Heat Pump	Experimental
2017	Jignesh K.Vaghela[146]	EES is used for the analysis of theoretical performance of an automotive air-conditioner with alternative refrigerants to R134a, as R410a and others	A theoretical approach to alternative refrigerant use in an Automotive air-conditioner are presented with respect to replacing R134a with R410, R1234yf etc. The thermodynamic properties of the refrigerants are compared and a standard rating VC cycle is also analyzed. R1234yf was derived as the best replacement for a drop in scenario for R134a. Even though the COP was lower with yf, the low GWP makes it more suitable. R410a was not adopted due to its higher saturation pressures.	R134a to R410a, R1234yf	Automotive Air Conditioning	Theoretical

Year	Authors	Summary	Notes	Refrigerants	System	Method
2017	Adrián Mota-Babiloni, Joaquín Navarro-Esbrí, Pavel Makhnatch, Francisco Molésa[147]	The use of R32 and mixtures to substitute R410a and R22 in domestic air conditioning systems is explored in terms of USA and Europe and the most recent research works have been collated.	R32 in mixture form including HFC/HFOs from literature are analyzed to develop better mixing parameters. The current literature available from specific mixtures and their GWP values as well as thermophysical properties, to flammability issues, possible toxicity issues, compatibility with materials, two phase flow including condensation, evaporation, heat transfer coefficients and system performance has been summarized.	R22, R410a to R32 and its mixtures	Residential Air Conditioning	Theoretical / Review
2019	Qiu Jinyou, Zhang Hua, Sheng Jian, Wu Zhihong[148]	The Drop In replacement of R410a in a residential air-source heat pump water heater unit with L41b and the use of an IHX were explored.	A drop in COP was reported ranging between 1.4 - 9.1% and 2.3-10.1% at various conditions in comparison to R410a. However, the IHX will allow the reduction of these losses. The heating capacities were also lower ranging between 6.9-18.6% and 7.6 - 20.9%. With the use of the IHX, L41b can be adopted for existing system to replace R410a.	R410a to L41b	Domestic Water Heater, Air Source Heat Pump	Experimental

As presented in Table 2.1-3, there have been several researchers in recent years focusing on testing alternative low GWP refrigerants and mixtures as drop-in replacements for R410a. However, a majority of the work has been focused on either air conditioners or refrigeration units, whilst only a few have focused on chillers or heat pumps.

From these literature, the most recent work focusing of replacing R410a were presented on using a refrigerant mixture of R32/R290 for a domestic air conditioning unit under Chinese Standards by Tian et. al. [143], whilst Mota-Babilioni et. al.[147] also focused on reviewing the suitability of using R32 and some of its mixtures as alternatives for domestic or residential air conditioners. A theoretical approach was taken by Prof. J.K. Vaghela [146] to test the possibilities of using R410a as a drop in in automotive air conditioners. Jinyou et. al. [148] also presented the use of L41b (R1234ze(E)/R32 at 27/73 mass fractions) for a residential air-source heat pump. The selection of this refrigerant was based on the work presented by Schultz et. al. [138] under AHRI, which examined the use of R410a alternatives for an air cooled water chiller.

The most significant research pertaining to a water cooled vapor compression chiller was carried out by Fukuda et. al. [144], at the same research institution. His work presents the analysis of the same experimental setup with the use of a ternary and binary mixture of CO_2/R32/R1234yf for replacing R410a. However, the studies were not carried out under the AHRI 551/591 (SI) standards. This allowed the use of refrigerant side properties for calculation of the heating and cooling effects. Though this is a possibility for experimental setups, in the industry it is often very difficult to tap into the refrigerant loop and most of the heat transfer calculations will be based on the water side. Doing so is recommended by the AHRI standards as well.

As mentioned before, many global and local policies are driving the HVAC&R industry to improve their eco-consciousness and there is a lot of contribution to this by research institutions. In Japan, the F-Gas policies, are currently pushing the industry to change high GWP refrigerants to low GWP refrigerants and mixtures [53]. One of the goals of the industry is to thus use drop in refrigerants to replace the widely used high GWP refrigerants. However, the performance and behavior of these new refrigerants and mixtures need to be compared with the performance of current refrigerants as a minimum

scenario. One of the current refrigerants which is widely used and in need of replacement due to its high GWP is R410a [46], [149].

However, as highlighted in Table 2.1-3, the current studies on R410a as a drop-in refrigerant on a water cooled Mechanical Vapor Compression (MVC) chiller did not utilize the AHRI Standard 551/591. This creates several difficulties in the replicability of these experiments by different research bodies for other chillers under various environmental conditions and the fairness in comparison based on other work would be lost. Following an international standard will overcome this, by allowing for an easier replicability and comparison of R410a as a drop-in refrigerant for MVC chillers. Hence there is the requirement to employ an international standard and carry out a baseline experimental investigation for a water cooled MVC chiller operating on R410a. This will allow a fair as well as replicable study allowing comparison with other drop-in refrigerants to be tested in the future.

To the best of my knowledge there has not been prior research carried out on a Mechanical Vapor Compression (MVC) Chiller operating on R410a using AHRI Standard 551/591 (SI) [59].

Hence a cycle performance analysis for a MVC Chiller operating on R410a, in order to compare with other potential 'drop-in' refrigerants with low GWPs is proposed. This will allow the above mentioned gap to be filled. The AHRI Standards will allow a fair comparison with potential low GWP 'drop-in' refrigerants which will be tested as future work. The experiments were conducted for cooling capacities between 1.0 – 1.6 kW, whilst the refrigerant charge amount was also varied, in order to determine the optimum charge. The cycle analysis for the experiments was conducted using both the first law analysis for determining parameters such as the Coefficient of Performance (COP) and the, 2nd law or exergetic analysis for further in-depth investigations was also utilized to identify irreversibilities within the cycle and to calculate the exergetic efficiency. This research and the related results and conclusions are presented within Chapter 2.

2.2 Experimental Methodology

2.2.1 Experimental Setup and Instruments

2.2.1.1 Schematic

The experimental setup used is shown in Figure 2.2-1 The set up consists of three individual loops; the Refrigerant Loop is shown in pink; the two separate loops shown in green and red dashed lines are for the Chilled Water Loop, and Cooling Water loop, respectively. The 4 main components of the of the chiller comprised of the compressor, evaporator, condenser and expansion valve. The water circuits consisted of two constant temperature water baths to provide the necessary loads and to remove the rejected heat.

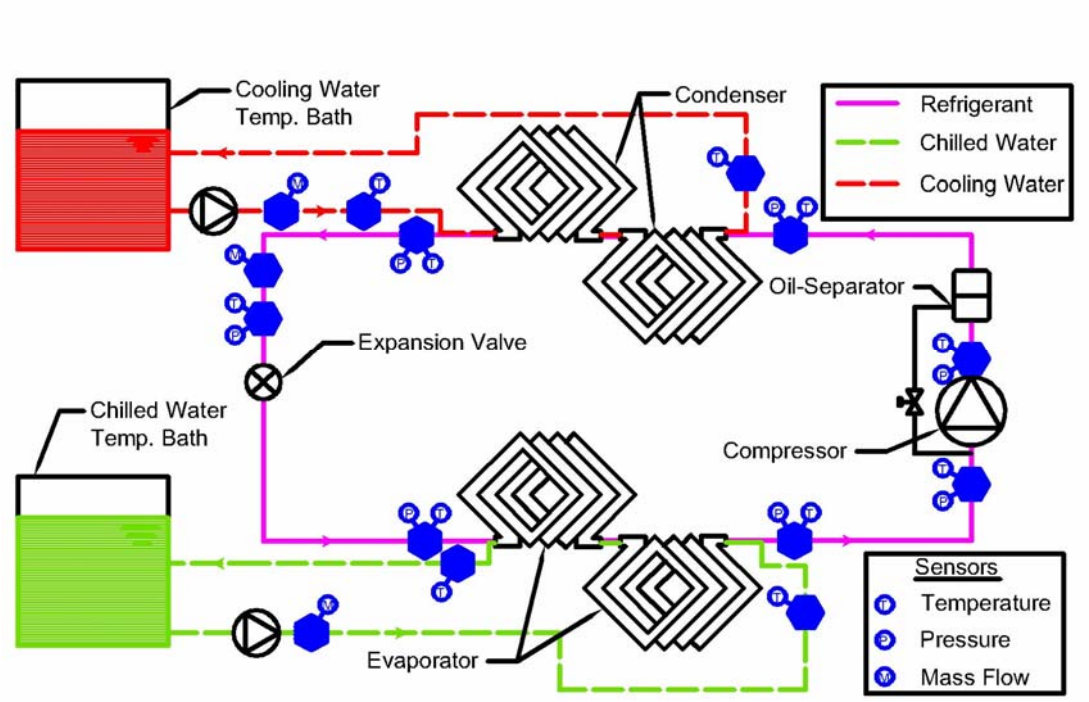

Figure 2.2-1 The schematic of the vapour compression chiller setup

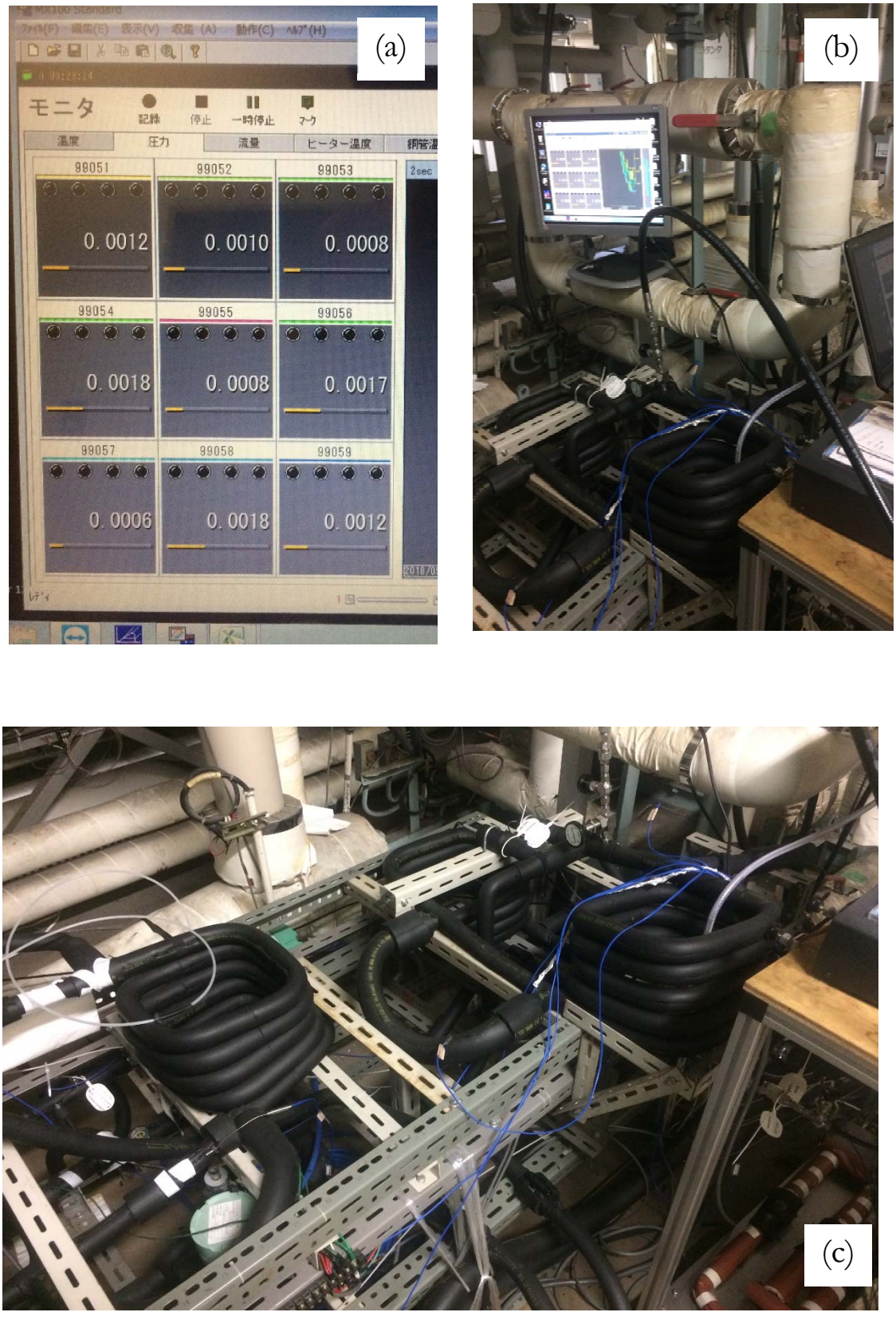

Figure 2.2-2 Images of the vapour compression chiller setup; (a) The data display platform; (b) the condenser coils; (c) the evaporator and condenser coils

2.2.2 Test Conditions

2.2.2.1 AHRI Standard 551/591 (SI)

The test conditions were adopted according to the Air Conditioning, Heating and Refrigeration Institute (AHRI) Standard 551/591 (SI) [59]. The chiller falls under Section 2.1.1 of the scope as being classified under possessing a water-cooled, air-cooled, or evaporative-cooled condenser. Under Table 1 of the AHRI standard (refer to Appendix for full version Figure A-1), which is presented here as a summarized version in Table 2.2-1 the necessary Standard Rating Conditions are provided. This chiller was analyzed for cooling mode, whilst the heat pump analysis for heating mode are not presented here. The standard requires that the Chilled Water inlet temperature be maintained at 12 °C, while a 5 °C difference between the evaporator inlet and outlet is maintained by controlling the outlet temperature to be 7 °C. The flow rate of the chilled water at standard rating conditions required to be 0.0478 L/s.kW. The condenser side cooling water also met specific requirements such as an inlet temperature of 30 °C, with again a 5 °C difference to maintain the outlet temperature at 35 °C. The water flow was adjustable to meet the rated capacity.

Table 2.2-1 The summarized AHRI Standard 551/591 testing conditions for a water cooled chiller

Operating Category	Evaporator Conditions			Tower (Water Conditions)		
All Cooling	Entering Temp. °C	Leaving Temp. °C	Flow Rate $Ls^{-1}kW^{-1}$	Entering Temp. °C	Leaving Temp. °C	Flow Rate $Ls^{-1}kW^{-1}$
	12.00	7.00	0.0478[1]	30.00	35.00	Note 2

1: Rated water flow is determined by the water temperatures at the rated capacity. Then normalized flow rate shown, per unit evaporator capacity, is for reference only at Standard Rating Conditions.
2: Rated water flow is determined by the water temperatures at the rated capacity and rated efficiency.

Part Load performance was also carried out, by varying the compressor frequency. The test conditions were satisfying Table 2 under Section 5.4.2 of the standard (Refer to Appendix Figure A-2).

2.2.3 Experimental Procedure

The heat pump system initially underwent a vacuum test, in which the refrigerant loop is vacuumed and the pressure is observed to ascertain whether there are any leaks. A high pressure test was also conducted, where pressurized Nitrogen is charged and the pressure behavior is measured. This allowed the verification that at higher pressures, the system still maintained a good pressure seal.

In order to begin the charging of a new refrigerant the system is once again vacuumed. With the expansion valve closed, the required refrigerant charge amount (starting from the least amount) is charged at the charging port located just in between the expansion valve and evaporator. Then, the water circuits are operated in order to vaporize the refrigerant. With this the expansion valve is slightly opened and the compressor is powered on at around 60 Hz in order to warm up for around 4 minutes. After this, the required set points for the temperatures and flow rates are used to begin the experiment. The pulse control for the expansion valve, is used to control the refrigerant flow to the desired amount. For each charge amount, the load is varied by controlling the flow rates of the chilled and cooling water as well as by using the inverter to control the input frequency of the compressor. By adjusting these parameters, the cooling capacity is varied between 1.0 kW and 1.6 kW, whilst the refrigerant charge amount is varied between 0.67 kg to 0.80 kg in order to determine an ideal refrigerant charge amount. The data such as pressure, temperature and flow rates are recorded using LabView software [150], then processed with the aid of Mathematica [151].

2.2.4 Uncertainty Analysis

2.2.4.1 Instrument Accuracy

The instrument accuracies are shown in Table 2.2-2 for the sensors used in the chiller setup.

Table 2.2-2 The instrument accuracies of the sensors used for the VC Chiller setup

Parameter	Type	Range	Accuracy
Temperature	T-type Thermocouple	-5°C - 70°C	±0.05°C
Pressure	Absolute Pressure Transducer (High)	~5MPa	±0.15 % Full Scale[(a)]
	Absolute Pressure Transducer (Low)	~2MPa	±0.2 % Full Scale[(a)]
Refrigerant Flow	Coriolis Flowmeter	22-220 kg/hr	±0.22 % of reading[(a)]
Water Flow	Coriolis Flowmeter	30-300 L/hr	±0.5 % of reading[(a)]
Compressor Power	Digital Power Meter	~	±0.1 W of reading
Note: (a) [142]			

2.2.4.2 Extended Uncertainty Calculation

The uncertainty or error analysis is conducted according 2 methods, firstly for single variable parameters such as the processed meter readings for T_{Exp} or P_{Exp}, the Type A and Type B uncertainties are used to find the Extended Uncertainty [152]. Type A uncertainties are calculated based on a statistical method, whilst Type B uncertainties fall into the other category which includes instrument error or even errors from calibrations.

For any parameter dependent on more than one variable, (such as the COP), a Taylor Series Method (TSM) is used for propagating the uncertainties of each variable to give a final overall uncertainty [152].

The calculations for the Extended uncertainty, $U_{\%}$ using Type A and Type B uncertainties, with a coverage factor $k_{\%}$ estimated from a t-distribution is shown below.

$$U_{\%} = k_{\%} u_c \qquad (2.2\text{-}1)$$

The uncertainty u_c is expressed as follows, as a function of Statistical Uncertainty Type A and Instrument Uncertainty Type B.

$$u_c^{\,2} = s_x^{\,2} + \sum_{k=1}^{N} b_k^{\,2} \qquad (2.2\text{-}2)$$

Statistical uncertainty is represented by s_x or the Sample Standard Deviation.

$$s_x = \sqrt{\frac{\sum_{i=1}^{N} (x_i - \bar{x})^2}{N-1}} \qquad (2.2\text{-}3)$$

$\bar{x}$ represents the Sample Mean

$$\bar{x} = \frac{\sum_{i=1}^{N} x_i}{N} \qquad (2.2\text{-}4)$$

For the Type B uncertainties, the instrument uncertainties or errors need to be known.

$$b_k = \frac{\%\ Error \times \mathrm{Re}ading}{t\%} \qquad (2.2\text{-}5)$$

$$b_k = \frac{Absolute\ Error}{t\%} \qquad (2.2\text{-}6)$$

For the multivariable parameter, the following TSM is used [152].

As an example, for a parameter r, which is a function of x and y,

$$r = f(x, y) \qquad (2.2\text{-}7)$$

The combined uncertainty u_c

$$u_c = \overbrace{\left(\frac{\partial r}{\partial x}\right)^2 b_x^{\,2} + \left(\frac{\partial r}{\partial y}\right)^2 b_y^{\,2}}^{\text{Systematic Error Correlation Effects}} + \overbrace{\left(\frac{\partial r}{\partial x}\right)^2 s_x^{\,2} + \left(\frac{\partial r}{\partial y}\right)^2 s_y^{\,2}}^{\text{Random Error Correlation Effect}} \qquad (2.2\text{-}8)$$

$$u_c = \left(\frac{\partial r}{\partial x}\right)^2 b_x{}^2 + \left(\frac{\partial r}{\partial x}\right)^2 s_x{}^2 + \left(\frac{\partial r}{\partial y}\right)^2 b_y{}^2 + \left(\frac{\partial r}{\partial y}\right)^2 s_y{}^2 \quad (2.2\text{-}9)$$

$$u_c = \left(\frac{\partial r}{\partial x}\right)^2 \left(b_x{}^2 + s_x{}^2\right) + \left(\frac{\partial r}{\partial y}\right)^2 \left(b_y{}^2 + s_y{}^2\right) \quad (2.2\text{-}10)$$

$$u_c = \left(\frac{\partial r}{\partial x}\right)^2 \left(u_x{}^2\right) + \left(\frac{\partial r}{\partial y}\right)^2 \left(u_y{}^2\right) \quad (2.2\text{-}11)$$

As it is simplified, the combined uncertainty, can be given in terms of the combined uncertainty of each individual variable (which can be calculated as shown before, based on the Statistical Error and Instrument Error) and the partial derivatives with respect to each variable.

After u_c is found, the Final Expanded Uncertainty is found using Equation 2.2-1.

2.2.5 R410a Refrigerant information

R410a is a near-azeotropic mixture of R32 and R125, which was developed by Honeywell [153]. It was introduced in the hopes of replacing R22, which a high ODP refrigerant in use before the early 2000s [153].

Table 2.2-3 The refrigerant properties of R410a compared with those of R32

Property	R410a	R32
GWP100	2088 [(c)]	675 [(c)]
ODP	0	0
Critical Temp	344.49K (71.34°C)[(a)]	351.26K (78.11°C) [(a)]
Critical Pressure	49011 kPa [(a)]	5782 kPa [(a)]
Normal Boiling Point	220.45 K (-52.7°C) [(b)]	221.5 K (-51.65°C) (a)
Latent Heat of Vaporization @ Boiling Point	256.68 kJ/kg [(b)]	381.86 kJ/kg [(a)]
Flammability	A1 Non-flammable [(b)]	A2 [(e)] Slightly Flammable [(c)] / 2L Mildly Flammable [(d)]
Note: (a) [154]; (b) [153]; (c) [155]; (d) [156]; (e) [157]		

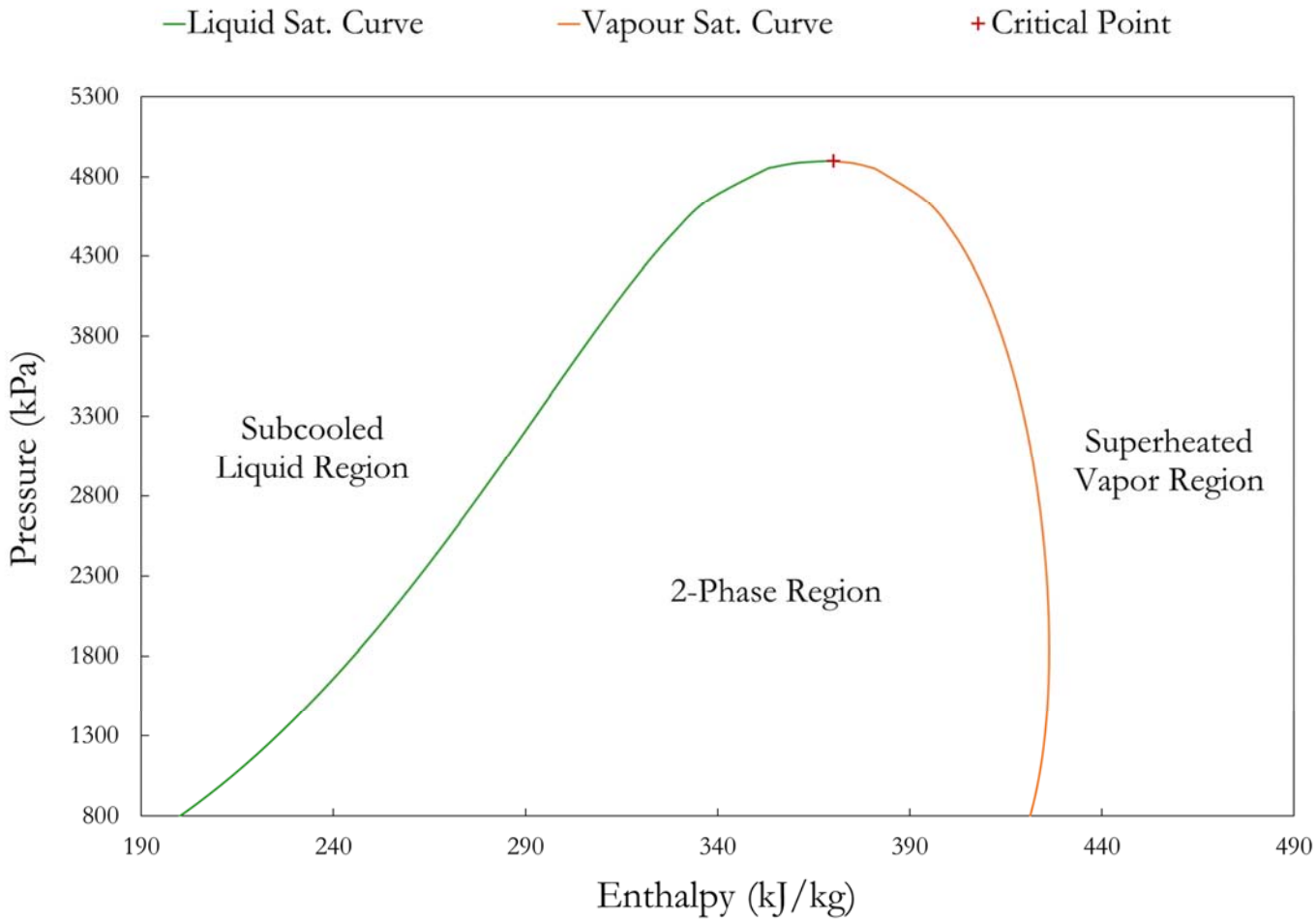

Figure 2.2-3 The Pressure – Enthalpy (p-h) diagram for R410a showing the 3 distinct phases and the critical point

2.2.6 Refrigerant Charging

2.2.6.1 Mass Based Calculation

The refrigerant sample preparation is similar to the one mentioned in Chapter 3 where a gravimetric approach is considered for mixtures which are prepared at the facility. Since larger masses of the mixtures are required, liquid nitrogen is not used for cooling the refrigerant and ice is utilized instead. An electric heater is used to vaporize the main supply refrigerant. In this case, since R410a is available from the industry, there is no mixing process tacking place, but direct charging into the system This is described below.

2.2.6.2 Charging Process

Once the required amount of mass is determined, the refrigerant bottle / tank is place on a weighing scale and the mass recorded (as shown in Figure 2.2-4). Next the scale is tared and the refrigerants is slowly charged into the chiller system using the connection point located in between the expansion valve and evaporator. Once the required mass figure is shown on the scale, the valve is closed. In this process, a minor amount of refrigerant will remain in the connection tube, but is ignored due to its small volume.

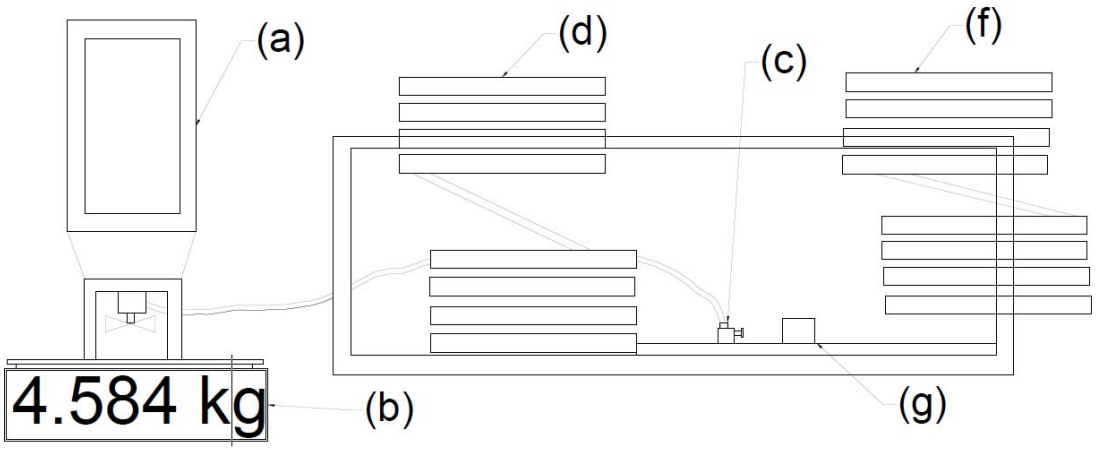

Figure 2.2-4 Mass charging process; (a) refrigerant tank; (b) scale; (c) charging port; (d) evaporator; (f) condenser; (g) expansion valve

2.2.7 Heat Leak Test

A heat leak test had been previously carried out. The correlation between temperature and heat leak amount for the two heat exchangers are presented as follows. These adjustments are included in the final tabulation values.

$$Q_{Evap,Loss} = \left[\left(\left(\dot{V}_{CH} \times C1\right) + C2\right) \times \left(\left(\frac{T_{CH,in} + T_{CH,out}}{2}\right) - T_{Room}\right)\right] + \left(\left(C3 \times \dot{V}_{CH}\right) + C4\right) \quad (2.2\text{-}12)$$

$$Q_{Cond,Loss} = \left[\left(\left(\dot{V}_{CW} \times D1\right) + D2\right) \times \left(\left(\frac{T_{CW,in} + T_{CW,out}}{2}\right) - T_{Room}\right)\right] + \left(\left(D3 \times \dot{V}_{CH}\right) + D4\right) \quad (2.2\text{-}13)$$

Table 2.2-4 The evaporator heat loss coefficients

Evaporator Loss Coefficients	
Coefficient	Value
C1	1.3674560E-06
C2	2.2640678E-03
C3	-6.0373438E-05
C4	4.2713616E-05

Table 2.2-5 The condenser heat loss coefficients

Condenser Loss Coefficients	
Coefficient	Value
D1	2.5094638E-06
D2	2.2729434E-03
D3	1.6276613E-05
D4	-1.9321645E-03

2.3 Data, Results and Discussion

2.3.1 Experimental Results

The experimental data are processed using Mathematica then presented in the following sections under each calculated parameter.

2.3.2 First Law Analysis

The cycle analysis is based on several assumptions which include the following;

- Steady state conditions
- Black-box model (where only the input and output at each specific subsystem is considered)
- Closed system with respect to the refrigerant circuit, however each subsystem which is defined as a component (i.e. Evaporator, Compressor, etc.) is considered as an open system or control volume where either refrigerant and water flow and heat exchange exists

For each component, which can be considered as a control volume, the mass and energy balance is given below.

$$\sum_i \dot{m}_i - \sum_e \dot{m}_e = 0 \qquad (2.3\text{-}1)$$

$$\sum_i \dot{m}_i h_i - \sum_e \dot{m}_e h_e + \dot{Q}_{Net} + \dot{W}_{Net} = 0 \qquad (2.3\text{-}2)$$

The kinetic and potential energies are neglected in this case. At all conditions, steady state is assumed.

To begin the cycle analysis, the energy balance (EB) of the chiller is calculated.

$$EB = \frac{q_{Evap} + w_{Comp} - q_{Cond}}{q_{Cond}} \quad (2.3\text{-}3)$$

The EB for each experiment is shown in Table 2.3-1 where the values are all below 0.038, which signifies the calculations and measurements are at stable conditions and can be considered as accurate according to previous research by Kyaw Thu et. al. [158].

Table 2.3-1 The energy balance for all refrigerant charge amounts at all cooling capacities

Charged Mass (kg)	Cooling Capacity (kW)	Energy Balance (-)
0.67	1.20	0.028
	1.40	0.025
	1.60	0.017
0.70	1.00	0.034
	1.20	0.025
	1.40	0.018
	1.60	0.017
0.73	1.00	0.037
	1.20	0.026
	1.40	0.018
	1.60	0.015
0.75	1.00	0.035
	1.20	0.024
	1.40	0.016
	1.60	0.014
0.77	1.00	0.038
	1.20	0.027
	1.40	0.024
	1.60	0.029
0.80	1.00	0.036
	1.20	0.025
	1.40	0.018
	1.60	0.014

2.3.2.1 Pressure – Enthalpy Diagram

Another fundamental tool for cycle analysis involves the Pressure – Enthalpy diagram or chart (P-h diagram / chart) (Figure 2.3-1). The refrigeration cycle is represented by the orange line with 7 points highlighting the 7 key points in the cycle.

Figure 2.3-2 shows the p-h chart for the fixed refrigerant amount of 0.70 kg, with varied cooling loads from 1.0 kW to 1.6 kW.

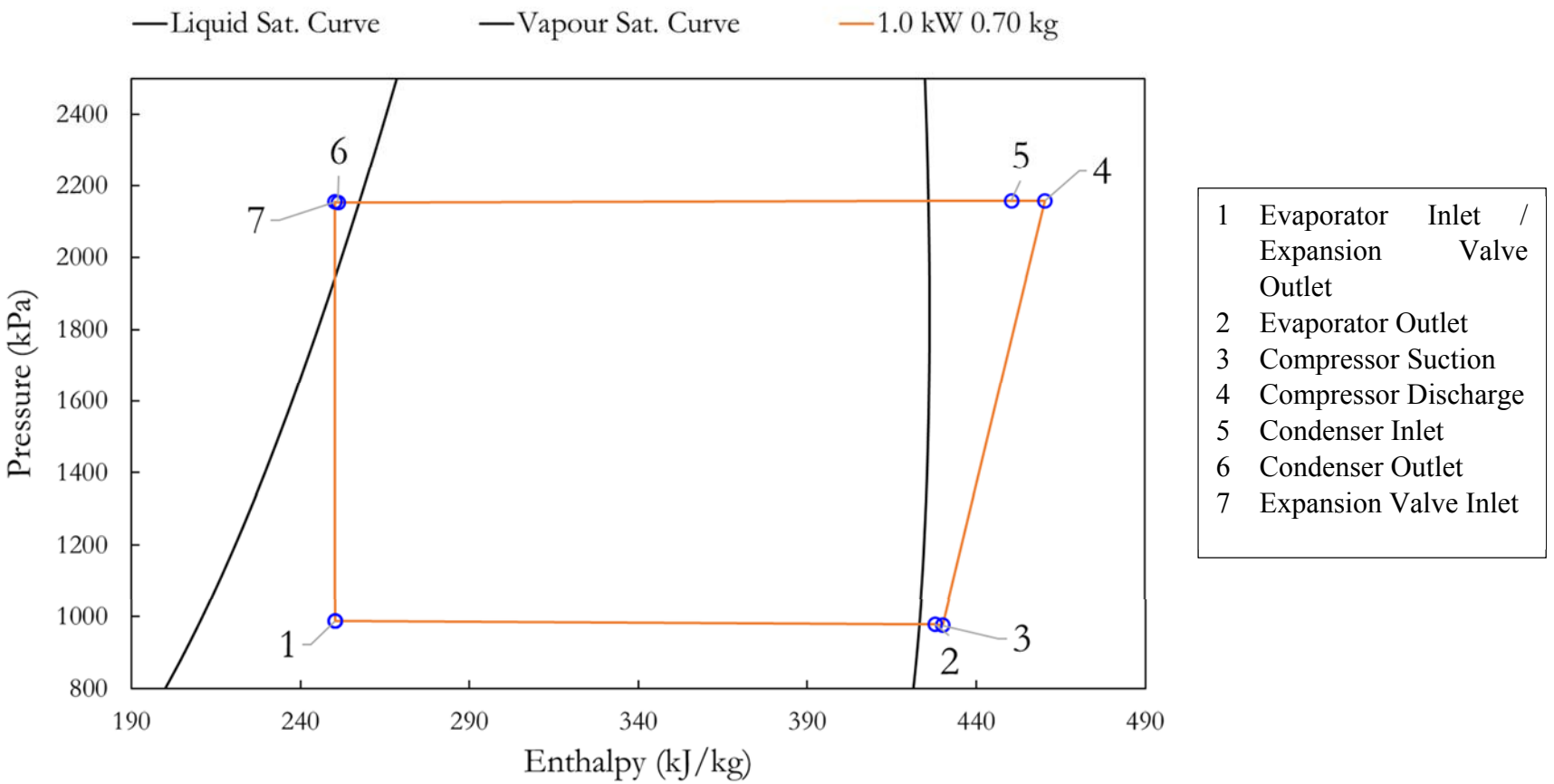

Figure 2.3-1 The Pressure – Enthalpy (p-h) diagram for the VC Compression cycle with 7 measurement points labelled

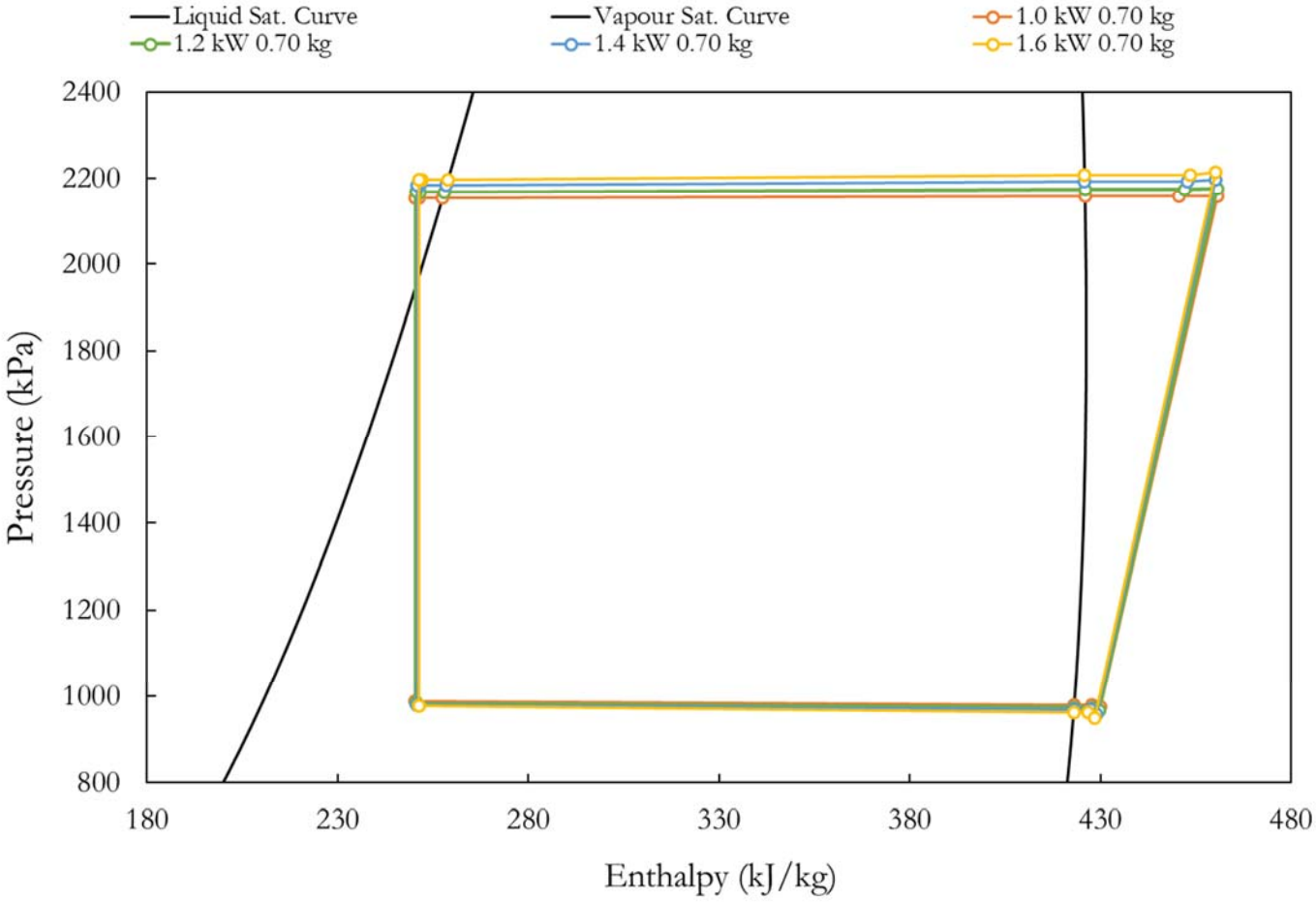

Figure 2.3-2 The p-h diagram for the VC Cycle at 0.70 kg of refrigerant charge with cooling capacities varied from 1.0 – 1.6 kW

2.3.2.2 Cooling Capacity Calculations and Compressor Power

The cooling effect or heat transfer at the evaporator (Q_{Evap})is calculated based on the chilled water temperature, flow rater and properties as specified under AHRI Standards [59].

$$Q_{Evap} = \dot{V}_{CH} \times \rho_{CH} \times c_p \times (T_{CH,in} - T_{CH,out}) - Q_{EvapLoss} \quad (2.3\text{-}4)$$

The heat rejection at the condenser is given as Q_{Cond},

$$Q_{Cond} = \dot{V}_{CW} \times \rho_{CW} \times c_p \times (T_{CW,out} - T_{CW,in}) + Q_{CondLoss} \quad (2.3\text{-}5)$$

Under Section 7.2 of the AHRI Standard [59], the method for calculating the water side properties is mentioned. Using these guidelines, the Density (ρ) and Specific Heat Capacity (c_p) for the Chilled and Cooling Water are calculated as follows.

The calculation requires a polynomial equation, which is dependent on Temperature. The table of constant are given herewith,

Table 2.3-2 The density constants $\rho_4 - \rho_0$ utilized for calculating the secondary fluid water densities, based on the AHRI Standard Recommendations

ρ Constants	SI (kg/m^3)
ρ_4	$-1.2556 \cdot 10^{-7}$
ρ_3	$4.0229 \cdot 10^{-5}$
ρ_2	$-7.3948 \cdot 10^{-3}$
ρ_1	$4.6734 \cdot 10^{-2}$
ρ_0	1000.2

$$\rho = (\rho_4 \times T^4) + (\rho_3 \times T^3) + (\rho_2 \times T^2) + (\rho_1 \times T) + \rho_0 \quad (2.3\text{-}6)$$

Table 2.3-3 The specific heat capacity constants C_{p5} – C_{p0} utilized for calculating the secondary fluid water specific heat capacities, based on the AHRI Standard Recommendations

C_p constants	SI (kJ/kg.K)
c_{p5}	$-3.2220 \cdot 10^{-11}$
c_{p4}	$1.0770 \cdot 10^{-8}$
c_{p3}	$-1.3901 \cdot 10^{-6}$
c_{p2}	$9.4433 \cdot 10^{-5}$
c_{p1}	$-3.1103 \cdot 10^{-3}$
c_{p0}	4.2160

$$c_p = \left(c_{p5} \times T^4\right) + \left(c_{p4} \times T^4\right) + \left(c_{p3} \times T^3\right) + \left(c_{p2} \times T^2\right) + \left(c_{p1} \times T^1\right) + c_{p0} \quad (2.3\text{-}7)$$

c_p is calculated at the average temperature (T_{avg}) between the water inlet and outlet, whilst ρ is based on the inlet temperature.

$$T_{avg} = \frac{T_{in} + T_{out}}{2} \quad (2.3\text{-}8)$$

The compressor power was measured using a digital power meter, which includes the total power consumption including its performance efficiency.

$$W_{Comp} = P_{Comp} \quad (2.3\text{-}9)$$

According to AHRI Standard [59], the equation for the *COP* or COP_R (referring to the refrigeration/cooling process) is described in the section below.

2.3.3 Coefficient of Performance

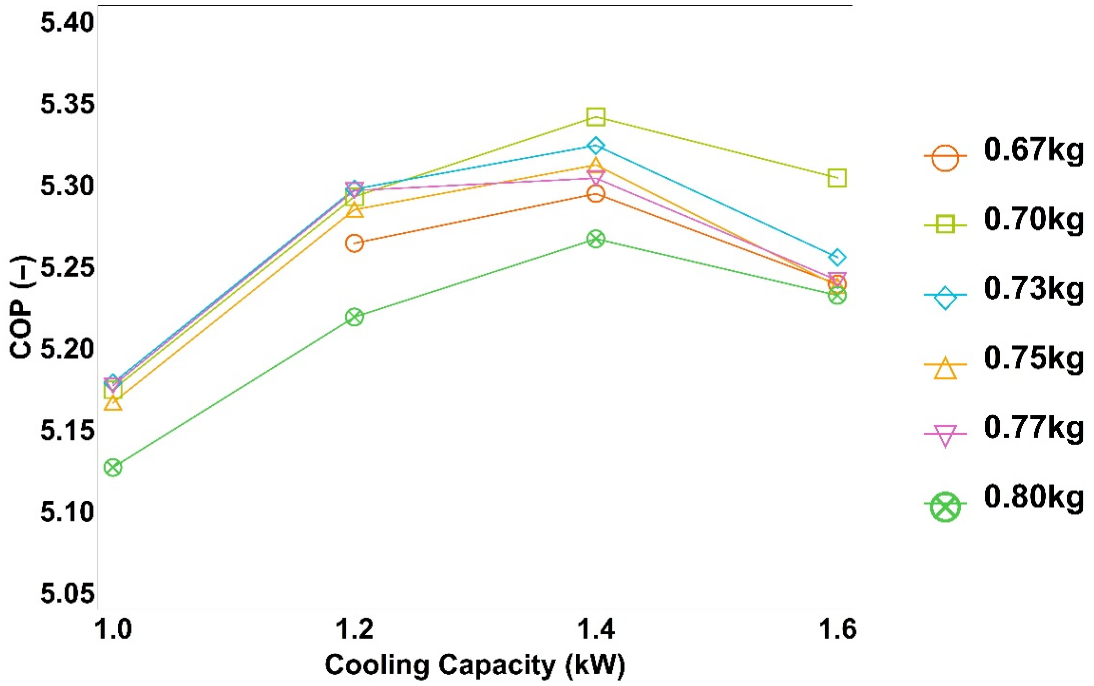

Figure 2.3-3 The Coefficient of Performance (COP) for varied charge amounts between 0.67 – 0.80 kg versus the cooling capacities between 1.0 – 1.6 kW

The first and most common indicator used for testing performance is the Coefficient of Performance (COP) of the refrigeration cycle.

$$COP = \frac{Q_{Evap}}{W_{Compressor}} = \frac{V_{CH}\rho_{CH}c_{P,CH}\Delta T_{Evap}}{P_{input,Compressor}} \qquad (2.3\text{-}10)$$

The cooling effect or heat transfer at the evaporator is calculated based on the chilled water temperature, flow rate and properties as specified under AHRI Standards [59].

The specific heat capacity of water is calculated based on the average value between the inlet and outlet chilled water temperatures.

$$T_{CH,avg} = \frac{T_{CH,in} + T_{CH,out}}{2} \qquad (2.3\text{-}11)$$

The mass flow rate of the chilled water is also based on Equation 2.3-12 which converts the volume flow rate read from the flow meter to mass flow rate, based on the density of the water at the inlet temperature.

$$V_{CH} = \frac{m_{CH}}{\rho_{CH}} \qquad (2.3\text{-}12)$$

As presented in Figure 2.3-3, the COP for different charge amounts all show a similar trend, where a peak occurs at 1.4 kW cooling capacity. The COP at cooling capacities both lower than 1.4 kW and higher than 1.4 kW, all present lower values in comparison. There are several possible conclusions regarding the optimum cooling capacity and the optimum mass charge derived from this peak like behavior of COP.

Table 2.3-4 The COP with calculated Extended Uncertainties for all refrigerant charge amounts and cooling capacities

Charged Mass (kg)	Cooling Capacity (kW)	COP (-)	± Error (-)	Perc. Error (%)
0.67	1.2	5.264	0.059	1.04
	1.4	5.295	0.059	1.06
	1.6	5.239	0.059	1.09
0.7	1.0	5.175	0.058	1.00
	1.2	5.293	0.060	1.04
	1.4	5.342	0.060	1.06
	1.6	5.304	0.059	1.07
0.73	1.0	5.179	0.058	1.00
	1.2	5.297	0.059	1.03
	1.4	5.324	0.060	1.06
	1.6	5.256	0.059	1.07
0.75	1.0	5.167	0.058	1.00
	1.2	5.285	0.059	1.03
	1.4	5.312	0.060	1.06
	1.6	5.238	0.059	1.07
0.77	1.0	5.177	0.058	1.00
	1.2	5.297	0.059	1.04
	1.4	5.304	0.060	1.06
	1.6	5.242	0.059	1.06
0.8	1.0	5.127	0.057	0.99
	1.2	5.219	0.059	1.02
	1.4	5.267	0.059	1.05
	1.6	5.232	0.059	1.07

2.3.3.1 Optimum Cooling Capacity

Firstly, it seems that the optimum performance of the Chiller for AHRI conditions occurs at 1.4 kW of cooling. Any part-load performance at lower cooling capacities, or at higher full load cooling capacities, the performance in terms of the COP will reduce. This could suggest the chiller should be utilized for a larger proportion of the daily load, at 1.4kW cooling capacity to provide the best overall performance.

2.3.3.2 Optimum Refrigerant Charge Amount

The highest COP is exhibited at 0.70 kg of refrigerant charge, which can be said to be the optimum refrigerant charge amount for AHRI conditions considering that 1.4 kW is the optimum capacity of the chiller. Even though, at lower cooling capacities, the charged amounts of 0.73, 0.75 and 0.77 kg, show similar performance, at an increased capacity level of 1.6 kW, the decrease in COP for 0.77 kg, is quite low in comparison to the other masses. Thus the optimum charge amount can be determined to be 0.77 kg since, irrespective of the cooling capacities, it exhibits the best performance.

2.3.3.3 COP Behavior Analysis

Looking into further details as to why the COP exhibits a peak, the capacities from 1.0 - 1.4 kW are analyzed as one section, then in the second section the COP trend for 1.4 – 1.6 kW is analyzed.

The COP is a function of the heat absorbed from the chilled water within the evaporator and the amount of power consumed by the compressor. From 1.0 kW - 1.4 kW, the increase in cooling capacity is achieved via an increase in both the Refrigerant Mass flow (controlled via the Expansion Valve), as well as an increase in Chilled Water Flow rate. This allows the heat exchanger to handle the extra load, since the heat transfer rate depends on the flow rate of the thermofluids.

However, at one point the further increase in flow rates will possibly not improve the heat transfer rate, due to the limitation in heat exchanger contact area. This could be a possible reason for the reduction in COP for section 2 from 1.4 – 1.6 kW. This is further justified

since the flow rates of the refrigerant and chilled water have similar values for a fixed capacity, across all charge amounts. Hence, the increase in flow rates, above the threshold value, which happens to be at the 1.4 kW cooling capacity, is met with limited heat exchanger capacity or surface area. It is also seen that the increased heat load which must be rejected at the condenser result in the larger lift across the compressor. This will increase the enthalpy change between the discharge and suction at the compressor, which also results in the increased pressure at the condenser. The larger load on the compressor, will also result in the reductions of COP.

2.3.3.4 COP Behavior at Optimum Charge

Since the optimum cooling capacity has been chosen as 1.4 kW, the behavior of the COP with respect the charged mass amount is further studied, using Figure 2.3-4.

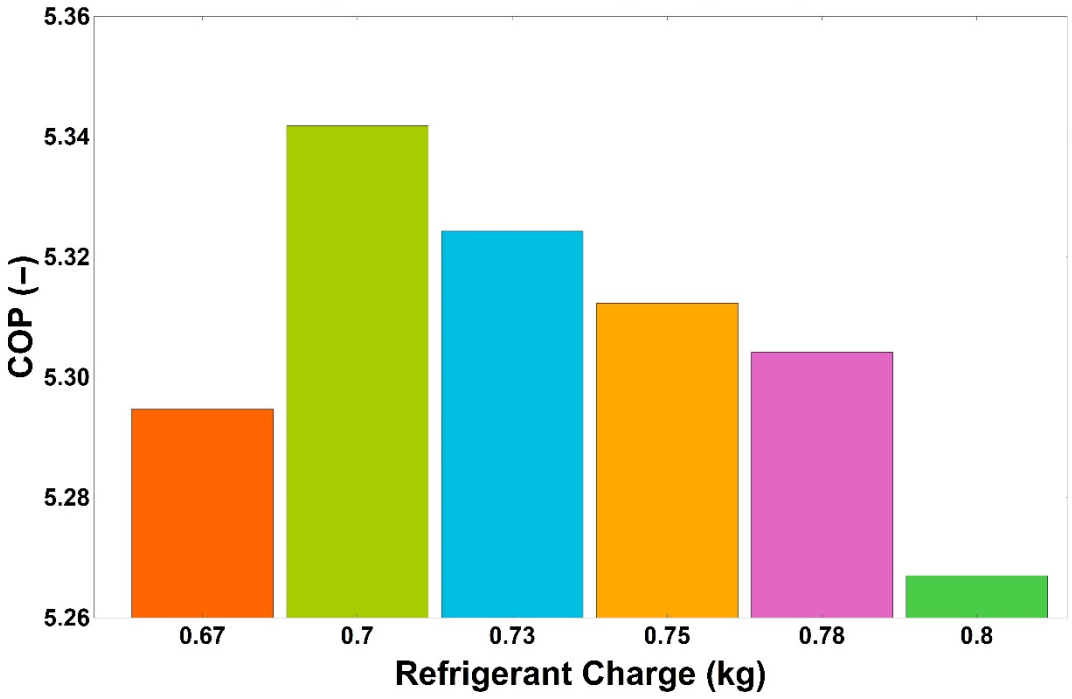

Figure 2.3-4 The variations of COP with refrigerant charge amount for the optimum cooling capacity of 1.4 kW

Beginning from the lowest charge amount 0.67 kg, as the charged amount is increased by 0.03 kg, a massive increase in COP is visible. The highest COP is exhibited by 0.70 kg of refrigerant charge for this particular chiller. Following this increase, any further addition of refrigerant results in the decrease of COP as seen in Figure 2.3-4. The possible reasons for this shall be separated into two parts; the increase in COP due to an increase in refrigerant charge up to 0.70 kg; the reduction of COP with increasing refrigerant charge up to 0.80 kg.

2.3.3.5 COP increase at 1.4 kW with increased charge amounts 0.67 – 0.70 kg

The initial increase in COP with the addition of 0.03 kg, to a total of 0.70 kg within the refrigerant circuit, suggests that the system is under charged when at 0.63 kg. Hence, when there is sufficient refrigerant to flow through the circuit, the performance of each individual component is increased. Firstly, in the heat exchangers there could be better heat transfer due to the readily available refrigerant amount. The subcool at the condenser outlet is the lowest at 0.67 kg and increases with the charge amount, possibly signifying the inadequate amount of refrigerant present within the system at low charge.

The evaporator temperature also slightly drops, when the refrigerant charge is increased, which could suggest that at low charge there is insufficient refrigerant within the evaporator tubes.

The compressor also seems to behave better with 0.70 kg charge amount, whilst at 0.67 kg. Possibly the amount of refrigerant vapor available for compression is not adequate enough, hence a larger power consumption occurs. The power consumption is the largest at 0.67 kg. This is main contributor to the reduced COP.

2.3.3.6 COP decrease at 1.4 kW with increased charge amounts 0.70 – 0.80 kg

Focusing on section 2 of Figure 2.3-4 any further increase in refrigerant mass above 0.70 kg, decreases the performance. Large charge amounts will result in the additional mass of refrigerant accumulating at the end of the condenser, where it liquefies. This phenomenon will cause larger subcooling as well, which is visible in Figure 2.3-5. The mass flow rate is also now controlled with the expansion valve, in order to maintain the same cooling capacity. The larger subcooling, coupled with the lower mass flow rates (see Figure 2.3-5) will result in the flooding of the condenser towards the end and also increase the condenser pressure. This would potentially result in a reduced effective capacity of the condenser, together with the increased load on the compressor to provide a larger temperature lift. This predicted increase in condenser pressure was also observed, giving a justifiable reason for the lower COP at larger charge amounts. A possible method to overcome this problem could be with the use of a liquid receiver, which allows the accumulation of extra liquid, and the distribution of this liquid, if larger loads occur.

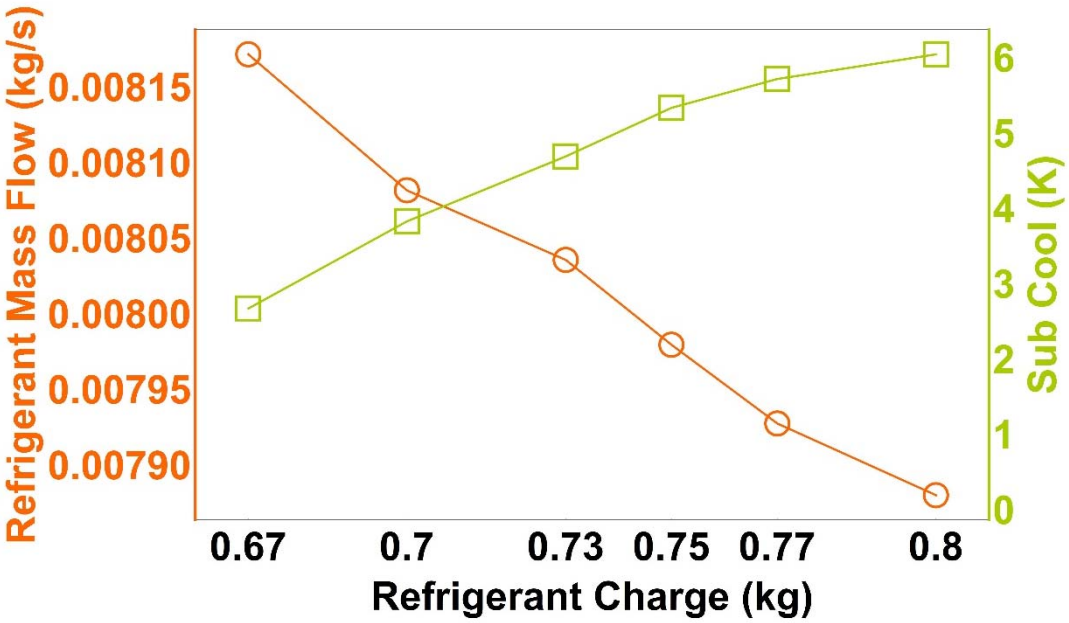

Figure 2.3-5 The variations of refrigerant mass flow and the condenser sub cool versus refrigerant charge amount at the optimum cooling capacity of 1.4kW

2.3.4 Second Law Analysis

This section will introduce the concepts of Exergy Destruction and will also present the Exergetic Efficiency of the chiller. The first law analysis section is based on the conservation of energy principle. The COP measures how much work input into the chiller through the compressor is required to provide the necessary cooling. The second law deals with the amount of work potential which is lost during this process. It introduced the concept of exergy, which is the work potential. In the case of reversible process, the work potential can be fully utilized, whilst in real life this is not the case. It is known that no process is ideally reversible, and hence there is the loss of some work potential, which is known as exergy destruction. Using the exergy destruction, it is then possible to calculate the exergetic or second law efficiency which will compare the operation of the chiller, to that of an ideal system. This content is presented below.

2.3.5 Exergy Destruction

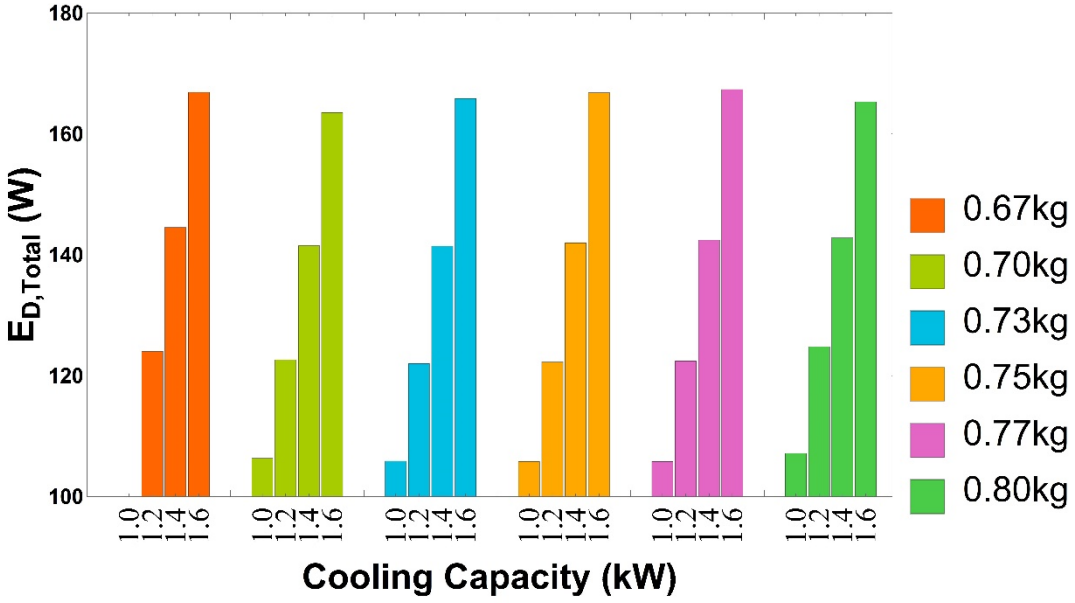

Figure 2.3-6 The total exergy destruction versus cooling capacity, for all refrigerant charge amounts

For the second law analysis, the exergy destruction is explored (shown in Figure 2.3-6 is the Total Exergy Destruction $E_{D,Total}$). The dead state exergy is defined with respect to the dead state conditions of T_0 = 298.15K and P_0 = 101.35 kPa. The amount of potential work

which is destroyed is represented in terms of each component of the refrigeration cycle. The following equations are hence utilized;

The General exergy balance for a control volume equation,

$$(X_2 - X_1)_{cv} = X_{heat} - X_{work} + X_{mass,in} - X_{mass,out} - X_{destroyed} \qquad (2.3\text{-}13)$$

$$\overbrace{E_{cv}}^{\text{Exergy change}} = \overbrace{\sum_{j=1}^{n}\left(1-\frac{T_0}{T_j}\right)Q_j + \left(W_{cv} + p_0\Delta V_{cv}\right) + \sum_i m_i e_{fi} - \sum_o m_o e_{fo}}^{\text{Exergy transfer}} - \overbrace{E_D}^{\text{Exergy destruction}} \qquad (2.3\text{-}14)$$

And in rate form,

$$\overbrace{\frac{dE_{cv}}{dt}}^{\text{Rate of exergy change}} = \overbrace{\sum_{j=1}^{n}\left(1-\frac{T_0}{T_j}\right)\dot{Q}_j + \left(\dot{W}_{cv} + p_0\frac{dV_{cv}}{dt}\right) + \sum_i \dot{m}_i e_{fi} - \sum_o \dot{m}_o e_{fo}}^{\text{Rate of exergy transfer}} - \overbrace{\dot{E}_D}^{\text{Rate of exergy destr}} \qquad (2.3\text{-}15)$$

The flow exergy e_f is given below (neglecting kinetic and potential energy effects),

$$e_f = (h_i - h_0) - T_0(s_i - s_0) \qquad (2.3\text{-}16)$$

For each individual component, the exergy balance equation is also given herewith in rate form, but can be used without the rate form as well,

Compressor exergy destruction,

$$\dot{E}_{D,Comp} = P_{Comp} + \dot{m}_{ref} \times (e_{f4} - e_{f3}) \qquad (2.3\text{-}17)$$

The heat exchanger exergy destructions,

$$\dot{E}_{D,Cond} = \dot{m}_{ref} \times (e_{f4} - e_{f6}) + \dot{m}_{CW} \times (e_{fCW,In} - e_{fCW,out}) \qquad (2.3\text{-}18)$$

$$\dot{E}_{D,Evap} = \dot{m}_{ref} \times (e_{f3} - e_{f1}) + \dot{m}_{CH} \times (e_{fCH,In} - e_{fCH,out}) \qquad (2.3\text{-}19)$$

The expansion device exergy destruction,

$$\dot{E}_{D,Exp} = \dot{m}_{ref} \times (e_{f6} - e_{f1}) \qquad (2.3\text{-}20)$$

The analysis for the exergy destruction in component form is presented in Figure 2.3-7 below for the mases of 0.67 kg, 0.70 kg and 0.80 kg, since they are the smallest, optimum and largest charge amounts. In general, based on Figure 2.3-8 it can be seen that the compressor shows the largest exergy destruction, whilst the heat exchangers come in second and the expansion valve has the least amount of $\dot{E}_D$. To provide a more in-depth analysis, the exergy destruction ($\dot{E}_D$) will be separated into 2 sections; firstly, the changes in $\dot{E}_D$ for the optimum charge of 0.70 kg, with varied cooling loads will be analyzed; secondly the change in $\dot{E}_D$ with respect to the refrigerant charge amount, at a fixed cooling capacity of 1.4 kW is presented.

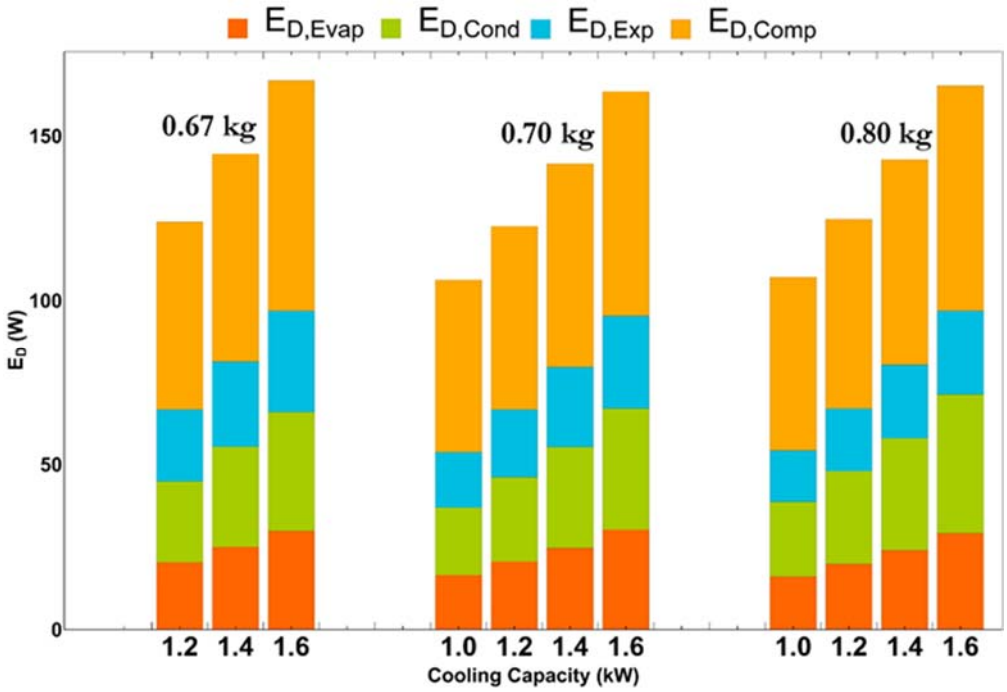

Figure 2.3-7 The exergy destruction versus cooling capacity for the 3 refrigerant charge amounts of 0.67, 0.70 and 0.80 kg

2.3.5.1 $\dot{E}_D$ at 0.70 kg and 1.0 – 1.6 kW

At a constant charge of 0.70 kg, the total $\dot{E}_D$ itself will increase as the cooling capacity is increased from 1.0 kW to 1.6 kW (as seen in Figure 2.3-7). Shown in Figure 2.3-8 as pie charts, the individual component exergy destruction also follows a similar trend and increases as the cooling load is raised.

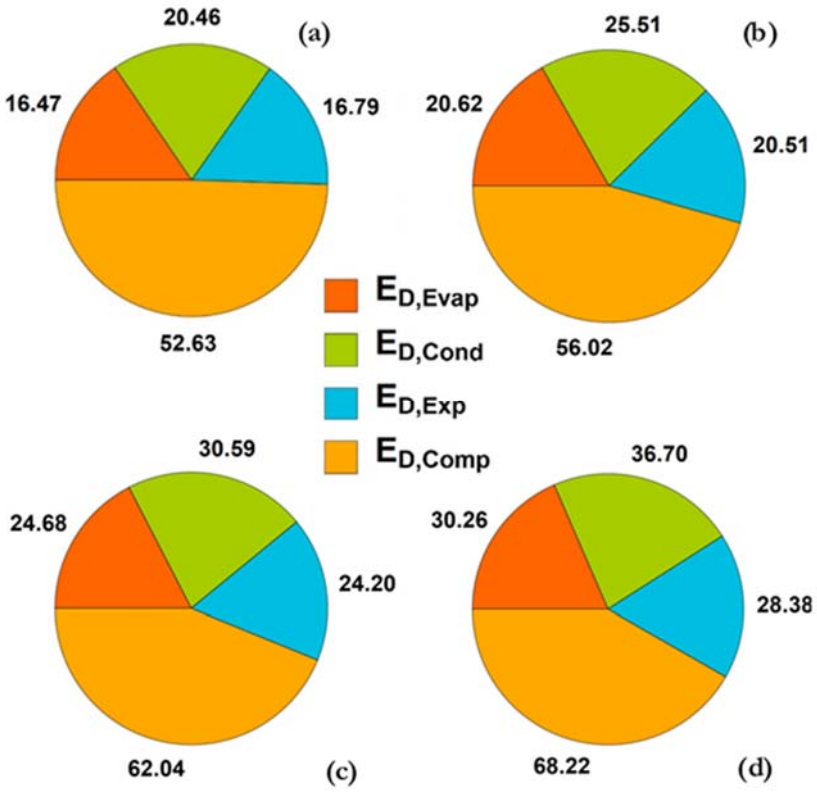

Figure 2.3-8 The component exergy destruction (W) at the optimum charge amount of 0.70 kg for the varied cooling capacities; (a) 1.0 kW; (b) 1.2 kW; (c) 1.4 kW; (d) 1.6 kW

The compressor $\dot{E}_{D,Comp}$ occupies the largest $\dot{E}_D$ at any capacity as mentioned before and is also increasing with the capacity. There are several possibilities for this behavior. Firstly, as the cooling capacity is increased, the pressure lift across the compressor was also increased, due to both an increasing condenser pressure and slight reduction in evaporator pressure (shown in Figure 2.3-2). This increased pressure lift results in a larger requirement of compressor work, which essentially contributes largely to the $\dot{E}_{D,Comp}$.

Another aspect which requires some attention is the possibility of friction losses, however, by examining the viscosity and dynamic viscosity shown below (Figure 2.3-9), it was noticed that since the suction temperature was slightly dropping, the resistance to flow would be less within the compressor. Thus the frictional losses would contribute less, when the cooling capacity is increased. However, if the increase in mass flow rates were sufficient enough, the overall frictional losses could have still contributed to the increasing $\dot{E}_{D,Comp}$.

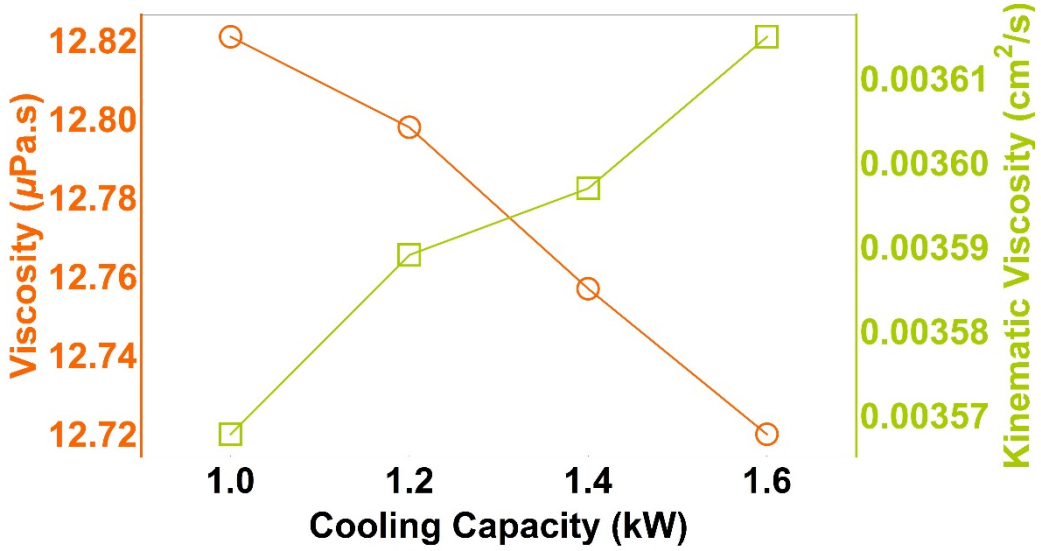

Figure 2.3-9 The viscosity and kinematic viscosity versus the cooling capacity at the optimum charge amount of 0.70 kg

The second largest $\dot{E}_D$ was exhibited by the condenser, $\dot{E}_{D,Cond}$. With increase the cooling capacity of the system for a fixed charge, the condenser has to reject a larger heat load. Hence, this will result in and increased $\dot{E}_{D,Cond}$. Also since the mass flow rate of refrigerant $\dot{m}_{ref}$ is increased, coupled together with the possible liquid accumulation at the end, could result in larger entropy generation, contributing to the increased $\dot{E}_{D,Cond}$.

The evaporator $\dot{E}_{D,Evap}$ on the other hand shows a smaller contribution to the total exergy destroyed in comparison to the condenser. However, as the cooling capacity is increased, the exergy destroyed also increases. The flow rate of refrigerant will similarly affect the evaporator as it did the condenser, whilst the increased heat gain, is also contributing to the exergy destroyed.

A comparison of the two heat exchangers also reveals how the condenser would naturally create larger exergy destruction due to larger enthalpy change of the refrigerant which needs to remove a total amount of heat equal to that of the sum of the power input of the compressor, and the heat gain of the evaporator.

$$\dot{Q}_{Cond} = \dot{Q}_{Evap} + \dot{W}_{Comp} \qquad (2.3\text{-}21)$$

The expansion device, shows the least exergy destruction. The expansion process is considered to be an isenthalpic process, where the contributor to the exergy destruction is the change in entropy. Since the pressure difference between the inlet and outlet conditions of the expansion valve are increased with larger cooling loads, there could be larger expansion loses as the subcooled liquid suddenly expands into the 2-phase state. Coupled together with the increase in $\dot{m}_{\text{ref}}$, the increasing $\dot{E}_{\text{D,Exp}}$ is also expected.

2.3.5.2 $\dot{E}_D$ at 1.4 kW and 0.67, 0.70 & 0.80 kg

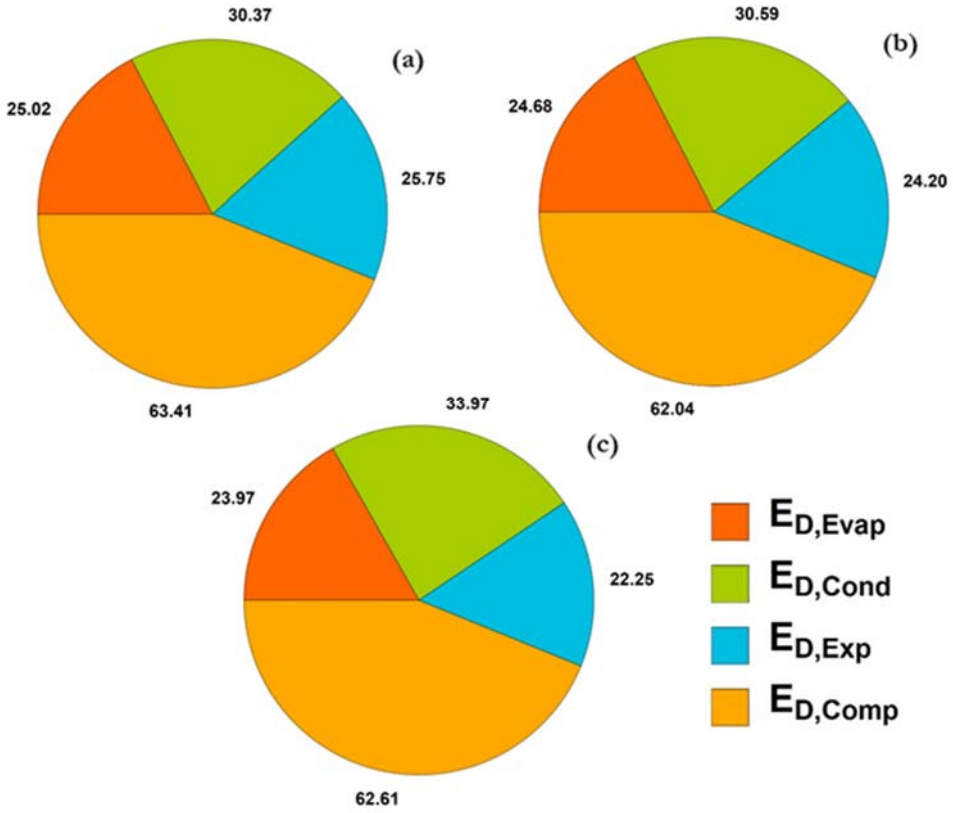

Figure 2.3-10 The component exergy destruction at the optimum cooling capacity of 1.4kw for the varied charge amounts of (a) 0.67 kg; (b) 0.70 kg; (c) 0.80 kg

Now considering, the scenario, where the optimum capacity to is 1.4 kW, the $\dot{E}_D$ with changing charge amount is also analyzed. Though the compressor $\dot{E}_{D,Comp}$ occupies the largest $\dot{E}_D$ and is followed by the heat exchangers $\dot{E}_{D,Cond}$, $\dot{E}_{D,Evap}$ and finally the expansion valve $\dot{E}_{D,Exp}$, the changes in the $\dot{E}_D$ do not seem to follow the same trend as the previous section.

The expansion valve seems to show less exergy destruction with increasing charge amount, possibly due to the reduced refrigerant mass flow rates $\dot{m}_{ref}$, which are controlled in order to maintain the cooling capacity at 1.4kW. The lower $\dot{m}_{ref}$ would result in lower expansion loses occurring at the expansion orifice.

From the heat exchangers, the evaporator shows a reducing $\dot{E}_{D,Evap}$, whilst the condenser shows an increasing $\dot{E}_{D,Cond}$. The possible reasons for this behavior could be the increasing inlet pressures with charge amount within the condenser, leading to larger entropy changes between the inlet and outlet conditions. Again there is a high chance of refrigerant accumulation at the exit, which also is signified through the increased subcooling at larger refrigerant charge amounts, which suggest a larger enthalpy change occurring at the condenser, which directly relates to a larger $\dot{E}_{D,Cond}$.

The evaporator, on the other hand shows a decreasing $\dot{E}_{D,Evap}$ trend, which could be caused by the slight decrease in T_{Evap} at larger charge amounts, which would aid in reducing the entropy related losses within the tubes. Also, with the $\dot{m}_{ref}$ control as well the reductions in chilled water flow rates V_{CH} in order to maintain an almost constant cooling load, the frictional losses will possible reduce, leading to the reductions in $\dot{E}_{D,Evap}$.

The compressor however, does not seem to exhibit a particular trend. This could be possibly due to both the reducing $\dot{m}_{ref}$ coupled with the increasing pressure lift which counteract each other.

2.3.6 Exergy Efficiency, η_{Ex}

$$\eta_{Ex} = -\frac{Q_{Evap}\left(1-\frac{T_0}{T_{Evap}}\right)}{\eta_{Elec}\times W_{Comp}} = COP\left(\frac{T_0}{T_{Evap}}-1\right) \qquad (2.3\text{-}22)$$

The exergetic efficiency is used to compare the performance of the chiller, with that of the ideal case. The equation for η_{Ex} is shown in Equation (2.3-22)

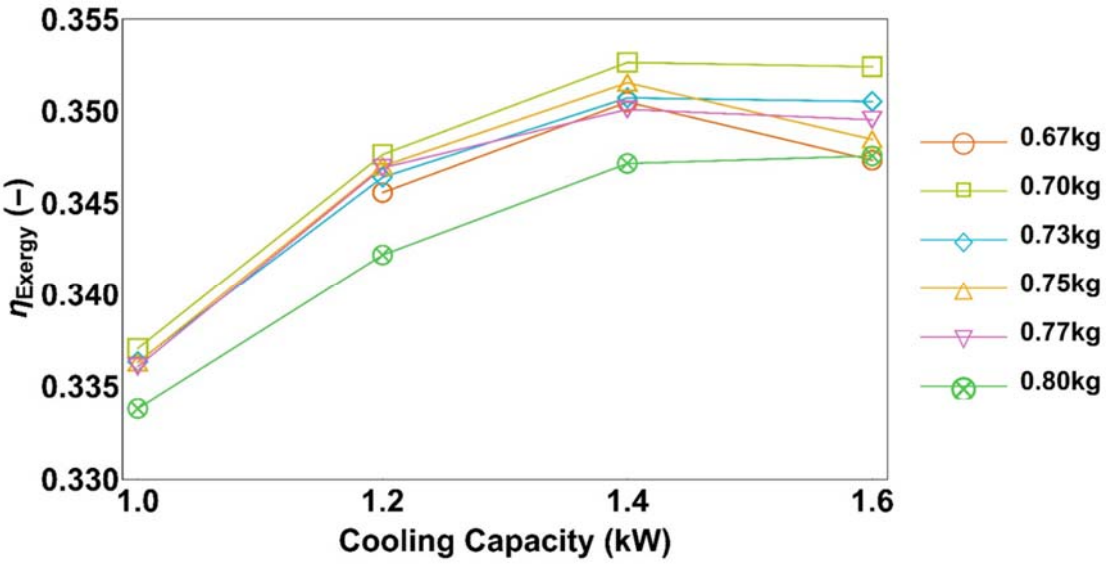

Figure 2.3-11 The exergetic efficiency versus cooling capacity for all refrigerant charge amounts from 0.67 – 0.80 kg

At an initial glance, the exergy efficiency (shown in Figure 2.3-11) shows a similar trend to that of the COP, where the exergetic efficiency seems to peak at 1.4 kW for all refrigerant charge amounts. The exergetic efficiency is dependent on the Evaporator Temperature T_{Evap} as well as the COP. Both these parameters seem to show a somewhat opposite trend, where the T_{Evap} will constantly drop with increasing cooling capacity, whilst the COP will increase till it reaches a peak, then drops (Shown in Figure 2.3-12)

2.3.6.1 Exergy Efficiency η_{Ex} at 0.67kg, 0.70 kg and 0.80 kg with 1.0 – 1.4 kW

For the fixed charge amounts, when increasing the cooling capacity from 1.0 kW to 1.4 kW, T_{Evap} seems to drop slightly, whilst the COP increases (Figure 2.3-12). Since the temperature drop, suggests a larger deviation from the dead state, it is expected that the exergetic efficiency should increase. This coupled with the increase in COP, result in the overall peaking in exergetic efficiency across almost all charge amounts.

However, after the optimum cooling capacity of 1.4 kW is reached, any further increase in the cooling, will result in lower COPs which was explained before. This will result in lower exergetic performance as well. The lower T_{Evap} , or increasing temperature difference from the dead state cannot produce much effect due to the larger drops in COP, which controls the exergetic efficiency in this case.

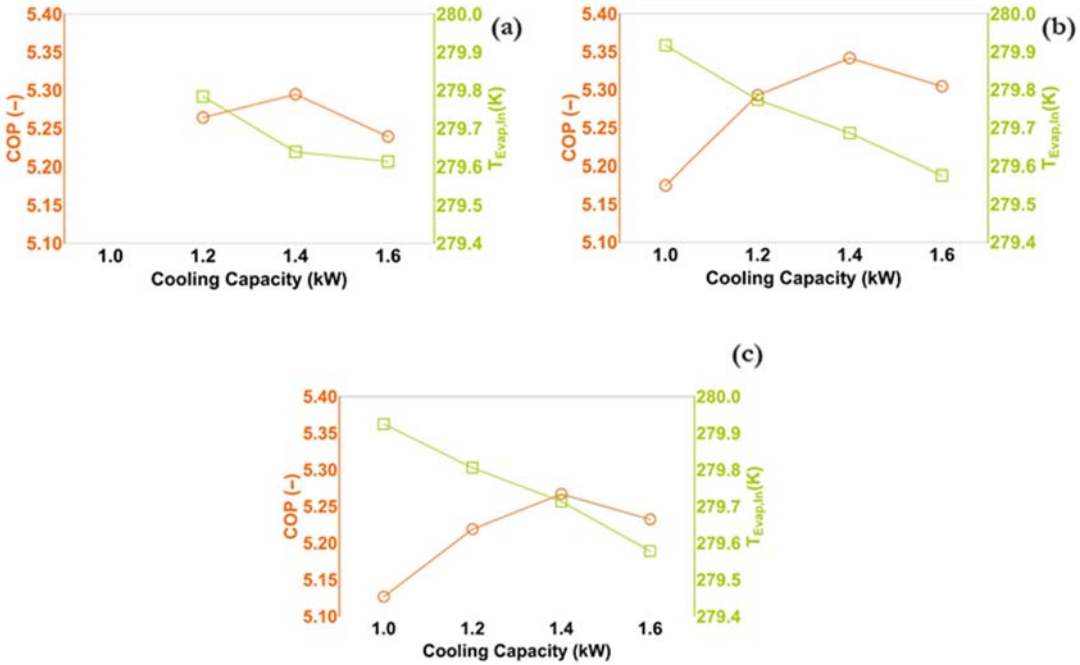

Figure 2.3-12 The variations in COP and evaporator inlet temperature versus cooling capacity for the refrigerant charge amounts of 0.67, 0.70 and 0.80 kg

It should also be noted that if the evaporator temperature T_{Evap} slowly increases and reaches T_0 , the reduction in Exergetic Efficiency is observed, where η_{Ex} will reach zero. Hence, for the case of cooling, the lower the evaporator temperature, the better the exergetic performance will be, provided that the COP change is not as influential.

Lastly, the highest exergetic efficiency of all the charge amounts occurs for the newly determined optimal charge and optimal cooling load of 0.70 kg at 1.4 kW. The optimal charge of 0.70 kg, constantly shows better exergetic efficiency, with respect all other charges as well.

Table 2.3-5 The exergetic efficiency with calculated extended uncertainties for all refrigerant charge amounts at all cooling capacities

Charged Mass (kg)	Cooling Capacity (kW)	η_{Ex} (-)	± Error (-)	± Perc. Error (%)
0.67	1.2	0.3456	0.0040	1.16
	1.4	0.3505	0.0041	1.16
	1.6	0.3473	0.0040	1.16
0.7	1.0	0.3371	0.0039	1.16
	1.2	0.3476	0.0040	1.16
	1.4	0.3527	0.0041	1.16
	1.6	0.3524	0.0041	1.15
0.73	1.0	0.3363	0.0039	1.16
	1.2	0.3464	0.0040	1.16
	1.4	0.3507	0.0041	1.16
	1.6	0.3505	0.0041	1.16
0.75	1.0	0.3363	0.0039	1.16
	1.2	0.3470	0.0040	1.16
	1.4	0.3515	0.0041	1.16
	1.6	0.3485	0.0040	1.16
0.77	1.0	0.3361	0.0039	1.16
	1.2	0.3469	0.0040	1.16
	1.4	0.3501	0.0041	1.16
	1.6	0.3495	0.0040	1.15
0.8	1.0	0.3338	0.0039	1.16
	1.2	0.3422	0.0040	1.16
	1.4	0.3472	0.0040	1.15
	1.6	0.3476	0.0040	1.16

2.4 Conclusion

The thermodynamic analysis for a Vapor Compression (VC) cycle with R410a as the working fluid was conducted using a water cooled chiller. The AHRI Standard 551/591 (SI) was utilized to determine the operating conditions. R410a was used as a 'drop-in' refrigerant such that no changes to the existing setup were carried out. The test conditions were carried out for a range of charge amounts varying from 0.67 – 0.80 kg, in order to determine the optimum charge. The cooling capacity of the chiller were also varied between 1.0 – 1.6 kW in order to determine part load behavior. The experimental results were analyzed using Mathematica software with respect to both first law and second law.

The energy balance of the chiller was below 0.04, which suggested the good correlation among the calculated heat transfer rates based on the chilled and cooling water as well as the accountability of the heat leaks. The coefficient of performance (COP) was then analyzed for all conditions, and the results allowed the determination of the optimum charge amount of 0.70 kg based on the largest COP of 5.342 as well as the determinations of the optimum cooling load which was 1.4 kW. The COP peaked at 1.4 kW for all charge amounts, which signify the best performance of the whole chiller occurring at around 87 – 88 % of full load conditions. The undercharge and overcharge conditions resulted in the drop of performance, which was again visible by examining the COP trend. The exergy destruction was also presented in component form. For fixed mass charge amounts, an increase in cooling capacity resulted in the total increase in exergy destruction. The individual components contribution to this increasing exergy destruction showed similar trends. The compressor exhibited the largest exergy destruction, which was followed by the condenser, evaporator and finally expansion valve. In the case of the optimum cooling capacity of 1.4 kW, the increase in mass charge of refrigerant resulted in the exergy destruction increase in the condenser, but no particular trend was visible for the compressor. However, the evaporator and expansion valve both showed reduced exergy destruction possibly due to the reduced refrigerant mass flow rates within the circuit.

The exergy efficiency was also presented in graphical form to show a similar trend to that of the COP. The exergetic efficiency peaked for almost all refrigerant charge amounts at 1.4 kW, whist the best exergetic efficiency was shown by the chosen optimum charge

amount of 0.70 kg. This allows the justification as well validation of the COP based optimum charge amount determination as well as the conclusion that 1.4 kW enabled the best performance of the chiller.

The results obtained for the ‘drop-in’ investigations of R410a, can thus be used for further comparison with alternative refrigerants with low GWPs which are to be tested. The exergetic analysis will also help identify the possible contributions of the components towards determining the final cycle performance of these new refrigerants and mixtures. The identification of irreversibilities through this method will enable further conclusions to be drawn about the possible improvements on the system which could be required for the use of alternative refrigerants as well as the current limitations of using ‘drop-in’ refrigerants to replace R410a for water cooled vapor compression chillers.

CHAPTER 3 NEXT GENERATION REFRIGERANT THERMOPHYSICAL PROPERTIES

The need for low GWP alternatives to replace the widely used refrigerants such as HFCs which poses high GWPs, has been in focus since the Kyoto Protocol where the effects of greenhouse gases was recognized [159]. This has prompted the re-introduction of some older generation natural refrigerants such as carbon dioxide, it has also encouraged the study of refrigerant mixtures which can provide lower GWP values and driven the industry to develop alternative low GWP refrigerants [22]. Pertaining to the latter, a new refrigerant HFO-1132(E) developed by Daikin with a GWP of 3 is in the initial stages of testing at the 'Next Generation Refrigerant Property Research Center' (Next-RP) at I^2CNER, Ito Campus. This refrigerant being tested falls under the chemical group of Hydrofluoro Olefins (HFOs) which have been identified as potential alternatives to the high GWP HFOs being widely used in the world [160]. The initial stages of introducing a new refrigerant require the formulation of an Equation of State (EOS) to predict its behavior and properties at various conditions. This formulation is based on several types of experimental data, which identify certain thermophysical properties such as the vapor pressure, viscosity, boiling points and critical parameters. The research presented in this work regarding this new refrigerant HFO-1132(E), will be on the Pressure – Temperature (PT) experiments carried out at low temperatures (250K - 300K) in order to determine the Vapor Pressure curve. Further to this, using the PT data, the derivation of the Vapor-Liquid Equilibrium, using a theoretical approach referred to as the 'Flash Method' and a Cubic Equation of State the Peng Robinson (PR) EOS is also presented within this work.

3.1 Introduction

The refrigeration timeline has been evolving either due to regulations brought on by international treaties, or due to the pursuit of better refrigeration technology. This has led to the use of different refrigerants, varying from natural refrigerants such as Carbon dioxide (CO_2) and Ammonia (NH_3) to artificially developed Chlorofluorocarbons (CFCs) such as R11 and R12, which were considered as ideal refrigerants during their time and Hydrofluorocarbons (HFCs) such as pure R32 or the mixture R410a. This presents the evolving nature of refrigerants and also highlights the next big step of developing the next generation or the $4^{th}/5^{th}$ generation of refrigerants as put to words by J.M. Calm [22]. The main target of this new generation of refrigerants is to combat the Global Warming crisis, which has been inadvertently contributed to by many refrigerants which possessed high Global Warming Potentials (GWP). Several potential candidates are being explored [161], [162], with respect to their thermodynamic properties, transport properties, flammability and performance in practical heat pumps. One interesting chemical group which are being tested are the Hydrofluoro olefins due their lower GWPs as a result of their Carbon-Carbon double bond structure and low atmospheric lifetime [160], [163]–[167].

Though HFOs hold a great promise for replacing high GWP refrigerants, they still are faced with some practical issues such as flammability [161], [162]. Hence, the use of refrigerant mixtures to achieve suitable properties which have been previously implemented in cases such as R410A, is potentially being utilized with HFOs as well. These mixtures which are identified as having low GWP and can overcome the issues the pure components possess, would require extensive thermophysical property testing as well as practical cycle performance evaluation before being proven as successors to the current generation of refrigerants.

As mentioned above, the thermophysical or thermodynamic properties of refrigerants are key in selecting the Next Generation Refrigerants and these properties can range from simple attributes such as pressure, temperature, density, to more complicated properties such as enthalpy, entropy, viscosity, velocity of sound and Vapor-Liquid Equilibrium (VLE) [168], [169]. In general, the thermophysical properties of refrigerants are essential

in determining the behavior, suitability and applications of refrigerants. Some of these properties are often presented in forms of diagrams such as the Pressure- Enthalpy (p-h) Diagram, or even as Pressure-Concentration (p-x) Diagrams [168], [169] for mixtures and are also translated into Equations of State (EOSs) allowing a wider and more accurate identification of properties. The determination of these properties are hence a fundamental step which occurs at the early stages of the introduction of a new refrigerant or potential refrigerant mixture. The amount of data and research pertaining to this is immense and a fraction of this is presented in Table 3.1-1.

Table 3.1-1 Literature review on several of the various thermophysical property research carried out for different refrigerants and mixtures since 1973 - 2019

Year	Authors	Summary	Comments	Focus
1973	J.E. Lane[170]	Numerical solutions to the differential equations describing meniscus in vertical tubes have been obtained in order to improve the calculation on surface tension.	The solution of non-linear differential equations is used to calculate the surface tension through the description of the meniscus. Hence, the newly developed solutions show better fitting in comparison to the traditionally used Sugden's Table values.	Correction Terms for Surface Tension
1976	R. De Santis, F. Gironi and L. Marrelli[171]	An Equation of State for including the hard-sphere repulsion compressibility factor pertaining to Carnahan and Starling as well as an attractive term, is introduced.	The proposed EOS show good accuracy with respect to pure refrigerants and their VLE properties.	EOS VLE Carnahan-Starling
1992	N.Kagawa, M.Uematsu, K.Watanabe[172]	An EOS is presented for the Binary Mixture of R22/R114. The available PVTx data were used for this formulation.	The proposed EOS for the R22/R114 mixture was validated with experimental data as well as the comparison between the theoretical heat pump cycle and practical cycle analysis.	EOS derivation, Helmholtz, PVTx, R22/R114, Cycle Analysis

Year	Authors	Summary	Comments	Focus
1992	Zhao Z.Y., Yin J.M.. Tan L.C.[173]	The PVT properties of R152a were measured along 18 isochores.	Utilizing the PVT data together with works by Higashi 1987, a new vapor pressure equation was correlated, with an Average Deviation on 0.12% and a maximum of 0.28%.	PVT, R125a, Vapor Pressure Equation
1995	G.Giuliani, S.Kumar, F. Polonara[174]	The experimental apparatus to be used for PvT data measurements is described. R22 and R134a are used to validate the device.	An absolute average deviation between 0.6-0.7% were reported for the R22 and R134a PvT data, using this new experimental apparatus.	PVT, Experimental Setup
1996	M Nagel,K Bier[175]	In order to replace R22 and R502, the ternary mixture of R134a, R125 and R32 are explored with respect to the phase equilibrium or VLE, through experimental measurements of binary mixtures from -70°C to Critical Temperature. The mixing behavior is based on a cubic EOS.	Based on their previous work, R143a was used instead on R32, and the predicted cubic EOS behavior for the VLE again show good correlation. The final calculations for saturation pressure for both binary and ternary systems have shown great accuracy, with respect to experimental results at different compositions. The flammability of each mixture is also presented in triangular phase diagram form.	VLE Cubic EOS Ternary R143a, R134a, R125

Year	Authors	Summary	Comments	Focus
1996	J. Wilhelm, E. Vogel[176]	The gas phase viscosity is measured for R134a due to large discrepancies by multiple research works. The viscosities were measured for a temperature range between 297 - 438K, and at densities from 12-90 $molm^{-3}$.	The experimental data for viscosities were then used to recalculate the isothermal values, with the use of a firs-order expansion, in terms of density. This allowed the comparison of the zero-density, which was within ±0.2%.	Viscosity R134a Low Density
1996	Yukihiro Higashi, Takeaki Ikeda[177]	VLE measurements near the critical region for R143a were carried out and presented. Using a vapor-pressure equation, a new critical point was also calculated and presented.	The new critical parameters are presented for R143a.	Critical Parameter, VLE, R143a
1996	Chun-cheng Piao, Masahiro Noguchi[178]	An 18 coefficient modified Benedict Webb Rubin EOS for R125 is developed. The PVT experimental data were used for the EOS development, together with saturation properties, isochoric heat capacities and speed of sound.	The R125 EOS based on the modified BWR EOS, is capable of predicting both gaseous super heated and compressed liquid phase behavior for pressure up to 68MPa, densities of 1700 kg^{m-3} and temperatures between 170K to 475K	EOS, BWR EOS, PVT, isochoric heat capacities, saturation properties, speed of sound , R125

Year	Authors	Summary	Comments	Focus
1997	S. B. Riffat, C. F. Afonso, A. C. Oliveira and D. A. Reay[76]	The introduction of CFC saw the reduction of Natural Refrigerant use. However, in order to limit the environmental impact of these artificial chemicals, a review of the use of Natural Refrigerants for Air-conditioning and Refrigeration systems is presented.	Ammonia, CO2, Water, Air and Hydrocarbons are proposed as alternatives to be re-used in HVAC&R equipment such as air-conditioners in order to replace HFCs. The low cost and low environmental impact were the key reason for their investigation. Some key areas for future research are highlighted such as the use of research of particular cycle performance such as ammonia in low charge larger capacity systems and the component focused research such as axial and centrifugal compressors for use of water vapor compression cycles at low temperatures.	Natural Refrigerants CO2, Water, Ammonia, HC and Air Required Future Research
1997	M.H.Barley, J.D.Morrison, A.O'Donnel, I.B.Parker, S.Petherbridge, R.W.Wheelhouse[179]	Under the Montreal Protocol, in removing Chlorine containing refrigerants, the use of binary mixtures of refrigerants is explored with respect to the VLE data. Combined mixtures of R32, R125, R143a and R134a are tested for a range of pressures and temperatures.	The experimental data were fitted using models to derive the VLE properties. Whilst further analysis was carried out regarding the azeotropic points for several mixtures.	VLE Wilson Equation Binary R32, R125, R143a and R134a

Year	Authors	Summary	Comments	Focus
1997	Gustavo A.Iglesias-Silva, Kenneth R.Hall[180]	A generalized orthobaric density equation is proposed for a multitude of refrigerants. R-11, R-12, R-13, R-14, R-22, R-23, R-32, R-123, R-123a, R-124, R-134a, R-141b, R-142b, R-143, R-143a and R-152a.	The fitting parameters for the density equation for the mentioned refrigerants are calculated based on experimental data. The triple point is calculated from the fit of the data, which uses asymptotic behavior in the critical region and the rule of rectilinear diameters. Though the vapor densities are also derived, they are not properly addressed.	Liquid Density R-11, R-12, R-13, R-14, R-22, R-23, R-32, R-123, R-123a, R-124, R-134a, R-141b, R-142b, R-143, R-143a and R-152a
1997	R. Heide[181]	The surface tension of some pure refrigerants and their mixtures are measured for a temperature range between −50 to 60°C using the capillary rise method. The possibility to formulate the mixture surface tensions based of pure refrigerants was also explored. R32, R125, R134a, R143a, R152a, R404A and R407C.	The calculation of mixture surface tensions based on the mass proportions showed a good correspondence to the measured values.	Surface Tension R32, R125, R134a, R143a, R152a, R404A and R407C
1997	Jee Young Shin, Min Soo Kim, Sung Tack Ro[182]	The convective heat transfer coefficients for forced convective heat transfer for both pure and refrigerant mixtures were measured experimentally. R22, R32, R134A, R290, R600a, R32/R134a, R290/R600a and R32/R125.	The experimental results were compared with Gungor and Winterton correlations for a multitude of test conditions such as heat fluxes and mass fluxes for horizontal tube configuration. Some behavior patterns for the zeotropic mixtures such as variation of coefficients were not linear and the degradation of heat transfer were also reported.	Heat Transfer Coefficients, R22,R32,R134a.R290 and R600a and mixtures

Year	Authors	Summary	Comments	Focus
1997	K. Srinivasan, L.R Oellrich[183]	The differences in reported values for the saturation properties of R143a are compiled and a unified equation is proposed.	The saturation vapor pressure and liquid densities are reported and the vapor densities are calculated based on the Clausius-Clapeyron EOS and Watson's correlation. The surface tension is also derived and compared with experimental data. The saturated liquid viscosity and thermal conductivity have also been correlated.	R143a Correlation Saturated Vapor Pressure, Liquid Density, Surface Tension, Saturated Liquid Viscosity, Thermal Conductivity. Vapor Density Clausius-Clapetron EOS, Watson's Correlation.
1997	Socrates Ioannidis, Dana E. Knox[184]	For a ternary mixture of R14, R23 and R13, the VLE behavior is predicted using a modified excess Gibbs Energy model. The results are compared with the 3PWS model and the van der Waals mixing rules. Using Huron-Vidal Mixing rule, the behavior of some complex systems are predicted with only 3 data points at a given temperature.	A predictive model was introduced in order to use limited experimental data at a single temperature to obtain possible VLE extrapolations.	VLE Predictive Model

Year	Authors	Summary	Comments	Focus
1997	T.Rachidi, A.Bernatchou, M.Charia, H.Loutfi[185]	A predictive method for determining thermophysical properties of E143a and C216 are explored in order to replace R12 in Vapor Compression Cycles.	The critical parameters are calculated based on Lyderson group method, acentric factor based on the Lee-Kesler Equation, Critical Compressibility on the relation proposed by Patel and Teja, Heat Capacity by Rihani and Doraiswamy, Specific Volume by Patel-Teja EOS, Saturation Pressure using iterative resolution of iso-fugacity.	Thermophysical Property Prediction critical parameters are calculated based on Lyderson group method, acentric factor based on the Lee-Kesler Equation, Critical Compressibility on the relation proposed by Patel and Teja, Heat Capacity by Rihani and Doraiswamy, Specific Volume by Patel-Teja EOS, Saturation Pressure using iterative resolution of iso-fugacity.
1997	M.O. Al-Shafe'I, K. Mečárik[186]	A modification to the Carnahan-Starling - de Santis EOS is presented to provide improved pvT behavior.	The validation using ASHRAE refrigerants show the improved accuracy of the new EOS.	EOS Thermodynamic Property
1997	Lambert J Van Poolen, Cynthia D.Holcomb, Vicki G.Niesen[187]	The liquid-vapor coexistence data is used to determine the critical parameters for R32, R124 and R152a.	The calculated critical parameters fall within the uncertainty range of those reported in literature.	Critical Parameter Prediction R32, R124, R152a.

Year	Authors	Summary	Comments	Focus
1998	Mark O. McLinden, Eric W. Lemmon, Richard T. Jacobsen[188]	A summary of the models used to predict thermodynamic properties of pure refrigerants and their mixtures is presented. The importance of experimental data is also presented and some gaps in research are highlighted.	Virial, Cubic, martin-Hou, Benedict-Webb-Rubin, and Helmholtz EOS and several of their extended models are evaluated. The formulations for 16 pure refrigerants are also recommended. Mixtures of these refrigerants, can then be derived based on mixing rules. For mixture behavior, 5 models were also compared, whilst no single model seems to fit all scenarios. However, the Helmholtz energy model is seen to be the best which is available. R32, R125, R143a, R134a and R152a and mixtures for natural refrigerants, propane, butane isobutane and CO2. The need of additional caloric data, PVT data and VLE data is also emphasized. The Helmholtz energy mixture model of Lemmon and Jacobsen is presented as the best model available at this point.	Thermophysical Properties, EOS Comparison, Cubic EOS, Helmholtz EOS
1998	Sergio Bobbo, Roberto Camporese, Roman Stryjek[189]	The VLE data were experimentally obtained for a binary mixture of RE170 and R236fa. The CSD EOS is also used to regress the VLE data.	The experimental data showed a negative deviation from the Raoult's law, due the hydrogen bonding between oxygen in RE170 and hydrogen in R236fa.	VLE RE170 and R236fa, CSD EOS

Year	Authors	Summary	Comments	Focus
1998	Kouichi Satoh, Hideo Nishiumi, Taku Kasatani[190]	The vapor pressure measurements for a treated R22 sample, to produce Fluoroether, which do not contribute to Ozone Depletion are reported.	The possibility to use Fluorocarbons with treatment, in order to het similar refrigerant properties was presented with respect to R22.	Vapor Pressure R22, Chemical Treatment Fluoroether
1998	Howard L.Wilson, W.Vincent Wilding[191]	Vapor Phase Pressure - volume and Temperature (P-V-T) for binary mixtures of R22, R32 and R134a are experimentally recorded. A monomer-hexamer chemical association model and the Soave EOS were used to compare the results.	The experimental results varied with respect to the models, averaged at around 1.5%.	PVT, Soave EOS, Binary R22, R32 and R134a
1998	G.Di Nicola, G.Giuliani, G.Passerini, F.Polonara, R.Stryjek[192]	Two methods for deriving VLE data from isochoric experiments are presented. The 'Flash Method' and 'Model Free' Method. The Caranahan-Starling- de Santis EOS was used for VLE behavior prediction.	R32, and R134a Binary mixtures VLE were predicted using the CSD EOS, with the aid of the 'Flash Method' and 'Model Free' Method. A 2% uncertainty for both methods are reported.	VLE, CSD EOS, R32 and R134a Binary, Flash Method, Model Free Method
1998	S.B. Kiselev[193]	A cubic crossover EOS for pure fluids, is developed based on the Patel-Teja Cubic EOS. Co2, Water, R32 and R125 are used for comparing the model behavior with experimental data.	The crossover Patel-Teja EOS show better representation of the thermodynamic properties neat the critical region.	Cubic EOS, Patel-Teja, CO2, Water, R32 and R125

Year	Authors	Summary	Comments	Focus
1998	JaewonLee,Joncheon Lee, Hwayong Kim [194]	Experimental VLE data was obtained for mixtures of R32/R142b, R32/R123. Whilst the Peng Robinson EOS was used to represent these data.	The PR EOS showed a good fitting to the mixtures which were tested.	PR Cubic EOS, VLE Data, Fitting
1998	Heng-Liang Zhang, Satoru Tada, Haruki Sato, Koichi Watanabe[195]	The PVTx properties for mixtures of R125/R143a as an alternative to R502 were measured in the superheated region.	Using the PVTx data, and a truncated Virial EOS, a correlation was developed with 0.2% fitting error to predict the behavior of this binary mixture.	PVTx, Virial EOS, Fitting
1999	S.B Kiselev, R.A Perkins, M.L Huber[196]	The transport coefficients for the pure refrigerant R32, R125, R134a and mixture of R32/R125 are presented near the critical region.	The transport property model developed is used to calculate thermal conductivity and diffusivity data, which is then compared with the experimental data, which show deviations less than 4-5%, at densities larger than $0.1\rho_c$ and temperatures up to $2T_C$	Transport Coefficient, Thermal Conductivity, Thermal Diffusivity, R32, R125, R134a and R125/R32 Mixture
1999	J Lia, R Tillner-Roth, H Sato, K Watanabe[197]	The Equations of State (EOS) using the Helmholtz free energy have been developed for several binary and a ternary mixture.	R125/R134a, R134a/R143a, R125/R143a and R125/R134a/R143a mixtures are represented with newly developed EOSs.	EOS, Refrigerant Mixtures

Year	Authors	Summary	Comments	Focus
2005	G.Di Nicola, G.Giuliani, F.Polonara, R.Stryjek[198]	The PVTx measurement using an isochoric setup were performed on mixtures of N2O/R41/R32 and N2O/R41/R23. The CSD Cubic EOS was then used to derive VLE properties.	The binary mixtures of N2O/R41/R32 and N2O/R41/R23 showed adequate agreement within the derived VLE properties and PVTX data, when compared with results from the Burnett PVTx data. However, a positive deviation was seen with respect to Raoult's law.	PVTx, VLE, CSD EOS ,N2O/R41/R32 and N2O/R41/R23
2005	G.Di Nicola, G.Giuliani, F.Polonara, R.Stryjeks[199]	The PVTx data using the Burnett method for HFC+ HC or Inorganic Compounds are analyzed. N2O/R41 binary system is analyzed. Some Virial coefficients are also presented.	The PVTx data used to determine the virial coefficients show uncertainties within ±2 cm3/mol and ±500 cm3/mol2.	PVTx data, Burnett, N2O/R41, Virial Coefficients
2005	Adnan Sözen, Mehmet Özalp, Erol Arcaklioğlu[200]	The use of ANN for deriving liquid and 2-phase boiling of two ozone friendly refrigerant/absorbent pairs, Methanol/LiBr and Methanol/LiCl.	The maximum error is less than 3% whilst the average error is around 1%. The ANN predictions also fall within the estimated uncertainties.	Artificial Neural Networks, Absorption, Thermophysical Property Prediction, Methanol/LiBr and Methanol/LiCl
2006	Qi Chen, Rong-hua Hong, Guang-ming Chen [201]	The PVTx properties for the gas phase of HFC161/R125/R32 were measured. An EOS was also used for fitting.	The truncated virial EOS is utilized to fit the PVTx data for the binary mixture of HFC161/R125/R32	PVTx, Virial EOS, Fitting, HFC161/R125/R32 HFC/HFC/HFC

Year	Authors	Summary	Comments	Focus
2006	Qi Chen, Rong-hua Hong, Guang-ming Chen[202]	The PVTx properties for the gas phase of HFC161/R125 were measured. An EOS was also used for fitting.	The truncated virial EOS is utilized to fit the PVTx data for the binary mixture of HFC161/R125	PVTx, Virial EOS, Fitting, HFC161/R125 HFC/HFC
2006	Qi Chen, Rong-hua Hong, Guang-ming Chen[203]	The PVTx properties for the gas phase of HFC161/R32 were measured. An EOS was also used for fitting.	The truncated virial EOS is utilized to fit the PVTx data for the binary mixture of HFC161/R32	PVTx, Virial EOS, Fitting, HFC161/R32 HFC/HFC
2007	Rong-hua Hong, Qi Chen, Guang-ming Chen[204]	The PVTx properties for the gas phase of HFC161/R143a were measured. An EOS was also used for fitting.	The truncated virial EOS is utilized to fit the PVTx data for the binary mixture of HFC161/R143a	PVTx, Virial EOS, Fitting, R1234yf/R143a, HFC/HFC
2007	Adnan Sözen, Mehmet Özalp, Erol Arcaklioğlu[205]	An alternative approach to determine thermodynamic properties using Artificial Neural Networks (ANN) is proposed. Tests are carried out on R508b.	The properties determined include Specific Volume, Enthalpy and Entropy. With high R-squared values showing the good correlation between the predicted values and available data.	Artificial Neural Networks, Thermophysical Property Prediction, R508b

Year	Authors	Summary	Comments	Focus
2007	Katsuyuki Tanaka, Yukihiro Higashi[206]	Surface Tension experiments for R290, R600A and mixtures	A modified differential capillary rise method has been used to determine the surface tensions. Mixing rules developed are also able to predict the measured values with varied molar fractions.	Surface Tension, R290, R600a and mixtures
2007	Ryo Akasaka, Yukihiro Higashi, Katsuyuki Tanaka, Yohei Kayukawa, Kenichi Fujii[207]	VLE measurements are used to validate a cubic EOS and the derived VLE with mixing rules and the binary interaction parameter was also determined.	The use of a cubic EOS to derive VLE properties is presented, where the determined binary interaction parameter was used to compare and predict the bubble point pressures, which show similar accuracy to the VLE correlations.	Cubic EOS, VLE, Mixing Rules, Binary Interaction Parameters, R290, R600a, R600, R32
2008	James M. Calm[22]	The progress of refrigerants from the early years, to some of the latest developments and potential future of refrigerants is presented.	The marked differences in generations of refrigerants is presented and more importantly the search for low GWP high performance refrigerants and mixtures is highlighted.	History, Generations of Refrigerants, Next Generation, Low GWP
2008	Qi Chen, Rong-hua Hong, Guang-ming Chen[208]	The PVTx properties for the gas phase of HFC161/HFC227ea were measured. An EOS was also used for fitting.	The truncated virial EOS is utilized to fit the PVTx data for the binary mixture of HFC161/HFC227ea.	PVTx, Virial EOS, Fitting, R1234yf/HFC227ea , HFC/HFC

Year	Authors	Summary	Comments	Focus
2009	N.G.Polikhronidi, I.M. Abdulagatov, R.G.Batyrova, G.V.Stepanov[209]	The PVTx properties of H_2O/NH_3 are measured near the critical regions.	The measurements for PVTx were carried out in both single and two-phase regions. The Krichevskii parameter is also calculated and fall in good agreement with the critical line.	PVTx, H_2O/NH_3
2010	Katsuyuki Tanaka, Yukihiro Higashi[210]	The thermodynamic properties of R1234yf are presented.	The critical temperature, critical pressure and critical density which were measured using the visual meniscus disappearance method and the vapor pressure curves which were correlated based on the Wagner Equation as well as surface tensions measured using the differential capillary rise method are shown. The VLE properties are also estimated based on the PR EOS and the HT EOS. The heat of vaporization is calculated based on the CC Equation.	Critical Parameters, Vapor pressure, Acentric Factor, VLE, PR EOS, CC Eqn, Wagner Eqn
2010	Ryo Akasaka, Katsuyuki Tanaka, Yukihiro Higashi[211]	The development of an EOS for R1234yf	The thermodynamic properties of R1234yf which are highly needed are present as an newly derived EOS based on the Patel-Teja PT EOS and the corresponding extended state model (ECS).	EOS, R1234yf, Patel-Teja EOS, ECS EOS

Year	Authors	Summary	Comments	Focus
2011	Qi Chen, Yang Tong, Ronghua Hong, Guangming Chen[212]	The PVTx properties for the gas phase of HFC161/R134a were measured. An EOS was also used for fitting.	The truncated virial EOS is utilized to fit the PVTx data for the binary mixture of HFC161/R134a.	PVTx, Virial EOS, Fitting, HFC161/R134a, HFC/HFC
2012	Aik Jong Tan [213]	The Greenhouse Gas emissions and energy use of the US, related to commercial buildings and the dairy processing industry are explored within this thesis.	The building sector emission of GHGs from HVAC use is termed as the largest contributor, due to its large electricity use, which results in indirect CO2 emissions. Whilst for the dairy industry, particular types if manufacturing processes and goods, were identified as key contributors to the emissions. These conclusions were compared with existing research as well.	USA HVAC Industry & Dairy Industry, GHG emissions, Energy Use
2013	G.Di Nicola, G.Passerini, F.Polonara, R.Stryjek [214]	The PVTx properties of CO2/R1234ze (E) are measured using an isochoric set up and a Cubic EOS is used for fitting and VLE Derivation.	The binary mixture of CO2/R1234ze(E) showed adequate agreement within the 2-phase region with the use of the CSD Cubic EOS for VLE behavior whilst the super heated region was within 1% of predicted values.	PVTx, VLE, CSD EOS , CO2,R1234ze(E)

Year	Authors	Summary	Comments	Focus
2013	Giovanni Di Nicola, Alessia Arteconi, Giorgia Nardini, Roman Stryjek[214]	A built experimental setup was used for measuring Solid-Liquid Equilibria (SLE), for several binary mixtures, CO2/R1234yf, CO2/R1234ze (E). Triple points were also measured.	Temperatures reaching 122.6K, were used to measure the SLE of these mixtures. The triple points are also provided. The Schroder Equation is used for interpreting the results.	SLE, Triple Point, CO2/R1234yf, CO2/R1234ze(E)
2013	Ryo Akasaka[215]	For the Binary Mixtures of R32/R123ze(E) and R32/R1234yf, the Helmholtz energy explicit property models are presented.	Using the estimated model, the uncertainties are within 1% for the bubble pressure and 0.25% for the liquid densities. The critical loci are also reasonably presented with the model. The critical temperature calculated falls within 0.8K.	Property Model, Binary Mixture, R32, R1234ze(E), R1234yf, Bubble Pressure, Liquid Density, Critical Point
2013	Ryo Akasaka, Katsuyuki Tanaka, Yukihiro Higashi[216]	The VLE measurements near the critical point for the binary mixture R1234yf/R32.	11,18 and 11 saturated densities were obtained for different mixture ratios. The Critical parameters including temperature, densities and molar volume were determined using the meniscus disappearing level and the intensity of the critical opalescence. The PϱTx measurements were also used to determine the critical parameters.	VLE, Critical Parameters, PϱTx

Year	Authors	Summary	Comments	Focus
2014	Ryo Akasaka, Yukihiro Higashi, Akio Miyara, Shigeru Koyama[217]	A fundamental EOS was developed for R1234ze(Z)	For a temperature range between 273 - 430K, and up pressures of 6MPa, was developed using the critical parameters, vapor pressures, densities of both liquid and vapor phases and the sound of speed in the vapor phase.	EOS, R123ze(Z)
2014	Yingxia Qi, Hua Zhang, Yefeng Liu, Weidong Wu, Xi Chen, Xi Yang[218]	The PVTx properties for R290/R134a mixture are measured and an EOS is used for fitting.	The truncated virial EOS is utilized to fit the PVTx data for the binary mixture of R290/R134a.	PVTx, Virial EOS, Fitting, R290/R134a
2015	Martin K. Vollmer, Stefan Reimann, Matthias Hill, and Dominik Brunner[219]	The atmospheric presence of HFC such as R1234yf, R1234ze(E), and HCFC R1233ze(E) are recorded since 2011 to 2014 and reported.	The presence of R1234yf was undetected in 2011, but has grown since then to 4.5% by 2014. The presence of R1234ze (E) was detected in half of all samples in 2014, whilst the HCFC was only present in very low mole fractions. Based on the data recordings from Jungrasujoch and Dubendorf in Switzerland, the global increase of HCFC was reported to be 0.5 $Ggyr^{-1}$ for 2014	HFC and HCFC atmospheric concentrations, R1234yf, R1234ze(E) and R1233ze(E)

Year	Authors	Summary	Comments	Focus
2015	Qi Chen, Haiming Qi, Shiqi Zhang, Ronghua Hong, Guangming Chen[220]	The PVTx properties for the gas phase of R1234yf/R134a were measured. An EOS was also used for fitting.	The truncated virial EOS is utilized to fit the PVTx data for the binary mixture of R1234yf/R134a.	PVTx, Virial EOS, Fitting, R1234yf/R134a, HFO/HFC
2015	Ryo Akasaka, Yukihiro Higashi, Yasufu Yamada, Takashi Shibanuma[221]	Critical parameters of binary mixture R134a/R1234yf. Helmholtz mixture model development. VLE calculations.	The critical parameters of the binary mixture were determined experimentally, then used for the derivation of the Helmholtz EOS. With the use of this the VLE properties were compared with experimental results to show good correlations.	Critical Parameters, VLE, EOS
2015	Yukihiro Higashi, Shugo Hayasaka, Chihiro Shirai, Ryo Akasaka[222]	The PϱT measurements of R1234ze(Z) and R245fa were conducted together with critical parameter measurements.	The PϱT behavior, vapor pressure curves and the saturated vapor and liquid densities were determined using isochoric setups. Together with critical parameter experiments, new correlations for the properties have been determined.	PϱT, Critical Parameters, R1234ze(Z) and R245fa
2015	Chieko Kondou, Ryuichi Nagata, Noriko Nii, Shigeru Koyama, Yukihiro Higashi[223]	Surface tension measurements for low GWP refrigerants R1234zf, R1234ze(Z) and R1233zd(E) were carried out.	Using the capillary rise method at different temperatures, the surface tensions were measured. Deviations between Refprop 9.1 software was also tabulated. This shows a propagated uncertainty of less than 0.2 mN/m. Empirical correlation to represent the data are also given.	Surface Tension, R1234zf, R1234ze(Z) and R1233zd(E)

Year	Authors	Summary	Comments	Focus
2018	NaeemAbas, Ali Raza Kalair, Nasrullah Khan, Aun Haider, Zahid Saleem, Muhammad Shoaib Saleem[224]	A Refrigerant Qualitative Parametric (RQP) model is used to help determine suitable alternative refrigerants both synthetic and natural to replace high ODP CFCs and high GWP HFCs. A study on a vapor compression cycle is performed using 16 refrigerants to determine their suitability.	Through the vapor compression cycle analysis, CO2, NH3 and some HCs as well as the synthetic R152a, R1234yf are reported as optimal refrigerants to replace environmentally harmful ones.	RQP Model, Refrigerant Selection Thermophysical properties and performance based, Vapor Compression Cycle, CO2, NH3, HCs, R125a, R1234yf
2018	Sergio Bobbo. Giovanni Di Nicola, Claudio Zilio, J. Steven Brown, Laura Fedele[225]	This review paper focuses on the availability of thermophysical properties of either natural refrigerants, HFOs and HFCs, which are possibly capable of replacing high GWP HFC for HVAC&R use.	The thermophysical properties which have been focused on include saturation and critical properties, vapor phase pVT data, liquid density, specific heat capacity, thermal conductivity, viscosity and surface tension.	Thermophysical Property Review, HFC, HFO, natural refrigerants, Saturation Properties, Vapor PVT
2018	Zhang Haiyang, Li Huiya, Gao Bo, Zhong Quan, Wu Wei, Liu Wenjing, Dong Xueqiang, Gong Maoqiong, Luo Ercang[98]	The gaseous densities of the binary mixture R1234yf/R600a are measured using a densimeter. A Helmholtz EOS was also developed using this information and other sources. The azeotropic characteristics were also investigated.	Using the Gaseous density data as well as the developed Helmholtz EOS, a relationship between azeotropic behavior, pressure, saturated liquid and vapor densities was formulated.	Gaseous Density, Binary Mixture, Helmholtz EOS, Azeotropic, R1234yf/R600a

Year	Authors	Summary	Comments	Focus
2018	Shahin Khosharaya, Mariano Pierantozzi, Giovanni Di Nicola[226]	A modeling approach using the Patel-Teja Eos is used for finding viscosity.	For seven binary mixtures, the binary interaction parameters have been regressed. Together with pure parameters, the viscosity is found for binary, and quaternary mixtures. The exclusion of density in this model is provide an advantage when data is not present.	Viscosity, Patel - Teja EOS
2018	Giovanni Di Nicola, Gianluca Coccia, Mariano Pierantozzi, Sebastiano Tomassetti[227]	Cubic EOSs were utilized to represent VLE of binary systems. An optimization of the combination was also presented for the best EOS for certain mixtures.	The RKS, PR, PR Mod and a general Cubic EOS were compared for a multitude of mixtures and the optimum pairing was presented with the AAD in pressures.	VLE, Cubic EOS
2018	Giovanni Di Nicola, Gianluca Coccia, Mariano Pierantozzi, Sebastiano Tomassetti[228]	The surface tension equations for low GWP halogenated alkene refrigerants and some blends are developed.	Using available literature on surface tension of low GWP refrigerants, correlations using semi-empirical models were carried out. The derived coefficients are then presented together with AAD. The proposed equations show some improvement to the available ones in literature.	Surface Tension
2018	Yukihiro Higashi, Naoya Sakoda[229]	The PvT properties, saturated densities and critical parameters for HFO1243zf are presented	The thermophysical data related to the PvT, critical point and saturated densities are measured with the use of Isochoric, VLE and Visual Meniscus Disappearance setups.	PvT, VLE, Critical Parameters, R1243zf

Year	Authors	Summary	Comments	Focus
2019	Mariano Pierantozzi, Giovanni Di Nicola[230]	A method for determining the surface tension of organic compounds is presented.	With the data collection of liquid viscosity on organic carboxylic-acids, the Pelofsky relationship was used to describe the relationship between surface tension and liquid viscosity.	Surface Tension

As seen in Table 3.1-1, there is immense value and importance in the experimental data as well as theoretical approaches for determine thermophysical properties of refrigerants and their mixtures. The vast amounts of data gathered by researchers have often been used for deriving EOS and which are then presented in databases, one of which is Refprop [154]. These EOSs and databases allows the easy access to refrigerant property information as well as refrigerant mixture information. However, due to the almost infinite conditions and combinations, the EOSs and databases do not provide an exhaustive set of information and can sometimes include limits or ranges in which the extrapolations and theoretical predictions are considered to be accurate. Hence the continued research into thermophysical properties of both existing refrigerants and especially, new refrigerants and mixtures is of immense importance to the development and progress of the whole HVAC&R industry.

The newly developed refrigerant HFO-1132(E) by Daikin, is currently in the initial stages of introduction and still lack many of the thermophysical properties relating to it. This refrigerant falls under the Hydrofluoro Olefin (HFO) category and currently has no properties published before. The task of measuring some of the thermophysical properties such as Vapor Pressure curves, Critical Parameters and Vapor-Liquid Equilibrium have been tasked to the NEXT-RP Laboratory.

In the hopes of contributing to the requirement of thermophysical data of this new refrigerant, and for the formulation of its EOS, the Pressure Temperature (PT) experiments using an Isochoric setup for the low temperature range of 250 – 300 K, in order to obtain the Saturated Pressure curve is proposed and carried out. Besides the acquiring the valuable PT data, a further step of deriving the Vapor-Liquid Equilibrium (VLE) properties of this refrigerant based on the 'Flash Method' utilizing the Peng Robinson Cubic EOS is also presented.

It is hoped that this work in measuring the Pressure Temperature (PT) data will be instrumental in gaining an initial understanding of the behavior of this refrigerant, as well as the contribution towards the formulation of an EOS specific to this refrigerant.

The mentioned PT data, together with the saturation curve and VLE derivations are presented within this work for the new refrigerant.

3.2 Experimental Methodology

3.2.1 Experimental Schematic and Instruments

3.2.1.1 Isochoric Setup Schematic

Figure 3.2-1 displays the schematic of the Low Temperature Isochoric Experimental set up, located at Next-RP Laboratory, I^{2}CNER. The experiment mainly consists of a constant volume or isochoric cell connected to a pressure transducer. The isochoric cell can be charged with the required refrigerant, then connected to the pressure transducer. After which the setup can be immersed in to the Silicon oil of the constant temperature bath. A platinum resistance thermometer is used to measure the steady state temperature of the isothermal bath. This set up allows the recording of both refrigerant pressure and refrigerant temperature, in order to obtain Pressure-Temperature data. For the temperature measurements the use of the zeroth law is necessary, where thermal equilibrium is reached between the silicon oil and refrigerant.

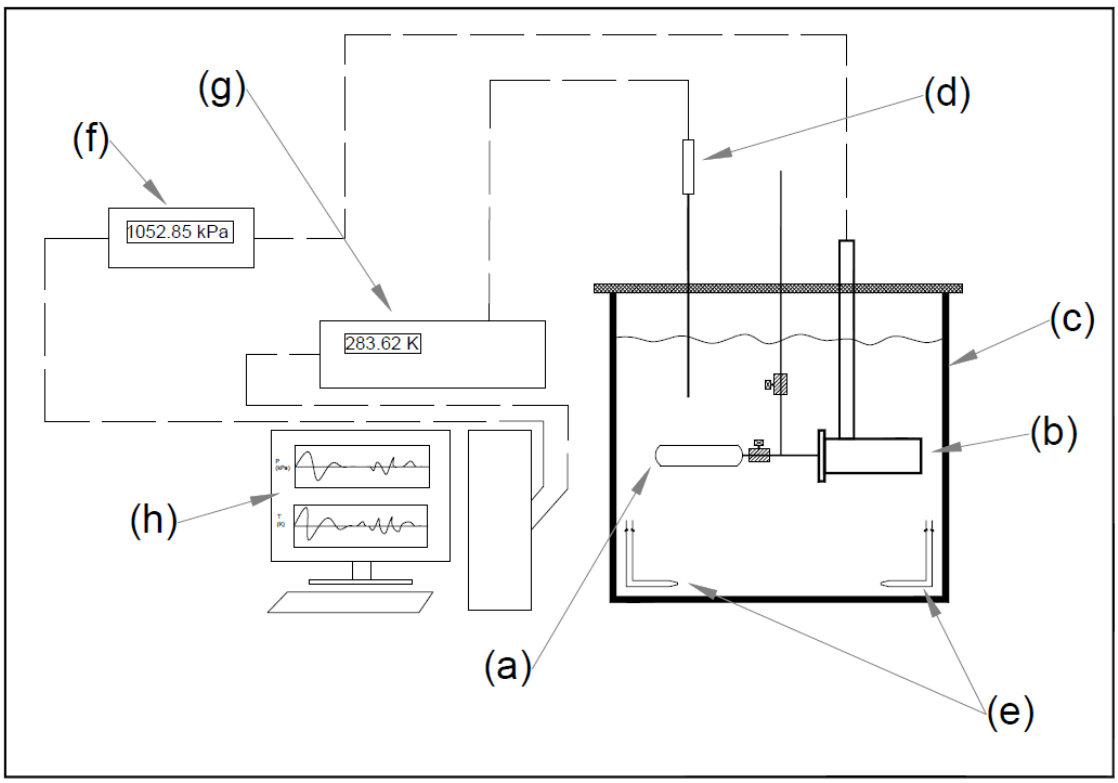

Figure 3.2-1 The schematic diagram of the Isochoric experimental setup; (a) isochoric cell; (b) pressure transducer; (c) isothermal bath; (d) platinum resistance thermometer; (e) thermal fluid pumps; (f) pressure display; (g) temperature display; (h) desktop

During the recording process the pressure and temperature readings are then converted from their primary form of voltage and frequency to Kelvin and Kilo Pascal, using a Wika ACL Resistance Thermometry Bridge [231], [232] and a Paroscientific Digiquartz pressure display, respectively [233]. These readings are then recorded using LabView software [150]. The analysis and fitting of the respective Pressure-Temperature curves were completed using Mathematica [151].

Figure 3.2-2 Photographs of the experimental setup; (a) The thermal bath; (b) the isochoric cell

3.2.2 Experimental Procedure

The testing method is straightforward, hence will be briefly described here. Only the pressure and temperature measurements of a given mass of refrigerant or refrigerant mixture are recorded. The required amount of refrigerant is charged into the isochoric cell. This process is described separately below for easier repetition. Once the charged and connected set up is immersed in the silicon oil, the required temperature set points are input into the Lauda temperature bath. Depending on the room temperature and set point temperature the time taken for stability can vary from a 3 hours up to 6 or 7 hours. Once thermal stability has been reached, and the temperature and pressure readings show minimum fluctuations, the necessary data is extracted from the data file. The extraction process, pressure and temperature average calculations and error analysis are all carried out using Mathematica [151].

3.2.3 HFO-1132(E) Refrigerant Information

Provided here is a brief description of the new refrigerant, HFO-1132(E). More information is unavailable at this point of time due both confidentiality reasons as well as the novelty of the refrigerant itself, making the available thermophysical properties limited since they are currently being tested.

HFO-1132(E), is classified as a Hydrofluror olefin (HFO), which signifies the presence of Hydrogen, Fluorine and a double bond between the 2 carbon atoms. HFOs have been identified as a potential alternative to high Global Warming Potential (GWP), refrigerants such as Hydrofluorocarbons (HFCs) [234]. The main reason for their low GWP, is the presence of the double bond between the carbon atoms, and faster reaction rates with atmospheric OH [167], [235]. The chemical name of HFO-1132(E) is trans-1,2-difluoroethylene [236]. This is an isomer of HFO-1132, and hence contains the bracketed '(E)' to indicate that it is 'trans-' better known [237]. An isomer is when two compounds have the same chemical formula or the same composition, but have different arrangements of each of the elements [238]. In the case of HFO-1132(E), it is known as a Geometric isomer, where the Fluorine atoms are positioned on opposite sides at each end as seen in

Figure 3.2-3 [239] . When the Fluorine atoms are on the same side at each end, it will be known as HFO-1132(Z), or Cis-1,2-difluoroethylene (Figure 3.2-4 [240]).

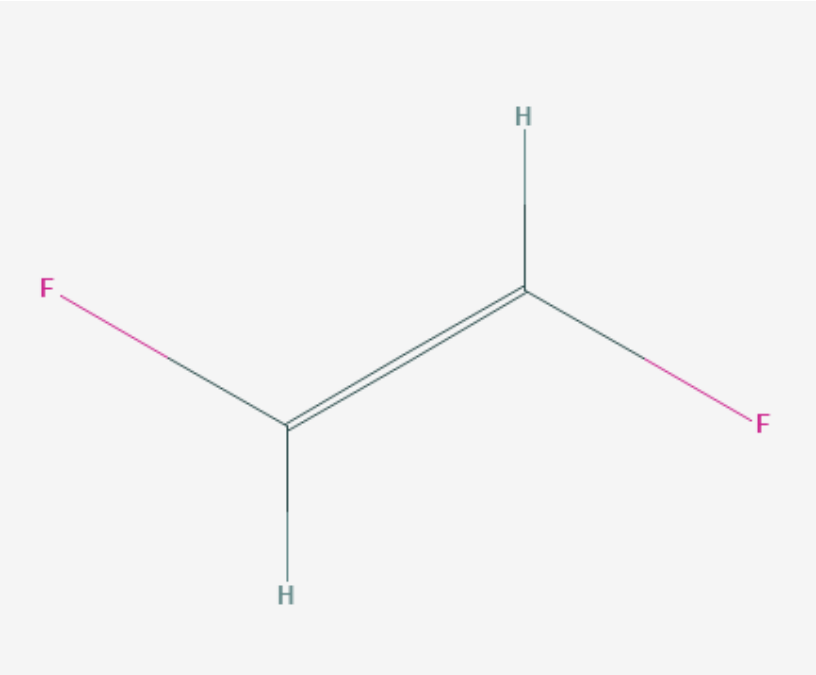

Figure 3.2-3 The chemical structure of HFO-132(E) [239]

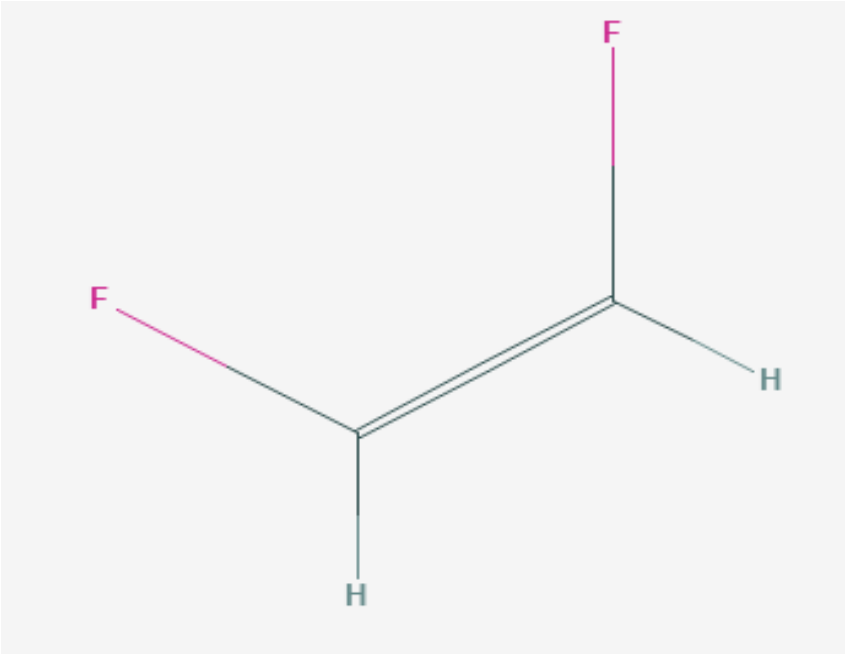

Figure 3.2-4 The chemical structure of HFO-1132(Z) [240]

3.2.4 Refrigerant Charging Process

Initially the required refrigerant mass is calculated. The measurements of the refrigerant mass is carried out using a gravimetric methods via a Mettler Toledo Analytical balance [241]. Since only pure refrigerants / pre mixed refrigerants have been tested using the current set up, the measuring process itself is also quite simple and does not require the direct mixing of refrigerants at the laboratory.

Refrigerant charging requires 2 isochoric cells, one such cell (Cell A) is used for measuring the refrigerant amount before and after charge, whilst the second cell (Cell B), is the isochoric cell which will then be submersed in the silicon oil and used in the set up. The main reason for using the secondary Cell A, to transfer the refrigerant to Cell B, is to obtain a better reading of the mass of refrigerant used for charging. Cell B, is usually immersed in the Silicon oil and it is difficult to remove all the oil, in order to measure the vacuumed cell weight accurately. Using the secondary Cell A, allows a more accurate reading of the mass before and after charge, to obtain the actual refrigerant amount which will be present in Cell B.

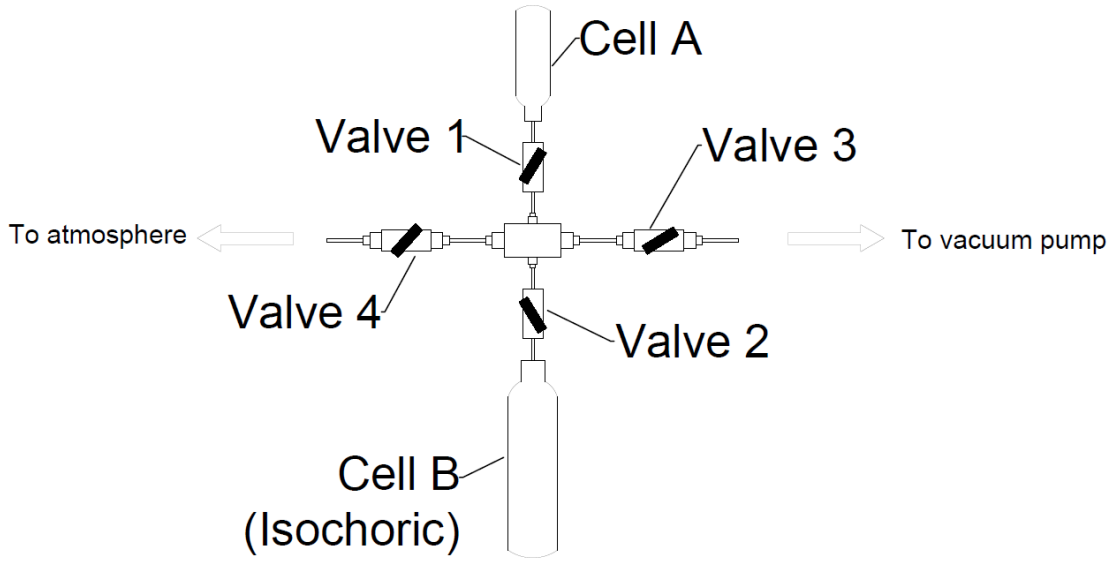

Figure 3.2-5 Diagram of vacuum process configuration with Cell B the isochoric cell being charged with refrigerant from Cell A

Referring to Figure 3.2-5 Cell A, is initially evacuated and weighed (each time the mass will be recorded), next the required amount of refrigerant is charged into Cell A (or has

been pre-charged and supplied by the respective manufacturer). The total weight of Cell A is recorded to know how much refrigerant is available. Next, Cell A is connected to Cell B and the vacuum as shown in above. After which the connection and Cell B, is evacuated. The evacuation process is done in two steps. First the Vacuum rotary pump is used to evacuate the cell (around 30 minutes), after the pressure reading on the Pa scale has reached its left limit, the secondary stage is begun, by using the turbo-molecular pump (TM Pump). This uses a series of turbines to remove gas molecules, such that ultra-low pressures can be achieved reaching 10^{-6} Pa [242].

After a few minutes of operating the TM Pump, a filament is used together with a Ionization Vacuum Gauge to measure the pressure more precisely [243]. The digital pressure gauge at 10^{-3} Pa is checked to see the vacuum state. Now the Valve 3 is closed, and the refrigerant is ready for charging. However, in order to make sure that all the refrigerant from Cell A to transferred to Cell B, Liquid nitrogen or Ice is used and Cell B is immersed in it. This allows the refrigerant to flow into Cell B due to a lower partial pressure and then cool down (liquefy), which assures that almost all the refrigerant will be charged into the new cell B. Now the Valve 1 to cell A is closed, and Valve 2 of Cell B is closed, and the cell B is allowed to cool to room temperature in order to remove the ice and moisture which has condensed and liquefied on the outside of the cell. This is important so that no water is mixed with the silicon oil as it will affect its performance, since the freezing point temperature of water is 273K, whilst our experiment will go to temperature reaching near 240K. The Cell A, is meanwhile measured after the charging process, and the difference in mass, provides the amount of refrigerant charged into Cell B. It is noted that, this measurement does not include the small amount of refrigerant in the connection tubing between the two cells. However, due to its very small volume, it is ignored.

The refrigerant containing Cell B, is now connected to the experimental isochoric set up, which can be removed easily from the oil bath. After it is connected as shown in Figure 3.2-2(b), the setup is moved to the vacuuming area, where according to Figure 3.2-6, the connection tubing between the isochoric cell and pressure transducer are vacuumed. After the vacuuming is complete. The isolation valve for the setup is used to seal the vacuumed section. Then the refrigeration sample isolation valve is opened, allowing the refrigerant to expand through the tubing into the pressure transducer, thus showing an increase in the pressure which is visible of the digital pressure gauge.

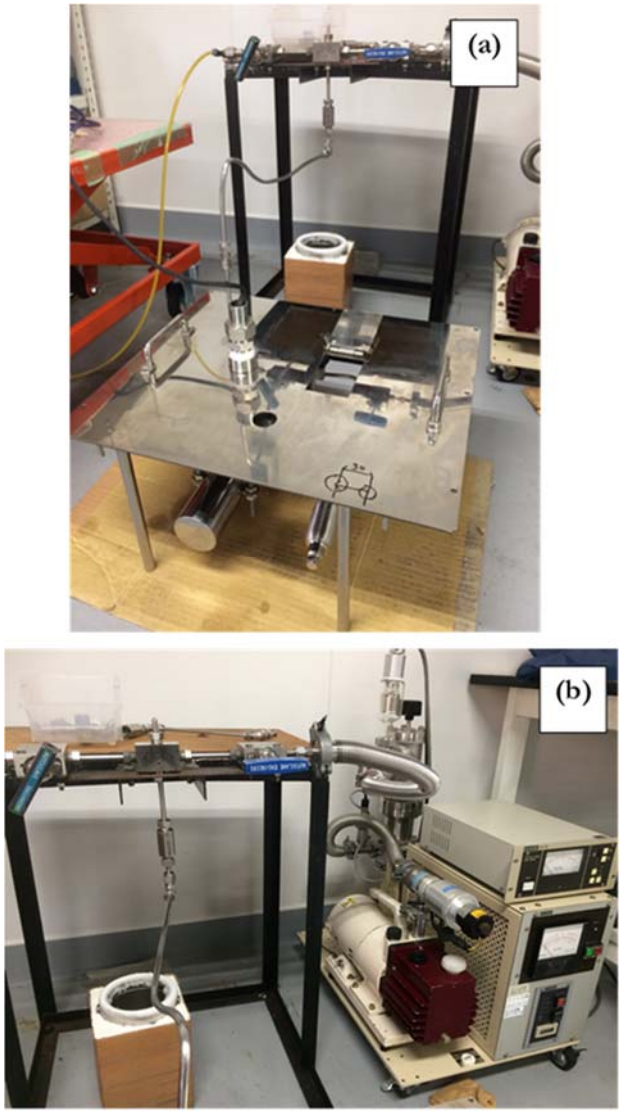

Figure 3.2-6 Figure of the vacuuming process in which; (a) the isochoric cell is connected to the tubing port; (b) vacuum is connected to the port as well and started

3.2.5 Pressure Sensor Calibrations

3.2.5.1 Evacuated State

In order to see the behavior of the pressure sensor across the temperature scale, at evacuated state, a Pressure-Temperature calibration process was carried out. The set up in initially evacuated, using the rotary pump and turbomolecular vacuum pump described before. This is done at room temperature. After which the setup is immersed in the silicon oil and the pressure is recorded at temperatures from 240K – 310K at ΔT=10K intervals to observe the behavior of the sensor.

3.2.5.2 Known Refrigerant R32

In order to measure the accuracy and repeatability of the pressure transducer, a known refrigerants, Difluoromethane which has been well documented and the thermophysical properties are readily are available of Refprop 10 software [154], is used to carry out

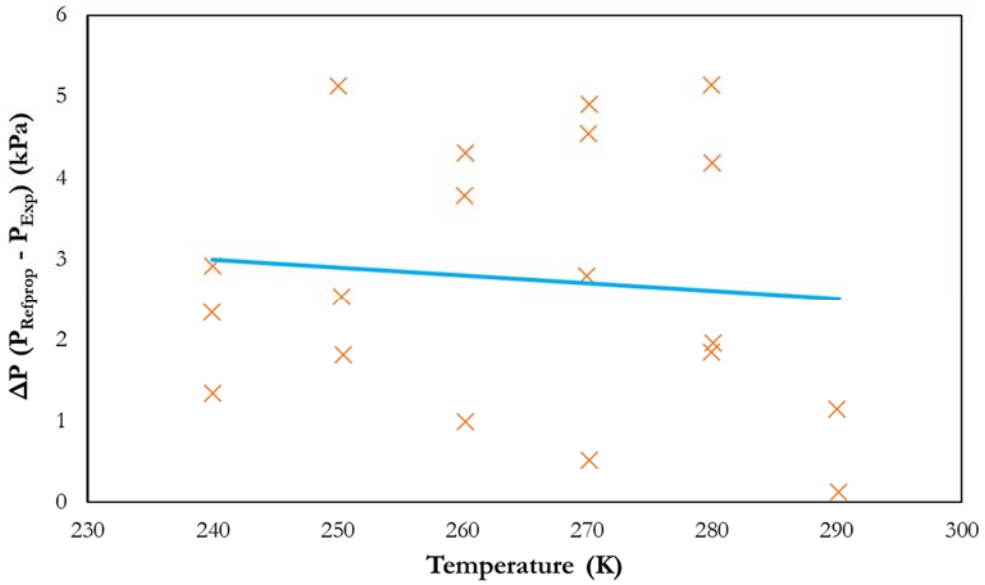

Figure 3.2-7 The pressure sensor calibration curve based on R32 experimental pressures and their deviation from Refprop 10.1

Pressure-Temperature experiments and compare with the Refprop Pressure values.

By using the difference between the Refprop and Experimental values, Del P (ΔP), a calibration curve for the pressure transducer is introduced.

$$\Delta P(kPa) = P_{REFPROP} - P_{Experiment} \qquad (3.2\text{-}1)$$

Linear Fitting

$$y = -0.0097x + 5.3201 \qquad (3.2\text{-}2)$$

Thus the new Experimental Pressure Calculated ($P_{Exp,Calc}$), based on the calibration curve is,

$$P_{Exp,Calc} = -0.0097T_{Exp} + 5.3201 + P_{Exp} \qquad (3.2\text{-}3)$$

3.2.6 Uncertainties

3.2.6.1 Instrument Uncertainty

The uncertainty calculations take into consideration both Type A and Type B uncertainties. The calculation method has already been introduced in Chapter 2 under Section 2.2.4. Shown below are the instrument uncertainties which are used for Type B calculations. It is also duly noted that the Expanded Uncertainty Calculations are limited to the low temperature range of 250-300 K, since these measurements were done using the described low temperature isochoric setup, whilst the higher temperature measurements up to the critical point were done using a separate setup, of which the instrument errors, and raw data are not accessible to the author. The final uncertainties for the Pressure and Temperature Readings are given in Table 3.2-1.

Table 3.2-1 The instrument accuracies for the pressure sensor and temperature sensor used for the Isochoric setup

Parameter	Type	Range	Accuracy
Temperature	Platinum Resistance Thermometer [a]	-40°C ~ 160°C	30<T<0 ±0.010K -40<T<0 ±0.015K
Pressure	Absolute Pressure Transducer [b]	0 ~ 6.9 MPa	±0.01 % Full Scale
Temperature Readings	Resistance Thermometry Bridge [c]	-200°C ~ + 962°C	±0.1 - 1.25 mK
Pressure Readings	Digiquartz Intelligent Display [d]	~	±0.008% of Full Scale
Note: (a) Calibration Certificate (provided in Appendix) & manufacturing information [244]; (b) [245]; (c) [232]; (d) [233]			

3.2.7 Challenges

3.2.7.1 The increased fluctuations of the Pressure and Temperature readings (Pipe flow rate decrease to reduce shaking / fluctuation)

During the experiments, it was visible that the pressure and temperature readings would fluctuate, even after several hours and thermal stability had been reached. It was determined that one possible reason was the higher pump flow rates, which were creating eddies and hence were causing both physical vibrations to the sensors and also creating

small volumes of silicon oil slightly different temperatures, similar to that of turbulent flow.

Thus it was proposed to reduce the flow rates of the Lauda unit. It was also proposed to change the flow nozzle which could have been resulting in larger eddies and turbulent flow. Shown in Figure 3.2.8(a), is the nozzle with multiple outlets. These could have resulted in more turbulent flow within the isothermal bath. Hence the flow outlet was changed to a simpler single nozzle layout as seen in Figure 3.2-8(b).

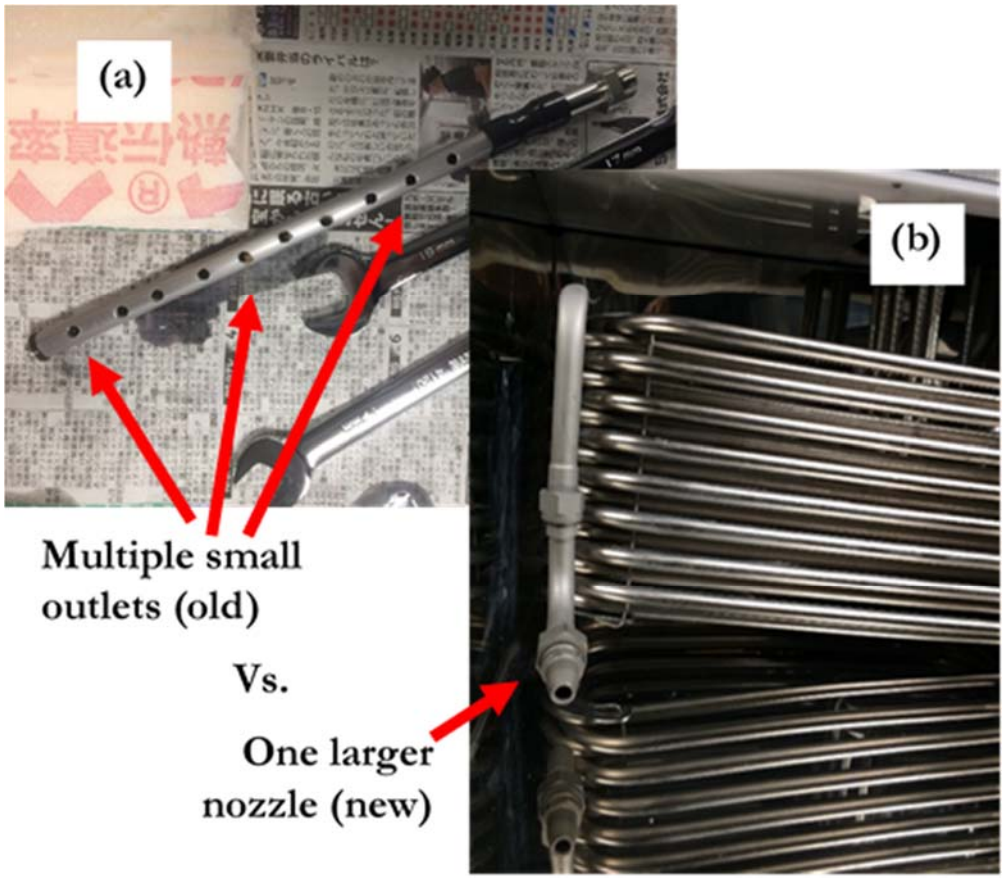

Figure 3.2-8 Isothermal bath silicon oil circulating nozzle structure; (a) previous version; (b) current version

3.2.7.2 Silicon Oil Level (Silicon oil amount top up, it reduces during cooling)

The silicon oil which was used in the isothermal bath, was subjected to temperatures from 300K to 250K. These temperatures resulted in the expansion and contraction of the liquid itself. Hence, during higher temperatures the oil level was adequate enough to cover the isochoric vessel and pressure sensor, whilst at the colder spectrum, it was observed that the oil level seemed to have decreased due to contraction. This could have caused more unsteady behavior at the lower temperature ranges, since the whole setup was not being immersed fully. Thus the silicon oil level was increased, such that the whole set up was covered even during the lower temperatures.

3.2.7.3 Pressure leak

During the vacuum tests as well as high pressure tests, it was noticed that a small leak was present, which would result in the reduction of pressure, even at constant or increasing temperatures. Thus the whole setup was tested using both a Helium leak detector and Snoop Leak Detector [246]. The latter employed the manual spotting of micro-bubbles which would appear when a leak of gas was present. Once the leak points were identified, as connection joints (Figure 3.2-9) in several locations of the setup, the connections were cleaned and properly tightened. This allowed the correction of the leaks, in order to maintain the pressure inside the isochoric cell.

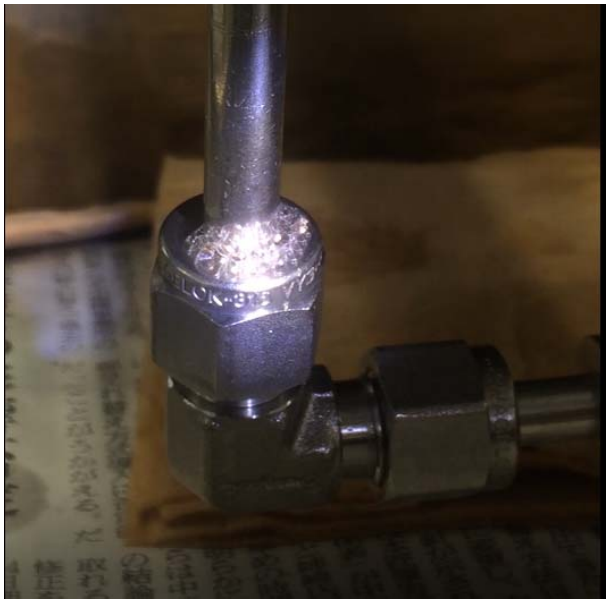

Figure 3.2-10 One of the leaking points at the connection between tubing identified through micro-bubble formation due to the use of Snoop leak detection fluid

Figure 3.2-9 Current insulation method for the heat leaks through the top panel use insulative cloth in addition to the layer on insulative material present

3.2.7.4 Set up top panel heat leak

During the experiments, it noticed that the top surface of the setup, will either be hot during high temperatures, or start to condense water vapor from the room, during lower temperatures. This suggests that even though there is an insulation layer underneath it, it is not providing adequate insulation and will result in heat leaks. Currently, insulation cloth is being used to prevent the leak, but it proposed to add an additional insulation layer [247] on top as well, to reduce the load on the Lauda system, and to provide better thermal stability.

3.2.7.5 Difficulty in accessing valves

Due to the presence of 4 support columns, which help hold the isochoric cell, the access to the 2 main valves is difficult. It is required to use these main valves, during the charging process and vacuuming process. Thus, the 4 support columns for the isochoric cell were removed, since the isochoric cell could already be supported without additional columns.

3.2.8 Isochoric Experimental Setup Review

The introduced isochoric experimental setup forms the basic foundations of thermophysical property experimentation through the measuring of Pressure – Temperature (PT) properties. The author has had the opportunity of carrying out Pressure – Temperature (PT) Thermophysical property measurements at two separate facilities on two Isochoric setups. Based on this experience and work, the author would like to suggest a 3rd Isochoric setup, which hopes to overcome some of the limitations of the currently available setups.

This will be presented under the Future work section.

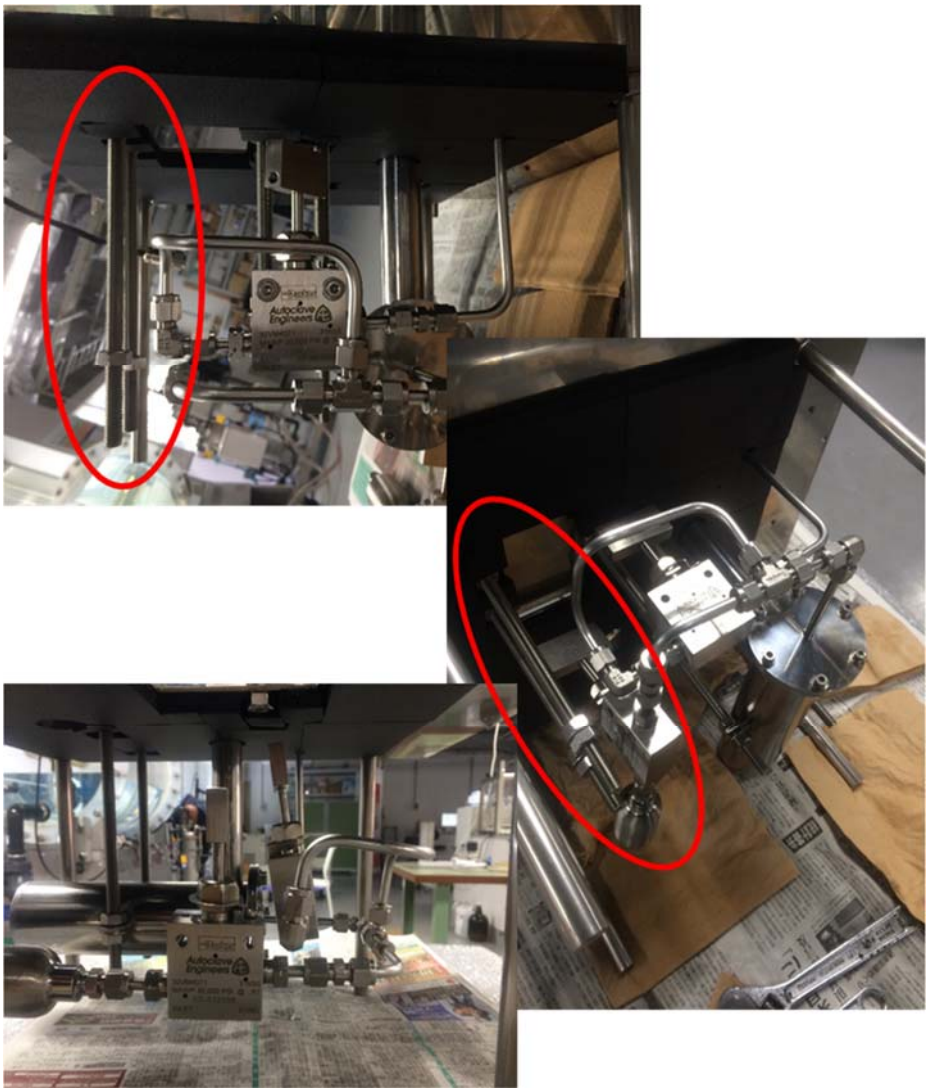

Figure 3.2-11 The removal of 4 additional support columns in order to provide better access to the valves and isochoric cell

3.3 Data, Results and Discussion

3.3.1 Pressure Temperature (PT) Graph

The Isochoric experiments were carried out for the new refrigerant HFO-1132(E) for a temperature range between 250K – 350K. These experiments were separated into two experimental setups; the main setup described in this work is used for the low temperature measurements for a range between 250K – 300K; the high temperature setup focused on data collection for a range of 300K – 350K. Presented below is the Pressure (kPa) vs Temperature (K) graph for all data points (see Figure 3.3-1).

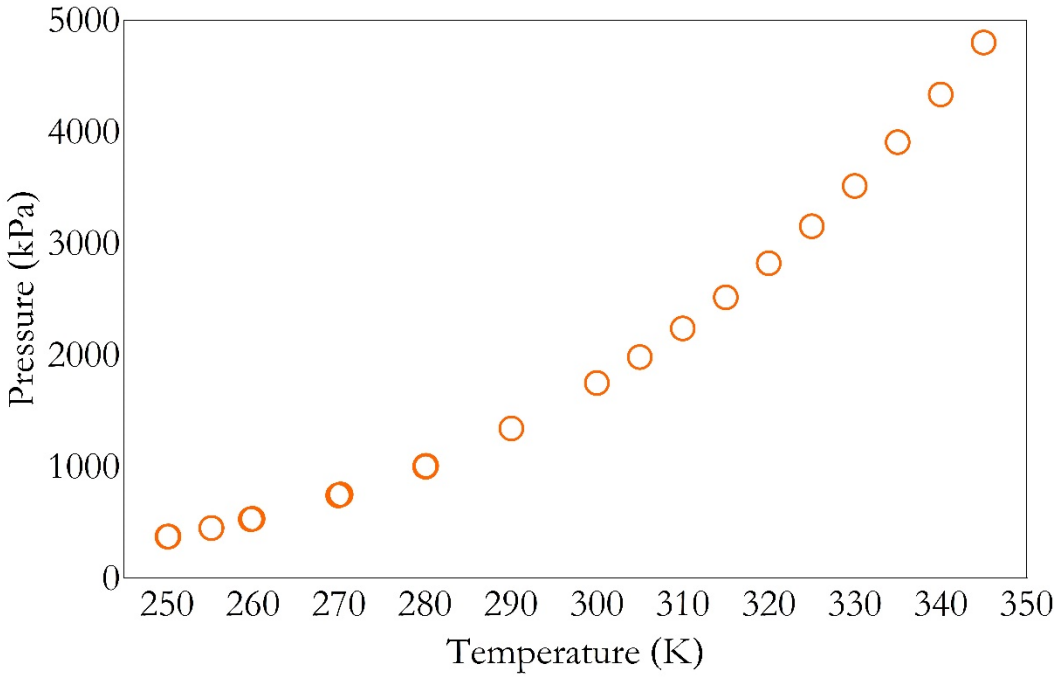

Figure 3.3-1 The Pressure versus Temperature (PT) plot for R1132(E)

3.3.2 Experimental PT Data

The data for the low temperature region are presented in Table 3.3-1 and Table 3.3-2 (as well as Figure 3.3-2) with Expanded Uncertainty analysis completed as mentioned before, whilst the high temperature data are presented in Table 3.3-3 without any uncertainty analysis since the raw data was not available.

Table 3.3-1 The experimental temperature readings with the calculated extended uncertainties

T_{Exp} (K)	± Uncertainty U_{TExp} (K)	± Percentage Uncertainty (%)
280.12	0.02	0.01
280.15	0.02	0.01
280.07	0.15	0.05
280.03	0.02	0.01
290.06	0.02	0.01
300.00	0.02	0.01
280.09	0.02	0.01
270.20	0.02	0.01
259.75	0.02	0.01
250.18	0.02	0.01
255.17	0.02	0.01
255.17	0.02	0.01
255.17	0.02	0.01
255.15	0.02	0.01
250.07	0.02	0.01
250.07	0.03	0.01
250.06	0.02	0.01
255.16	0.02	0.01
255.18	0.02	0.01
255.14	0.02	0.01
259.96	0.02	0.01
269.92	0.02	0.01
269.92	0.02	0.01
269.92	0.02	0.01

Table 3.3-2 The experimental pressure with calculated extended uncertainties

P_{Exp} (kPa)	± Uncertainty (kPa)	± Percentage Uncertainty (%)
1002.83	1.04	0.10
1005.55	1.06	0.11
1004.87	1.04	0.10
999.72	1.04	0.10
1340.52	1.04	0.08
1748.09	1.04	0.06
997.13	1.04	0.10
748.76	1.04	0.14
527.18	1.04	0.20
373.22	1.04	0.28
448.45	1.04	0.23
448.56	1.07	0.24
448.38	1.04	0.23
448.03	1.04	0.23
372.01	1.04	0.28
371.96	1.04	0.28
371.96	1.04	0.28
447.86	1.04	0.23
447.74	1.04	0.23
447.66	1.04	0.23
530.99	1.04	0.20
740.86	1.04	0.14
740.38	1.04	0.14
740.37	1.04	0.14

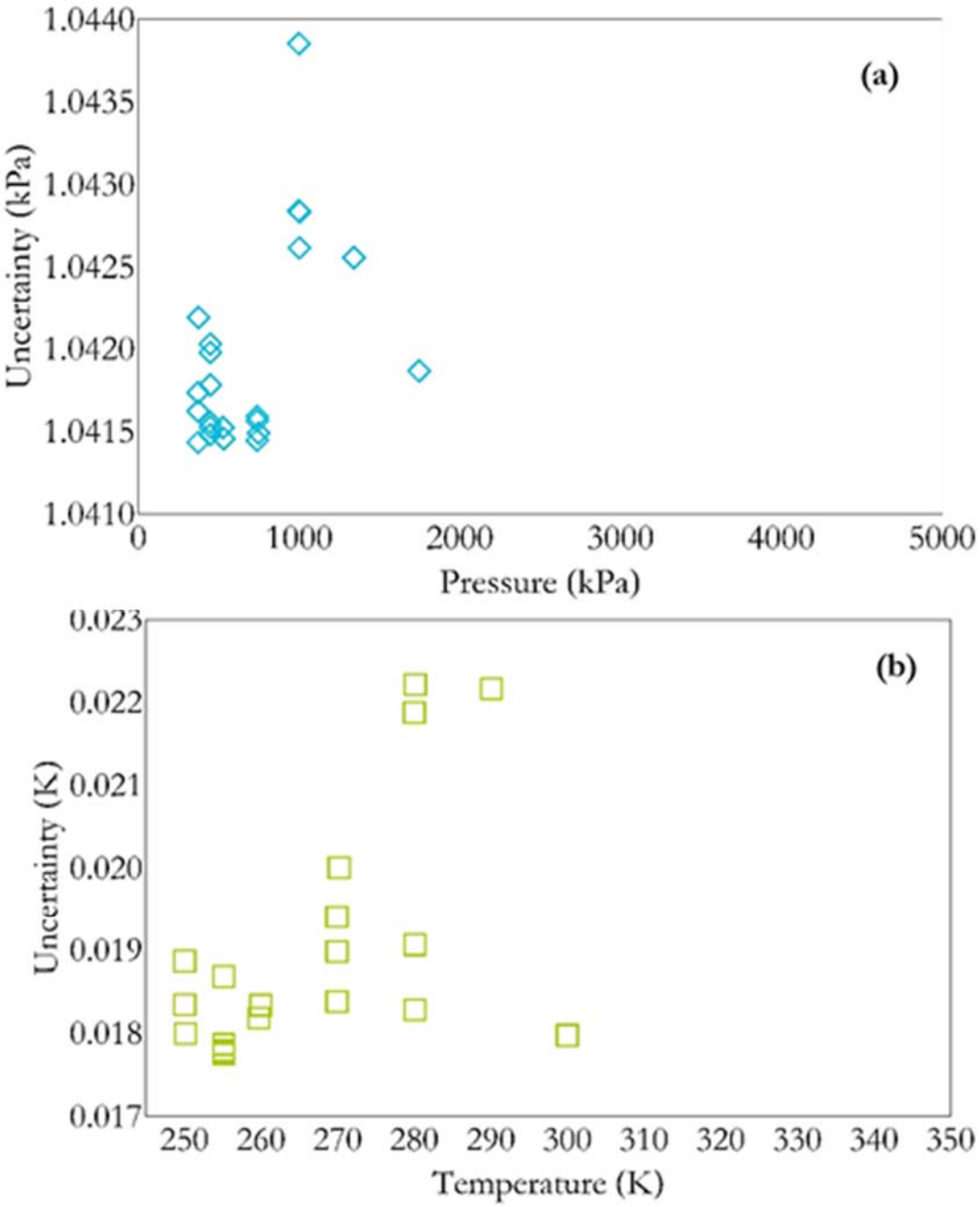

Figure 3.3-2 The uncertainties in graphical form of; (a) ΔP_{Exp} versus P_{Exp} ; (b) ΔT_{Exp} versus T_{Exp}

Table 3.3-3 The high temperature experimental (300 - 350K) data for Temperature and Pressure

Temperature (K)	Pressure (kPa)
300.00	1747.36
305.00	1979.93
310.00	2236.15
315.00	2515.32
320.00	2820.85
325.00	3151.87
330.00	3512.69
335.00	3905.23
340.00	4332.87
345.00	4797.88
348.72	5174.46

3.3.3 PT Vapor Curve Fitting

The initial step of analyzing the PT data, is to be done by finding a best fit equation for describing the behavior of Figure 3.3-1 (PT Curve). To do so, several models or equations were considered, in order to get Pressure as a function of Temperature. The fitting process was carried out via Mathematica [151], where the Absolute Average Deviation of Pressure (AAD_P) was minimized, in order to find the optimized coefficients for each equation.

$$\Delta P(kPa) = P_{Exp} - P_{Fit} \qquad (3.3\text{-}1)$$

$$\Delta P.\,\text{Perc}(\%) = \frac{\left(P_{Exp} - P_{Fit}\right)}{P_{Exp}} \times 100\% = \frac{\Delta P}{P_{Exp}} \times 100\% \qquad (3.3\text{-}2)$$

$$AAD_P(\%) = \frac{\sum\left(\frac{|\Delta P| \times 100\%}{P_{Exp}}\right)}{N} \qquad (3.3\text{-}3)$$

3.3.3.1 Clausius - Clapeyron Equation (CC)

The fitting process was started with a simple equation of state, the Clausius - Clapeyron (CC) Equation [248]. The CC equation is often used to determine the heat of vaporization (ΔH_{vap}) for a substance, when the PT behavior is known.

$$\ln(P_{CC}) = -\frac{\Delta H_{vap}}{RT} + a \qquad (3.3\text{-}4)$$

This can be often simplified to the well-known CC Equation shown below.

$$\ln(P_{CC}) = a - \frac{b}{T} \qquad (3.3\text{-}5)$$

The CC Equation if typically used for a limited temperature ranges at low pressure range due the inherent assumption of ideal gas behavior, temperature independence of heat of vaporization and that the volume of liquid in comparison to vapor for 1 mole of substance at saturation conditions is negligible [248]–[250].

Hence, it is evident that at high pressures the error in fitting will be larger (Table 3.3-5). Regardless, the coefficients obtained are given below in Table 3.3-4 and using these coefficients, the deviations in pressure (ΔP) between P_{Exp} and P_{Fit} and ΔP. Percentage ($\Delta P.Perc$) values are also shown in graphical form (See Figure 3.3-3). The Absolute Average Deviation of Pressure (AAD_P) for the CC fitting is 0.2498.

Table 3.3-4 The fitting coefficients for the CC equation using all data points

CC Equation	a	b	AAD_P (%)
	15.19	2319.16	0.2498

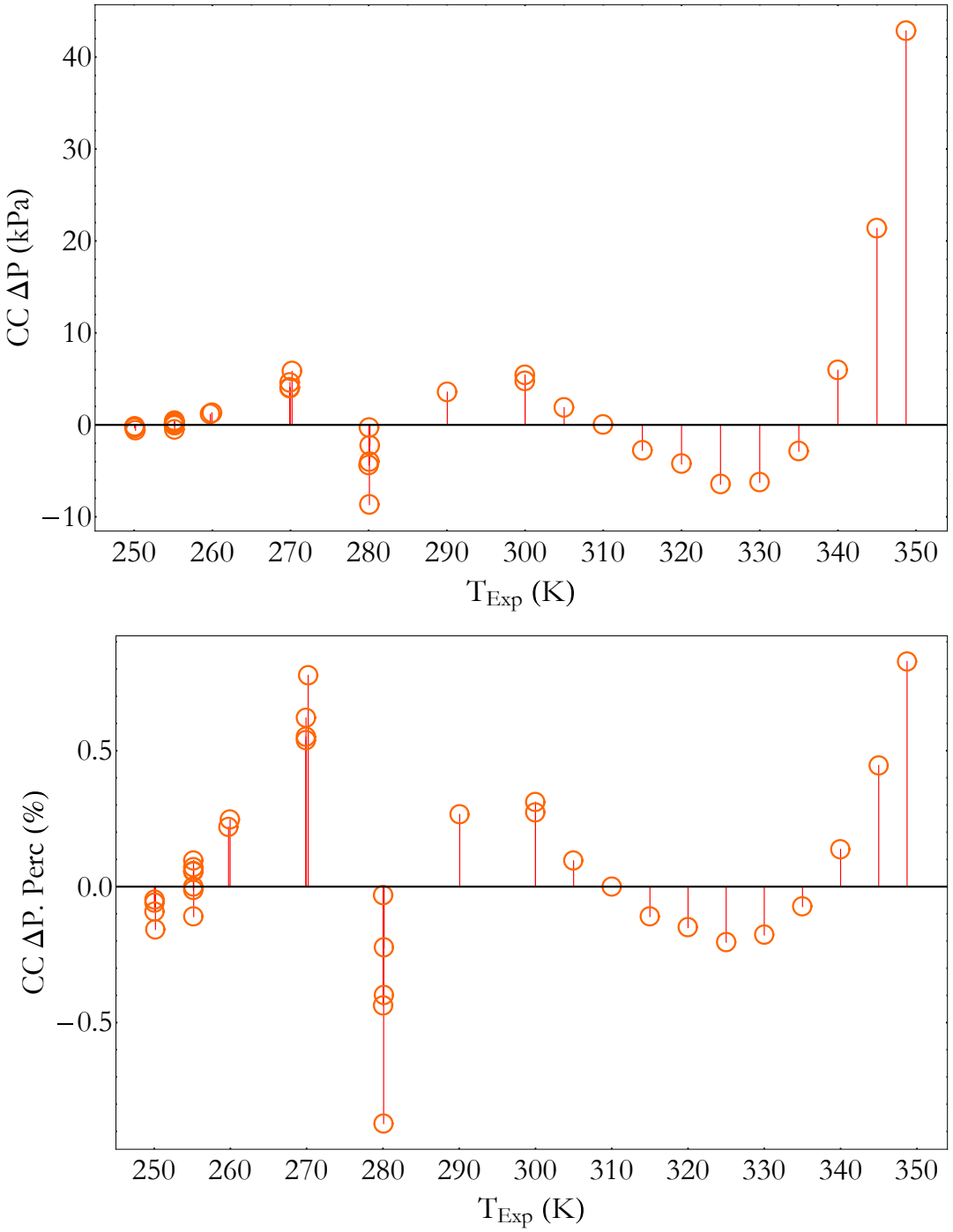

Figure 3.3-3 The fitting pressure errors for the CC equations

Table 3.3-5 The fitting errors for the CC equation together with the calculated pressure values

T_{Eexp}	P_{Eexp}	P_{CC}	ΔP (kPa)	ΔP. Perc (%)
280.12	1002.83	1006.84	-4.01	-0.40
280.15	1005.55	1007.80	-2.25	-0.22
280.07	1004.87	1005.20	-0.33	-0.03
280.03	999.72	1004.09	-4.37	-0.44
290.06	1340.52	1336.96	3.56	0.27
300.00	1748.09	1742.66	5.43	0.31
280.09	997.13	1005.82	-8.69	-0.87
270.20	748.76	742.94	5.82	0.78
259.75	527.18	526.03	1.15	0.22
250.18	373.22	373.81	-0.59	-0.16
255.17	448.45	448.13	0.32	0.07
255.17	448.56	448.13	0.43	0.10
255.17	448.38	448.13	0.25	0.06
255.15	448.03	447.79	0.24	0.05
250.07	372.01	372.23	-0.22	-0.06
250.07	371.96	372.30	-0.34	-0.09
250.06	371.96	372.14	-0.18	-0.05
255.16	447.86	447.92	-0.06	-0.01
255.18	447.74	448.24	-0.50	-0.11
255.14	447.66	447.66	0.00	0.00
259.96	530.99	529.69	1.31	0.25
269.92	740.86	736.27	4.59	0.62
269.92	740.38	736.30	4.07	0.55
269.92	740.37	736.39	3.98	0.54
300.00	1747.36	1742.61	4.75	0.27
305.00	1979.93	1978.05	1.88	0.09
310.00	2236.15	2236.15	0.00	0.00
315.00	2515.32	2518.10	-2.77	-0.11
320.00	2820.85	2825.09	-4.24	-0.15
325.00	3151.87	3158.32	-6.45	-0.20
330.00	3512.69	3518.94	-6.25	-0.18
335.00	3905.23	3908.10	-2.86	-0.07
340.00	4332.87	4326.92	5.94	0.14
345.00	4797.88	4776.52	21.36	0.45
348.72	5174.46	5131.62	42.84	0.83

3.3.3.2 Antoine Equation (AT)

A simple way to account for the inherent limitations of the CC equation was proposed by Louis Charles Antoine [250] . This equation could be used for higher pressures near the critical point [251], but is also mentioned to provide accurate correlations for pressure ranges between 1 – 200 kPa [248]. Regardless, the Antoine (AT) Equation [252], is also used for fitting the vapor pressure curve.

$$\ln(P_{AT}) = a - \frac{b}{c+T} \qquad (3.3\text{-}6)$$

The AT fitting showed a similar trend to that of the CC Equation, where there was an increasing error at higher temperatures and pressures. Though the AT equation, is well known to provide more accurate fittings [252], it still seemed to suffer inaccuracies when reaching very high pressures near the Critical Point (see Figure 3.3-4). The AAD_P for the AT equation is 0.2486.

Table 3.3-6 The fitting coefficients for the AT equations

AT Equation	a	b	c	AAD_P (%)
	15.11	2272.77	-2.86	0.2486

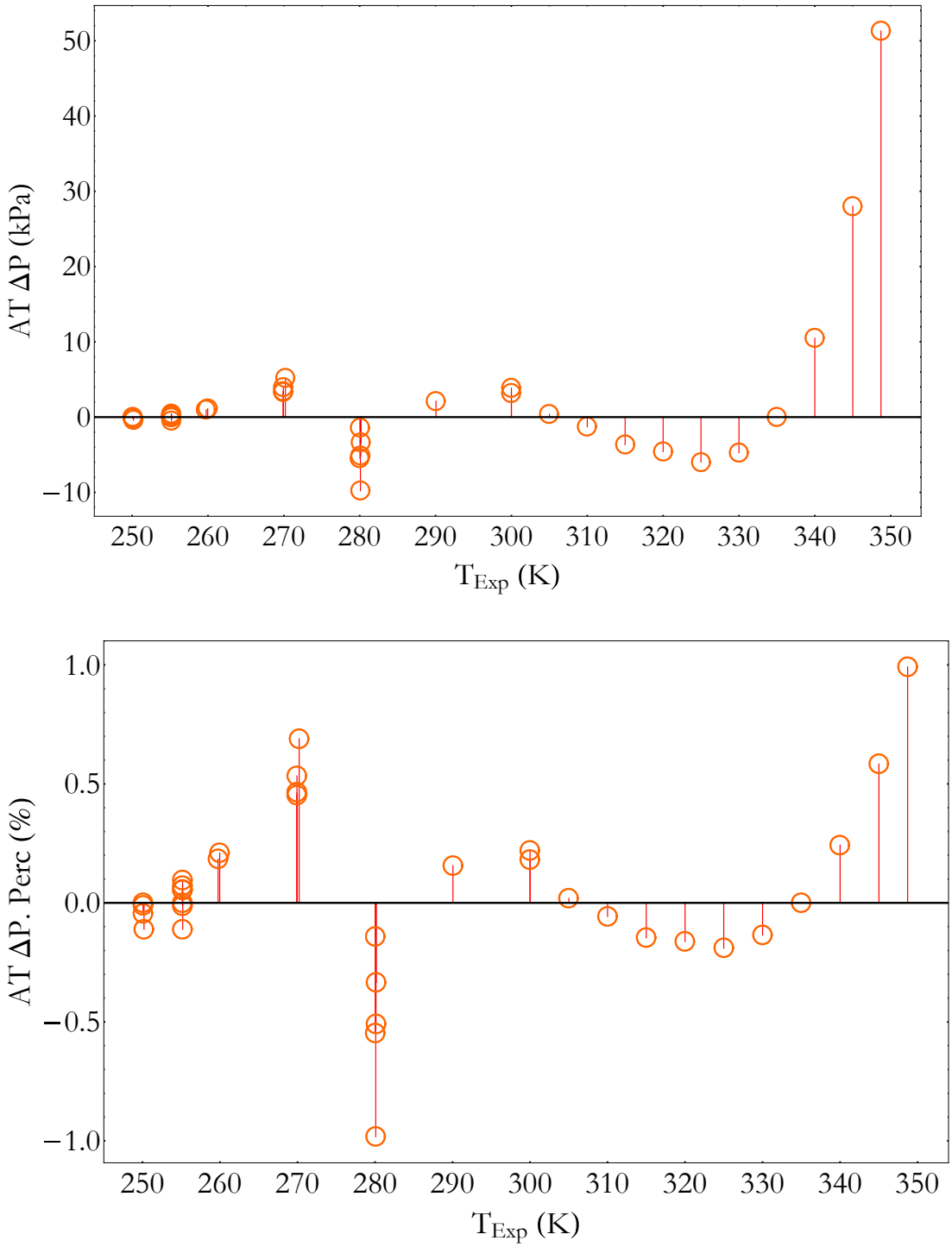

Figure 3.3-4 The fitting errors for the AT equation in absolute and percentage form

Table 3.3-7 The fitting errors for the AT equations together with the calculated pressures

T_{Eexp}	P_{Eexp}	P_{AT}	ΔP (kPa)	ΔP. Perc (%)
280.12	1002.83	1007.94	-5.12	-0.51
280.15	1005.55	1008.91	-3.36	-0.33
280.07	1004.87	1006.30	-1.43	-0.14
280.03	999.72	1005.19	-5.47	-0.55
290.06	1340.52	1338.42	2.10	0.16
300.00	1748.09	1744.24	3.85	0.22
280.09	997.13	1006.92	-9.79	-0.98
270.20	748.76	743.60	5.16	0.69
259.75	527.18	526.21	0.97	0.18
250.18	373.22	373.63	-0.41	-0.11
255.17	448.45	448.13	0.32	0.07
255.17	448.56	448.13	0.43	0.10
255.17	448.38	448.13	0.25	0.06
255.15	448.03	447.79	0.24	0.05
250.07	372.01	372.06	-0.04	-0.01
250.07	371.96	372.12	-0.16	-0.04
250.06	371.96	371.96	0.00	0.00
255.16	447.86	447.92	-0.06	-0.01
255.18	447.74	448.24	-0.50	-0.11
255.14	447.66	447.66	0.00	0.00
259.96	530.99	529.88	1.11	0.21
269.92	740.86	736.91	3.95	0.53
269.92	740.38	736.94	3.43	0.46
269.92	740.37	737.03	3.34	0.45
300.00	1747.36	1744.19	3.17	0.18
305.00	1979.93	1979.56	0.38	0.02
310.00	2236.15	2237.44	-1.29	-0.06
315.00	2515.32	2519.01	-3.69	-0.15
320.00	2820.85	2825.44	-4.59	-0.16
325.00	3151.87	3157.87	-6.00	-0.19
330.00	3512.69	3517.43	-4.74	-0.14
335.00	3905.23	3905.23	0.00	0.00
340.00	4332.87	4322.36	10.50	0.24
345.00	4797.88	4769.88	28.00	0.58
348.72	5174.46	5123.16	51.30	0.99

3.3.3.3 Wagner Equation (WAG)

Since the CC and AT equations are consider to be simple models, a slightly higher degree equation was needed to fit the results with better accuracy. For many Hydrofluorocarbons (HFCs), the Wagner equation has been utilized to determine vapor pressure curves [253]. Since the current HFO, will potentially be used to replace high GWP HFCs, there is the possibility of testing refrigerant mixtures which will include HFO + HFC + others (E.g. Natural Refrigerants) [254]. Some HFOs have also been already modeled with the Wagner equation as presented by Tanaka et. al. [210] for R1234yf. The Wagner (WAG) equation was hence chosen as potentially providing a better fit for a larger data range as well as due to the possibility of comparing with future HFO mixtures and their vapor pressure curves.

The fundamental Wagner equation consists of 27 terms, due to the powers of τ (τ =T-T_C) moving in steps of 0.5, from -2 to 9, and 6 additional terms of (1- τ). However, based on previous studies on some Hydrofluoroolefins with the use of truncated Wagner equations, such as on R1234yf by Di Nicola et. al. [255] and Tanaka et. al. in [210] in 2010 and by Fedele et. al. [256] in 2011, good fitting with low AAD_P were obtained. The review work done by Brown et. al [257], which show the feasibility of using a simplified Wagner equation with less terms for specifically hydrofluoro olefins, gives the necessary background to choose the following Wagner equation for representing the Vapor Pressure behavior.

$$P_{WAG} = P_C \times Exp\left[\frac{\left(A\times(1-\frac{T_{Exp}}{T_C})\right)^{1}+\left(B\times(1-\frac{T_{Exp}}{T_C})\right)^{1.5}+\left(C\times(1-\frac{T_{Exp}}{T_C})\right)^{2.5}+\left(D\times(1-\frac{T_{Exp}}{T_C})\right)^{5}}{\left(\frac{T_{Exp}}{T_C}\right)}\right]$$

(3.3-7)

The calculated coefficients are given below in Table form. Based on literature published by Lemmon et. al. [258] it is noted that the calculated coefficients fall within the expected range and follow the expected trends where A is in between (-6) – (-8), and B > 0, when C < 0. Figure 3.3-5 which shows that the error distribution has changed from those of CC and AT. Previously, there were increasing errors towards the critical point, but as seen

now the larger errors are only isolated to a few random temperatures. This has helped reduce the AAD_P value to 0.1733.

Table 3.3-8 The fitting coefficients for the WAG equations

WAG Equation	A	B	C	D	AAD_P (%)
	-7.18	1.69	-2.85	5.38	0.1733

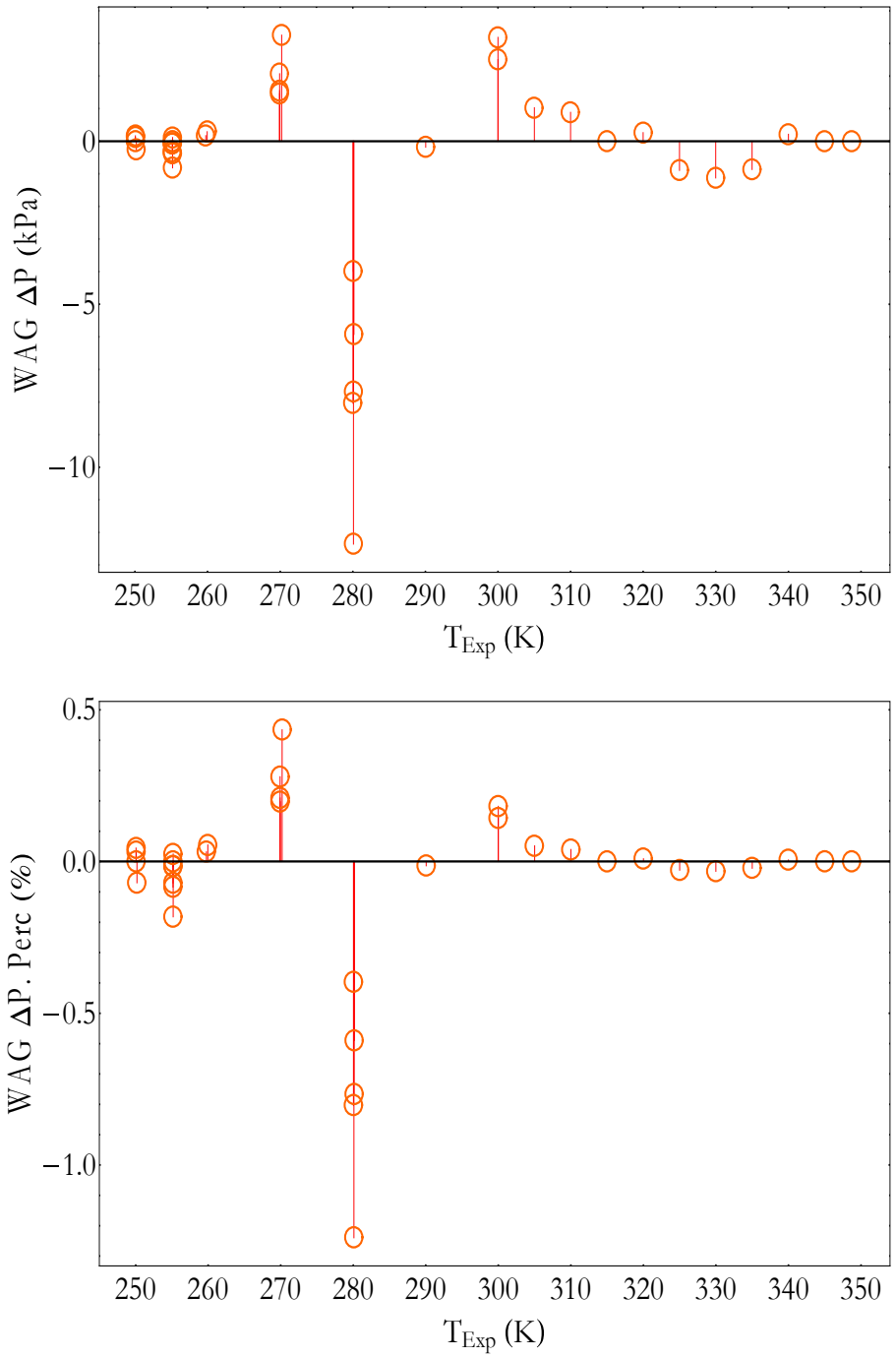

Figure 3.3-5 The fitting errors for the WAG equation in absolute and percentage form

Table 3.3-9 The fitting errors for the WAG equations together with the calculated pressures

T_{Eexp}	P_{Eexp}	P_{WAG}	ΔP (kPa)	ΔP. Perc (%)
280.12	1002.83	1010.51	-7.68	-0.77
280.15	1005.55	1011.47	-5.92	-0.59
280.07	1004.87	1008.86	-3.99	-0.40
280.03	999.72	1007.75	-8.03	-0.80
290.06	1340.52	1340.70	-0.18	-0.01
300.00	1748.09	1744.91	3.18	0.18
280.09	997.13	1009.48	-12.36	-1.24
270.20	748.76	745.51	3.25	0.43
259.75	527.18	527.01	0.17	0.03
250.18	373.22	373.48	-0.26	-0.07
255.17	448.45	448.45	0.00	0.00
255.17	448.56	448.44	0.11	0.02
255.17	448.38	448.45	-0.07	-0.01
255.15	448.03	448.10	-0.07	-0.02
250.07	372.01	371.89	0.12	0.03
250.07	371.96	371.96	0.00	0.00
250.06	371.96	371.80	0.16	0.04
255.16	447.86	448.24	-0.38	-0.08
255.18	447.74	448.56	-0.82	-0.18
255.14	447.66	447.98	-0.31	-0.07
259.96	530.99	530.70	0.29	0.05
269.92	740.86	738.80	2.07	0.28
269.92	740.38	738.83	1.55	0.21
269.92	740.37	738.91	1.46	0.20
300.00	1747.36	1744.86	2.50	0.14
305.00	1979.93	1978.91	1.02	0.05
310.00	2236.15	2235.27	0.88	0.04
315.00	2515.32	2515.32	0.00	0.00
320.00	2820.85	2820.59	0.26	0.01
325.00	3151.87	3152.76	-0.89	-0.03
330.00	3512.69	3513.81	-1.13	-0.03
335.00	3905.23	3906.10	-0.87	-0.02
340.00	4332.87	4332.65	0.21	0.00
345.00	4797.88	4797.88	0.00	0.00
348.72	5174.46	5174.46	0.00	0.00

With the improvement of the AAD_P, from 0.2490 to 0.1733 in comparison to those of the CC and AT equation fitting, the Wagner Equation seems to provides a better representation of the PT relationship.

3.3.3.4 Modified Benedict – Webb –Rubin Equation (MBWR)

As mentioned in section 3.3.3.3, the possibility of mixing HFOs which suffer from certain flammability issues, with HFCs might be important since 'drop-in' applications for existing systems might be of interest. HFCs can be represented with the Modified Benedict-Webb-Rubin (MBWR) equation as well [178], [259]. Hence, the MBWR equation is also used for the PT fitting.

$$P_{MBWR} = Exp\left[\left[\frac{\left(A\times(1-\frac{T_{Exp}}{T_C})\right)^{1}+\left(B\times(1-\frac{T_{Exp}}{T_C})\right)^{1.5}+\left(C\times(1-\frac{T_{Exp}}{T_C})\right)^{2}+\left(D\times(1-\frac{T_{Exp}}{T_C})\right)^{4}+\left(F\times(1-\frac{T_{Exp}}{T_C})\right)^{6.5}}{\left(\frac{T_{Exp}}{T_C}\right)}\right]\right] \quad (3.3\text{-}8)$$

Table 3.3-10 The fitting coefficients for the MBWR equations

MBWR Equation	A	B	C	D	F	AAD_P (%)
	-7.29	2.66	-2.90	0.57	3.09	0.1731

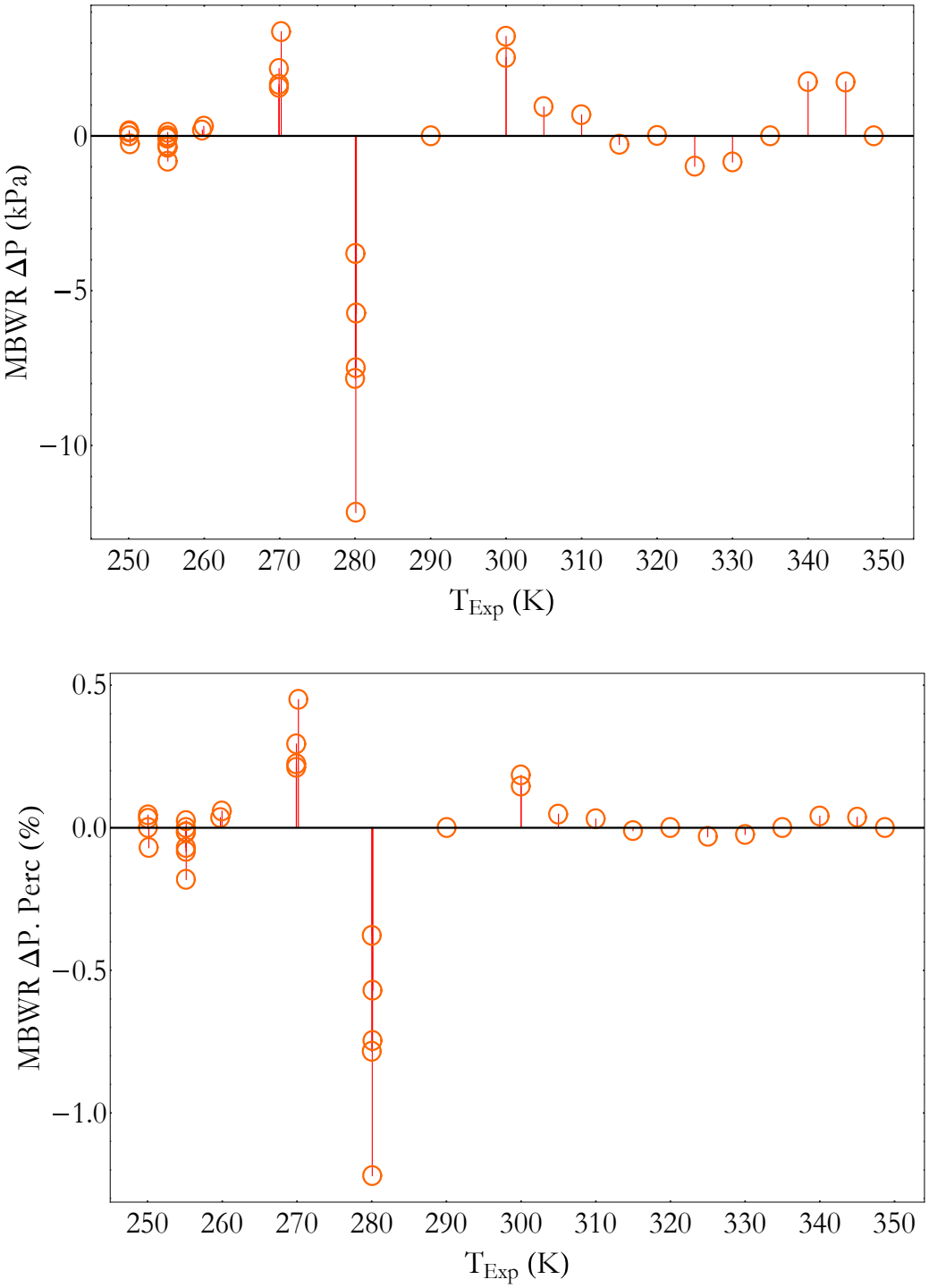

Figure 3.3-6 The fitting errors for the MBWR equation in absolute and percentage forms

Table 3.3-11 The fitting errors for the MBWR Equations together with the calculated pressures

T_{Eexp}	P_{Eexp}	P_{MBWR}	ΔP (kPa)	ΔP. Perc (%)
280.12	1002.83	1010.31	-7.49	-0.75
280.15	1005.55	1011.28	-5.73	-0.57
280.07	1004.87	1008.67	-3.80	-0.38
280.03	999.72	1007.56	-7.84	-0.78
290.06	1340.52	1340.52	0.00	0.00
300.00	1748.09	1744.88	3.21	0.18
280.09	997.13	1009.29	-12.17	-1.22
270.20	748.76	745.40	3.36	0.45
259.75	527.18	526.99	0.19	0.04
250.18	373.22	373.48	-0.26	-0.07
255.17	448.45	448.45	0.00	0.00
255.17	448.56	448.44	0.11	0.02
255.17	448.38	448.45	-0.07	-0.01
255.15	448.03	448.10	-0.07	-0.02
250.07	372.01	371.89	0.12	0.03
250.07	371.96	371.96	0.00	0.00
250.06	371.96	371.80	0.16	0.04
255.16	447.86	448.24	-0.38	-0.08
255.18	447.74	448.56	-0.82	-0.18
255.14	447.66	447.98	-0.31	-0.07
259.96	530.99	530.68	0.31	0.06
269.92	740.86	738.69	2.18	0.29
269.92	740.38	738.72	1.66	0.22
269.92	740.37	738.81	1.56	0.21
300.00	1747.36	1744.83	2.54	0.15
305.00	1979.93	1978.99	0.94	0.05
310.00	2236.15	2235.47	0.68	0.03
315.00	2515.32	2515.60	-0.27	-0.01
320.00	2820.85	2820.84	0.00	0.00
325.00	3151.87	3152.85	-0.98	-0.03
330.00	3512.69	3513.53	-0.84	-0.02
335.00	3905.23	3905.23	0.00	0.00
340.00	4332.87	4331.11	1.75	0.04
345.00	4797.88	4796.14	1.74	0.04
348.72	5174.46	5174.46	0.00	0.00

The BWR showed the best fit with the lowest AAD_P OF 0.1731, with the Wagner equation coming in at a close second with an AAD_P of 0.1733. The differences in the WAG and BWR fittings are very minute, since the AAD_P only vary by 0.001. The CC and AT fittings had much larger AAD_P coming in at 0.2498 and 0.2486 respectively.

3.3.4 Anomalies in PT data

When comparing the deviations in pressure using the ΔP graphs, for the AT and CC fitting the largest errors occurred at higher temperatures and pressures, which was expected. However, the WAG and BWR equations, exhibit higher errors at some distinct lower temperatures. The temperature exhibiting the largest error for the WAG and BWR fittings, happen to be 270K, 280K and 300K.

These temperatures also show higher errors for the CC and AT fittings as well. Hence, there seems to be some anomalies in these readings. Thus, 270K, 280K and 300K are neglected, and a re-fitting process is carried out. The newly obtained results are given below.

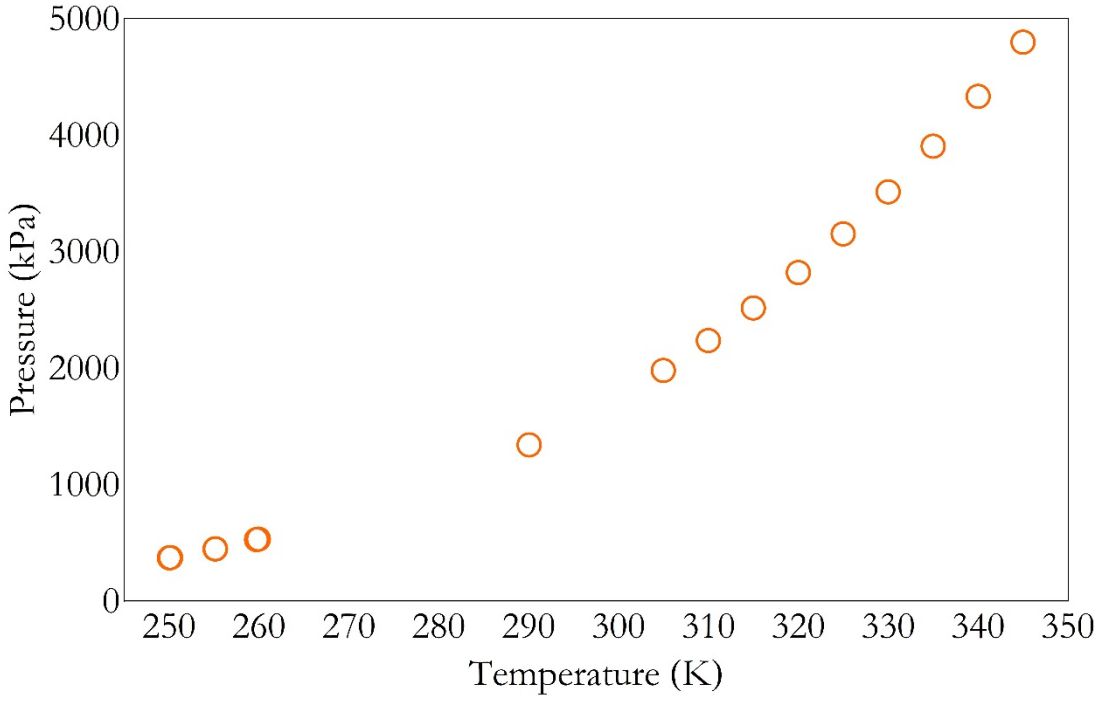

Figure 3.3-7 The Pressure – Temperature (PT) data with the removal of anomalies

Table 3.3-12 The CC and AT coefficients with the removal of PT anomalies

Eqn.	a	b	c	AAD_P
CC	15.19	2319.16		0.1546
AT	15.11	2272.76	-2.86	0.1519

Table 3.3-13 The WAG and MBWR coefficients with the removal of PT anomalies

Eqn.	A	B	C	D	F	AAD_P
WAG	-7.21	1.84	-3.28	8.03		0.0334
MBWR	-7.19	1.82	-1.12	-9.82	88.18	0.0325

With the removal of the 3 temperatures which were highlighted to be anomalies, it can be seen that the AAD_P, for all 4 equation fittings improve drastically. Hence, the removal of these readings can be justified. The trend in errors for the CC and AT equations still remain the same, where the largest errors still occur at larger temperatures and pressures. Whilst the absolute percentage errors (|ΔP Perc.|) for the WAG and BWR equations are all less than 0.15%, whilst the |ΔP Perc.| values for the CC and AT equations fall below 0.99%. (Processed data provided in Appendix Table A-3 to A-6)

It is also interestingly noted that the CC and AT fitting coefficients did not change from their previous state, even though the fitting error was reduced.

Now that the relationship between the PT data or the vapor pressure curve is provided using 4 equations (CC, AT, WAG and BWR), the fittings and respective coefficients can be used to calculate the either the Saturation Pressure or Temperature, at a given point. It also allows the calculation of other parameters, such as the acentric factor (ω) which will be essential for calculating Vapor-Liquid Equilibrium (VLE). The calculation and use of this parameter will be explained in the next section, under the VLE fittings.

3.3.5 Vapor-Liquid Equilibrium (VLE)

The purpose of finding the Vapor-Liquid Equilibrium (VLE), is to be able to use an equation of state to describe the behavior of the refrigerant when it is in the 2-phase region. Unlike, the simpler fitting carried out in the previous section, the equation used here will not only depend on temperature, but will also depend on volume.

$$P\,(T\,,V\,) \qquad (3.3\text{-}9)$$

In order to carry out the fitting, the approach applied is called the "Flash Method" for pure components. This method had been described in literature [192], [198] and is readily available in Chemical Engineering Books. The EOS used in for this work will be a cubic EOS, called the Peng-Robinson EOS [260]. It has been used by many researchers [165], [261] to deriving VLE properties and is considered as a good starting point for accurate VLE behavior prediction.

$$P=\frac{RT}{v-b}-\frac{a\times T}{v(v+b)+b(v-b)} \qquad (3.3\text{-}10)$$

3.3.5.1 PR EOS Terms

The Peng-Robinson Pressure P_{PR}, depends on several parameters including *R, T, v, a* and *b*. These are defined accordingly [260],

$$R = \text{Molar Gas Constant} = 8.314472\ \frac{kJ}{kmol.K}$$

$$T = T_{Exp}$$

$$v = \text{Molar Volume}\ \left(\frac{m^3}{kmol}\right)$$

$$\omega = \text{Acentric Factor}$$

a in itself is dependent on another 2 functions, given below,

$$a(T) = a(T_C) \cdot \alpha(T_R, \omega) \quad (3.3\text{-}11)$$

$$a(T_C) = 0.45724 \frac{R^2 T_C{}^2}{P_C} \quad (3.3\text{-}12)$$

$$\alpha = \left(1 + \kappa(1 - \sqrt{T_r})\right)^2 \quad (3.3\text{-}13)$$

$$T_r = \frac{T}{T_C} \quad (3.3\text{-}14)$$

$$\kappa = 0.37464 + 1.54226\ \omega - 0.26992\ \omega^2 \quad (3.3\text{-}15)$$

b is equal at all temperature to the value at critical temperature,

$$b(T) = b(T_C) \quad (3.3\text{-}16)$$

$$b(T_C) = 0.07780 \frac{RT_C}{P_C} \quad (3.3\text{-}17)$$

As it is evident, the PR EOS and its coefficients, require some information such as the Critical Parameters (T_C, P_C) of the refrigerant and the Acentric Factor (ω). The critical parameters have been determined via experiment and are presented below,

$$T_C = 348.72\ K$$

$$P_C = 5174.46\ kPa$$

3.3.5.2 Acentric Factor Determination

As for the acentric factor, it can be determined using the following formula, at certain condition defined at $T_r = 0.7$ [210].

$$\omega = -1 - \log\left[\frac{P}{P_C}\right]_{T_r=0.7} \quad (3.3\text{-}18)$$

$$T_r = \frac{T}{T_C} = 0.7 \quad (3.3\text{-}19)$$

As it can be seen, the Vapor pressure at a temperature of $T = 0.7\ T_C = 244.104$ K, is required to determine the acentric factor. Since, the experimental data are only available till 250 K, the previously determined vapor pressure curves using the 4 models (CC, AT, WAG, BWR) will hence be utilized, to determine the pressure at this temperature. This will provide us with 4 different acentric factors shown in Table 3.3-14 and Table 3.3-15 (Set 1: For all PT data and Set 2: For the PT data with anomalies removed).

Set 1: Full PT Data Set

Table 3.3-14 The acentric factor calculated for the CC, AT, WAG and MBWR equations based on the vapor pressure curves for all PT data points

Eqn.	CC	AT	WAG	MBWR
ω	0.24144	0.24195	0.24285	0.24289

Set 2: Anomalies Removed PT Data Set (270K, 280K and 300K Removed)

Table 3.3-15 The acentric factor calculated for the CC, AT, WAG and MBWR equations based on the vapor pressure curves for the PT data points with anomalies removed

Eqn.	CC	AT	WAG	MBWR
ω	0.24144	0.24195	0.24267	0.24233

It is noticed that ω_{CC} and ω_{AT} for the CC and AT equations do not change, for both data sets. This was expected since, the coefficients of these equations remained the same, even though the AAD_P reduced. However, the WAG and MBWR equations give 2 different ω_{WAG} *and* ω_{MBWR} due to their differences in fitting coefficients for the 2 data sets.

Using these 4 acentric factors (ω_{CC} ,ω_{AT} ,ω_{WAG},ω_{MBWR}) for both sets of data (Set 1: All Temperatures and Set 2: With the removal of 270K, 280K and 300K), the VLE fitting for the PR EOS is carried out, using the isofugacity condition. However, since the latter 4 acentric factors are based on more accurate vapor pressure curves, their results are will be explored further. The fitting using Set 1 which includes the anomalies will not be presented in extensive for, but the final AAD_P for these calculations will be shown.

The fugacity for the PR EOS, if given in its general form as see in Equation 3.3-20.

$$\ln\frac{f}{P} = Z - 1 - \ln(Z - B) - \frac{A}{2\sqrt{2}B}\ln\left(\frac{Z + 2.414B}{Z - 0.414B}\right) \qquad (3.3\text{-}20)$$

$$Z = \frac{Pv}{RT} \qquad (3.3\text{-}21)$$

$$A = \frac{aP}{R^2T^2} \qquad (3.3\text{-}22)$$

$$B = \frac{bP}{RT} \qquad (3.3\text{-}23)$$

The isofugacity is determines as shown below.

$$f^L - f^V < \xi \qquad (3.3\text{-}24)$$

$$\xi = 1\times10^{-11}$$

The accuracy of the fitting can be compared through the differences in pressures for the fitting curve P_{Fit} and the experimental pressure P_{Exp}, represented by the Pressure Error ΔP (kPa) and in the Percentage form as ΔP *Perc.* (%).

3.3.5.2.1 ω_{CC} VLE Derivation

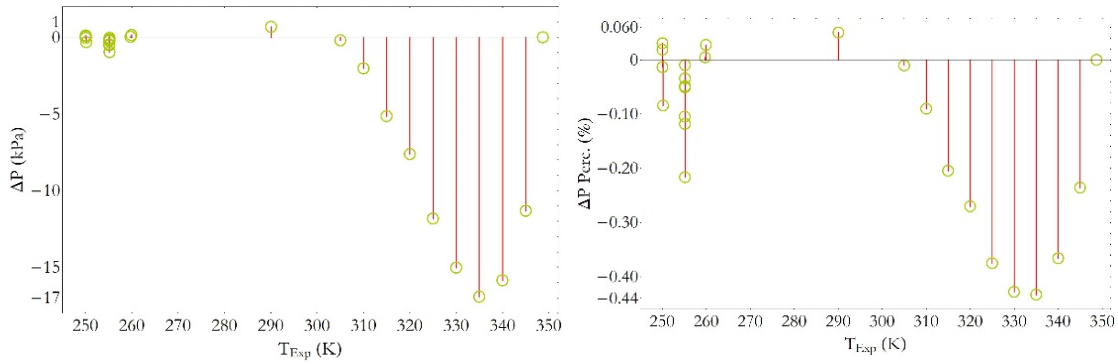

Figure 3.3-8 The fitting errors for VLE derivations using the CC acentric factor

3.3.5.2.2 ω_{AT} VLE Derivation

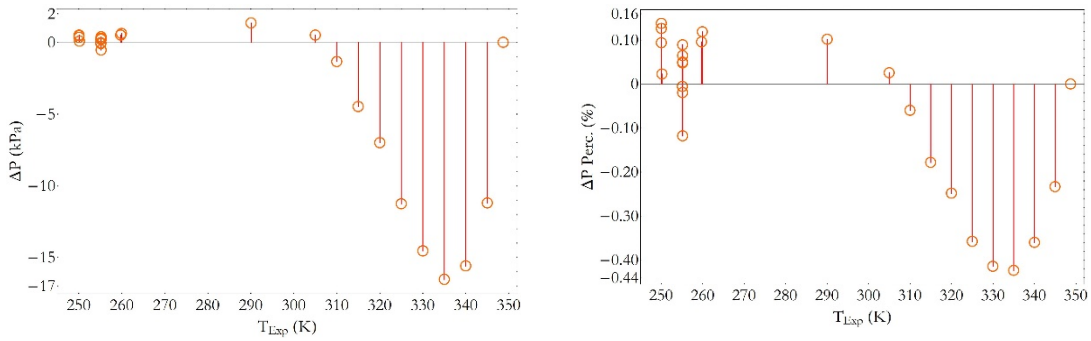

Figure 3.3-9 The fitting errors for VLE derivations using the AT acentric factor

3.3.5.2.3 ω_{WAG} VLE Derivation

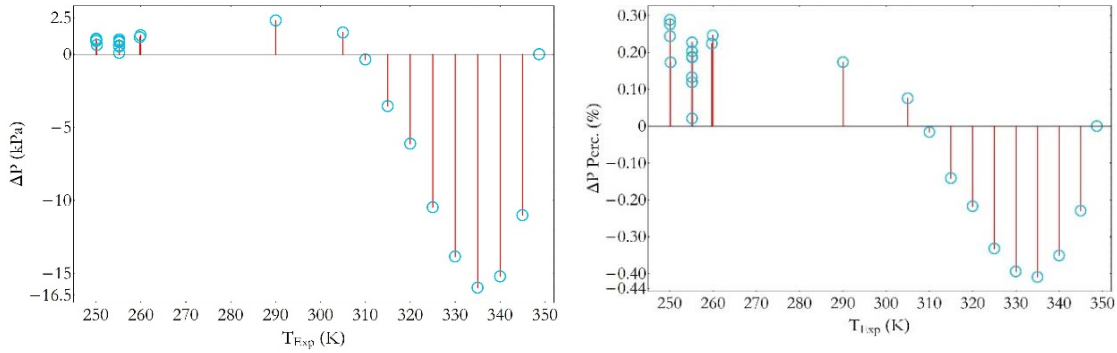

Figure 3.3-10 The fitting errors for VLE derivations using the WAG acentric factor

3.3.5.2.4 ω_{BWR} VLE Derivation

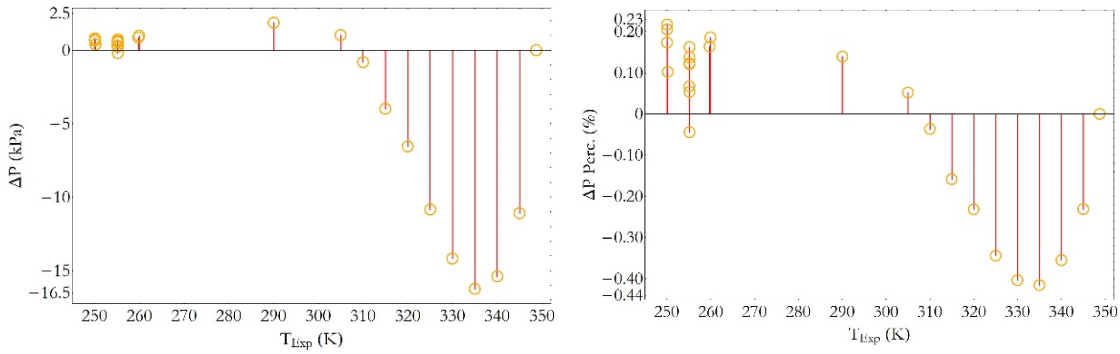

Figure 3.3-11 The fitting errors for VLE derivations using the MBWR acentric factor

3.3.5.3 PR EOS VLE Absolute Average Deviation in Pressure (AAD_P)

The calculated pressures $P_{Calc,CC}$, $P_{Calc,AT}$, $P_{Calc,WAG}$, $P_{Calc,MBWR}$ are given in the Appendix, together with ΔP and ΔP Perc. (%). In Table 3.3-17 andT Table 3.3-19 the AAD_P for each VLE Derivation using the 4 acentric factors (ω_{CC}, ω_{AT}, ω_{WAG}, ω_{MBWR}) are shown.

Set 1: Full PT Data Set

Table 3.3-16 The calculated acentric factors based on the initial vapor pressure fitting for all data points, using the four equations CC, AT, WAG and MBWR

Eqn.	CC	AT	WAG	MBWR
ω	0.24144	0.24195	0.24285	0.24289

Table 3.3-17 The AAD_P for the PR EOS VLE derivations using all PT data points and the respective acentric factors

Eqn.	CC	AT	WAG	MBWR
AAD_P	0.2345	0.2412	0.2989	0.3021

Set 2: Anomalies Removed PT Data Set (270K, 280K and 300K Removed)

Table 3.3-18 The calculated acentric factors based on vapor pressure fitting with anomalies removed for the four equations CC, AT, WAG and MBWR

Eqn.	CC	AT	WAG	MBWR
ω	0.24144	0.24195	0.24267	0.24233

Table 3.3-19 The AAD_P for the PR EOS VLE derivations using PT data points with anomalies removed and the respective acentric factors

Eqn.	CC	AT	WAG	MBWR
AAD_P	0.1345	0.1413	0.2029	0.1718

Using the final results, it is possible to see that for the VLE derivation using the PR EOS, the Absolute Average Deviation in Pressure $AAD_{P,CC}$ and $AAD_{P,AT}$ calculated using the ω_{CC} and ω_{AT} from the CC and AT equations, show the lowest values. The ω_{WAG} and ω_{MBWR} acentric factors, seem to cause larger deviations in the VLE predictions, since their $AAD_{P,WAG}$ and $AAD_{P,MBWR}$, are higher. This is true for both scenarios of Set 1: Full data fitting and Set 2: Anomalies removed.

In order to determine the equation which provides the best fit for the current research work, only the Set 2 data which has the anomalies removed will be used. This is justifiable since the AAD_P, of all four fittings has improved in comparison to using all the PT data.

Hence based on Set 2, it is noticed that the CC and AT equations are better at representing the new refrigerant, rather than the WAG and BWR equations because they provide lower AAD_P for the VLE calculations. Though this is true, the simple CC and AT equations did provide higher errors for the vapor pressure curve fittings, especially within the high temperature range. Arguing that the CC and AT equations can better represent this refrigerant will not be possible based on this. However, it is necessary to look into the entire process and the exact values of the AAD_P.

In the initial step for finding the vapor curve fitting using the pressure temperature (PT) data, the WAG and BWR equations showed a much higher accuracy in fitting, since the AAD_P were much lower at $AAD_{P,WAG} = 0.0334$ and $AAD_{P,MBWR} = 0.0325$,whereas the CC and AT equations only had and AAD_P of $AAD_{P,CC} = 0.1546$ and $AAD_{P,AT} = 0.1519$. Hence, for the vapor pressure curve, the WAG and BWR provide a superior fitting, especially in

a large temperature range, up until the critical temperature. The CC and AT equations suffer from larger errors towards the critical region, and their AAD_P was hence larger.

Now these vapor pressure curves are used for estimating the 4 acentric factors ω_{CC}, ω_{AT}, ω_{WAG}, ω_{MBWR}. Using these 4 acentric factors, it was possible to find the VLE conditions, by considering isofugacity. The most important condition in the PR EOS VLE derivation is to meet the isofugacity which justifies the equilibrium between the vapor and liquid states of the refrigerant. Since the isofugacity is already achieved for all 4 fitting, the AAD_P for the PR EOS fitting, can be used to ascertain whether the data is reliable, and if the fitting falls within an acceptable range.

Since this is a new refrigerant, there is no literature to compare the AAD_P for the VLE fitting, however, based on previous fittings in literature for different refrigerants, it can be seen that they range between values of 0.05 – 0.95 for the Carnahan – Starling – de Santis (CSD) EOS for a binary mixture of R32 + R134a [192], 0.001 – 3.520 for the mixture of R32 + R236ea [262] and from the review work carried out on VLE fitting with the PR EOS for numerous mixtures, the average AAD_P was between 0.15 – 4.19 [227]. Thus, the current fitting using the 4 acentric factors and the PR EOS do seem to represent the VLE behavior of the new refrigerant with acceptable accuracy.

It was noticed from the Figures 3.3.5.4.1 – 4 showing the pressure errors for the VLE, that a majority of the larger errors were located with the high temperature region. Hence the error distributions, could suggest some larger uncertainties for those readings, which were unfortunately not examinable, since they were only available as processed data.

The final recommendation of which equation should be used to represent the Vapor Pressure and potentially be used for acentric factor calculations can be divided into two scenarios. Firstly, if the vapor pressure curve fitting from low temperature up to the critical point is considered together with the VLE derivation, the MBWR equations provided that least errors in pressure across full larger temperature range, whilst also giving an adequate VLE fitting with and AAD_P of 0.1718.

However, in the scenario that there might be some uncertainty into the exact representation of the high temperature section, the simpler CC equation would provide a better fitting with respect to the Vapor pressure curve and the VLE.

3.3.6 Specific Molar Volume *v* for HFO-1132(E)

One of the other features of the PR EOS VLE derivation is the ability to determine specific molar volume, v (m^3/kmol) of the refrigerant. Due to the existence of VLE, both liquid and vapor specific molar volumes, v_L and v_V are calculated in the 2-phase region (Figure 3.3-12). The calculated v is also compared with the experimental value provided at the critical point.

$$v_C = 0.1479 \frac{m^3}{kmol}$$

Table 3.3-20 The specific molar volume comparison for the PR EOS derived v and the experimentally measured v_c

Molar Mass (kg/kmol)	ϱ_C (kg/m^3)	T_C (K)	P_C (kPa)	v_C (m^3/kmol)	$v_{C,PR}$ (m^3/kmol)	Δv_C (m^3/kmol)	Δv_C Perc. (%)
64.03	433.10	348.72	5174.46	0.1479	0.1801	-0.0322	-21.81

Though the error for the specific critical molar volume is high, there still needs to be sufficient experimental data to ascertain the overall specific molar predictions for pressure range below the critical point. This could be a potential area of research for the future work section.

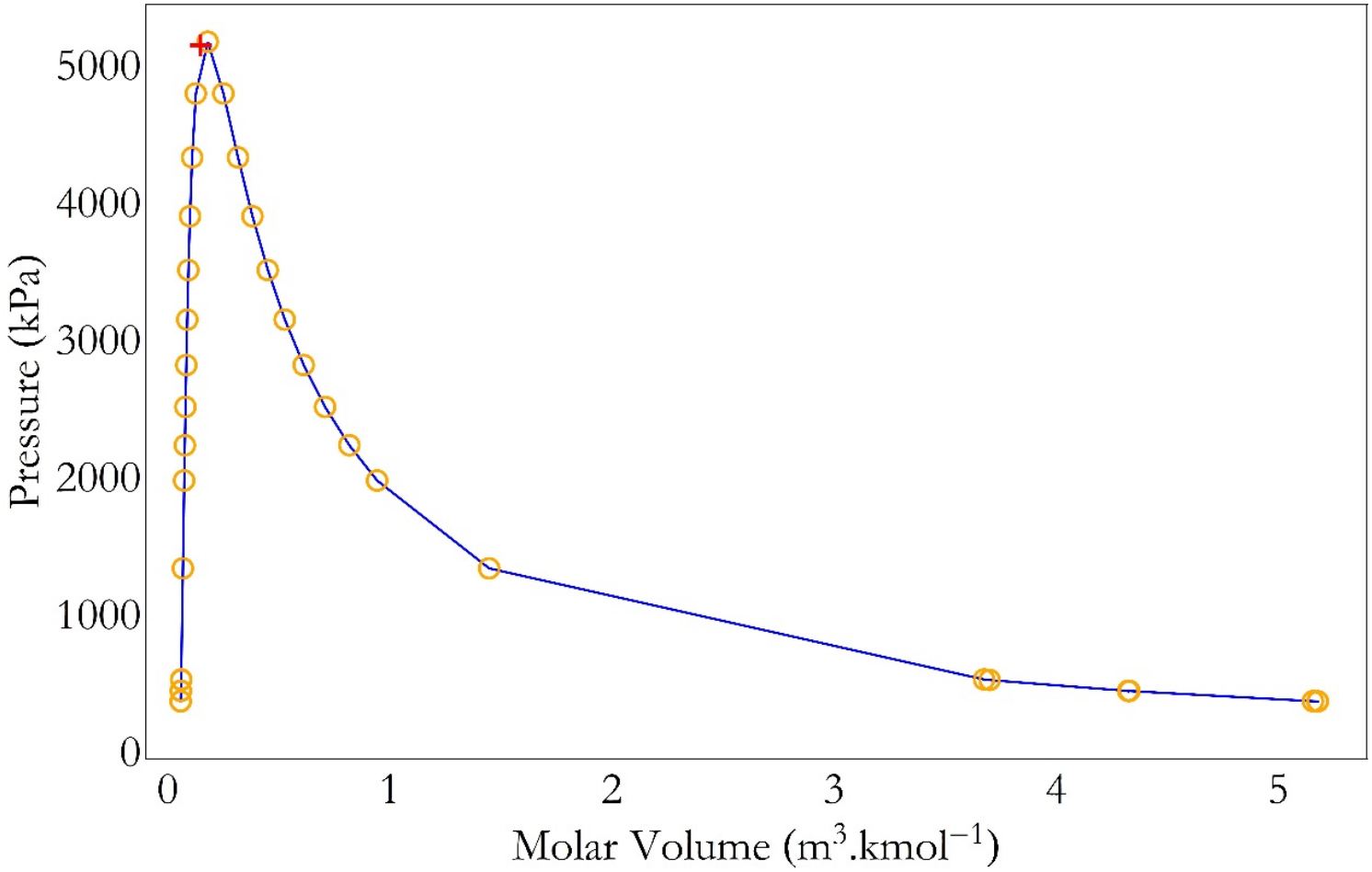

Figure 3.3-12 The PR EOS derived pressure versus specific molar volume for R1132(E) together with the critical specific volume v_c from experimental measurements (+)

3.4 Conclusion

The thermophysical property measurements for the newly developed R-1132(E) refrigerant has been begun with the vapor pressure measurements. These measurements were carried out using an isochoric set up which is able of operating for a temperature of 250 – 300K. The measure Pressure and Temperature (PT) data were then used to fit the vapor pressure curves based on 4 models. The fitting process was begun with the simplest Clausius – Clapeyron Equation (CC), then developed to the Antoine Equation (AT). After which the Wagner Equation (WAG and Modified - Benedict – Webb – Rubin Equations (MBWR) were also employed.

The fitting errors were represented through the Absolute Average Deviation in Pressure (AAD_P), which showed the lowest values for the MBWR, then the WAG, followed by the AT and CC equations.

Based on these fittings, the acentric factors were calculated, giving ω_{CC}, ω_{AT}, ω_{WAG} and ω_{MBWR}. Using these four acentric factors, the derivation of the Vapor – Liquid Equilibrium (VLE) were carried out using the Cubic Peng – Robinson (PR) Equation of State (EOS). Once again the error in derived VLE, were represented through the AAD_P. The AAD_P showed an opposite trend, where the simpler equations provided a better fit.

$$AAD_{P,CC} < AAD_{P,AT} < AAD_{P,MBWR} < AAD_{P,WAG}$$

This suggested two possible conclusions. Firstly, if both the vapor pressure curve fitting together with the VLE derivation for the wide range from 250 – 350K was considered, the MBWR seemed to provide the best fittings.

However, if more weight was placed on the VLE derivation as well as the lower temperature region of the vapor pressure curve, the simpler CC seemed to provide the best fit.

The PR EOS was also used for the calculation of the liquid and vapor specific molar volumes for the experimental temperature and pressure conditions. The critical point specific molar volume showed a somewhat large deviation from that of the PR EOS predicted value. However, the lack of experimental data with regard to the molar volumes prevented the comparison of the PR EOS predictions.

This work has allowed has presented the initial Pressure - Temperature data for the newly developed R1132(E) as well the VLE derivations using the PR EOS. The future work section will propose the next stage for the improving these results as well as contributing to the thermophysical property identification of R1132(E).

CHAPTER 4 GENERAL CONCLUSION

4.1 Vapor Compression Cycle Analysis

The analysis of the vapor compression cycle using R410a under the AHRI standard allowed the determination of the optimum cooling capacity of 1.4 kW and the optimum charge of 0.70 kg. These were validated through the behavioral analysis of the COP. Second law analysis allowed a further insight in to the occurrences of losses or irreversibilities within the components of the chiller. The results obtained can be further used as a baseline for comparing potential low GWP refrigerants and mixtures. This work is proposed to be carried out in order to determine a suitable refrigerant or mixture to replace R410a and other high GWP refrigerants in HVAC&R systems, particularly focusing on chillers.

4.2 Pressure – Temperature (PT) Thermophysical Property Measurements

The analysis of the Pressure – Temperature (PT) thermophysical properties of the newly developed refrigerant R1132(E) were conducted for temperatures ranges between 250-300K as well as 300-T_C . The results obtained were then analyzed for the fitting of the vapor pressure curves using the Clausius – Clapeyron, Antoine, Wagner and Modified – Benedict-Webb-Rubin (MBWR) equations. The vapor pressure curves were then used to calculate the acentric factor which was utilized for deriving the Vapor – Liquid Equilibrium for the new refrigerant. The Clausius - Clapeyron equation seemed to provide a better fit for the lower temperature ranges, whilst the MBWR equation was determined to provide a better fit when considering both the vapor pressure fitting and the VLE fitting. Continue studies on the properties of this refrigerant are required to hopefully introduce it as a Next Generation Refrigerant with low GWP and high performance. Some of the possible improvements to the methodology of measuring these properties is also presented in the next section.

CHAPTER 5 FUTURE WORKS

In this section, the author will compare two of the isochoric setups that have been used by the author for gathering Pressure – Temperature (PT) data and identify certain limitations in them and propose a third setup which hopes to overcome these issues.

The two experimental setups that have been studied are located at the NEXT-RP laboratory at I^{2}CNER and at the Polytechnic University of Marche (UNIVPM), Ancona, Italy

5.1.1 Setup 1 – NEXT-RP, I^{2}CNER

The isochoric setup which has been utilized for the experimental results provided in Chapter 3 of this work is catered towards measuring the Pressure – Temperature (PT) properties of refrigerants at low temperatures.

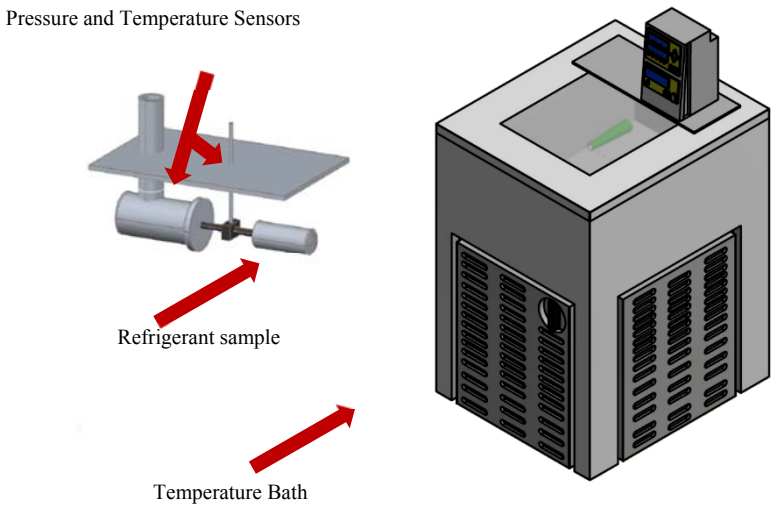

Figure 4.2-1 3D Model of the experimental setup at NEXT-RP Laboratory, I^{2}CNER

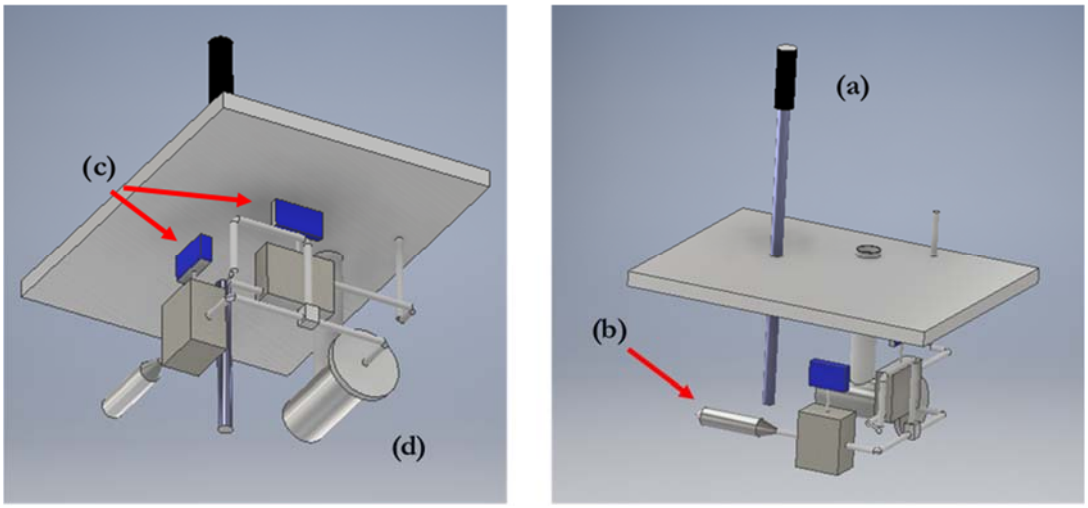

Figure 4.2-2 A closer look at the isochoric setup; (a) Pt Resistance Thermometer; (b) Isochoric Cell; (c) Valves which are hard to access; (d) Pressure Transducer

Table 4.2-1 The benefits and limitation of the isochoric PT experimental setup at NEXT-RP

Benefits	Limitations
The measurement of low temperature ranges from 240 – 310 K	The access to the valves are hindered by the layout of the setup
The smaller size of the isochoric setup allows easier mobility	The air gap between the pressure sensor and thermofluid cause temperature irregularities and condensation
The simple structure makes repair work and adjustments easier	The smaller size of the thermal bath provides less thermal stability
Automatic data recording using LabView	The lack of a larger top layer of insulation might cause larger heat leaks
More accurate refrigerant charge amount measurements	The vibrations of the thermal bath due to operation of compressor for cooling transfer to the sensors as well

5.1.2 Setup 2 – UNIVPM, Ancona

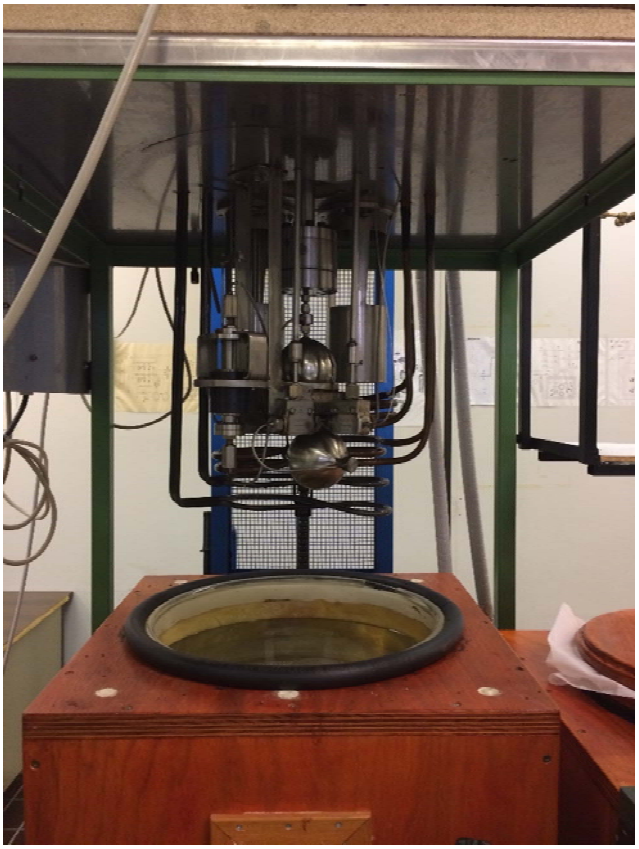

Figure 4.2-3 Photographs of the experimental setup at the UNIVPM, Ancona

Table 4.2-2 The benefits and limitations in the isochoric PT experimental setup at UNIVPM

Benefits	Limitations
The larger thermal bath provides better temperature stability	The pressure sensor require the manual operation of a 'Null Indictor' since it is a differential pressure transducer
The insulation around the thermal bath as well as on top of it, provide better thermal stability	The data recording process is manual
The tube fittings are not unfastened for refrigerant charging and hence will not be prone to leaks	The system cannot be moved due to its size
The calibration process for the pressure sensor is difficult	The access to tubes and fittings is difficult as well
	The lack of using Liquid Nitrogen for liquefying the refrigerant during charge might result in errors in mass charged

5.1.3 Setup 3 – Newly Proposed Isochoric Setup

Based on the benefits and limitations of both the previously studied setups and initial proposal for a new isochoric setup is given below.

Table 4.2-3 Proposals for overcoming the limitations in the isochoric PT experimental setup

Limitations	Solution
The access to the valves are hindered by the layout of the setup	Create a more simplistic and easily accessible layout
The air gap between the pressure sensor and thermofluid cause temperature irregularities and condensation	Use gap filler or thermal material to remove the air gap and prevent condensation around the pressure transducers [263]
The smaller size of the thermal bath provides less thermal stability	Increase the volumetric capacity of the thermal bath, either by directly using a larger volume bath, or by circulating liquid between two baths
The lack of a larger top layer of insulation might cause larger heat leaks	Add proper insulative material to top layer, which can follow a similar layout to that of the Italian setup, where the top layer is not removable and movable
The vibrations of the thermal bath due to operation of compressor for cooling transfer to the sensors as well	Have the thermal bath separate from the thermal tank in which the isochoric setup is places
The pressure sensor require the manual operation of a 'Null Indictor' since it is a differential pressure transducer	Use a digital pressure sensor which is submersible such that there will be no air gaps and can also provide the required automatic data readings possible through wireless connectivity [264]
The data recording process is manual	Use a similar LabView software of the NEXT-RP setup
The system cannot be moved due to its size	Make the system the same size as the current NEXT-RP setup, however with the inclusion of the larger thermal baths and easier access
The access to tubes and fittings is difficult as well	The simple layout should provide the best results to avoid this
The lack of using Liquid Nitrogen for liquefying the refrigerant during charge might result in errors in mass charged	By utilizing a smaller setup, this would still be possible
Some refrigerant properties are required at lower temperatures	Possibly utilize a lower temperature thermal bath which can cool below 250K

The circulation of liquid with the pump and nozzle will cause eddies and also disturbances to the PT readings	Use a cooling coil instead together with stirrers which would be easier to control and reduce any unwanted vibrations or movements
The temperature measurements are limited to the isothermal condition between the thermal fluid and the refrigerant	Include a second temperature sensor within the isochoric cell for a secondary temperature reading
The inability to see the existence of the 2 phase or the amount of refrigerant within the isochoric cell to notice any abnormal behavior or saturation states	Install an optical cell within the isochoric cell

This proposed setup will then be utilized for testing new refrigerant properties and also to test in-house mixed refrigerants with low GWP which will then be tested in the chiller for cycle analysis as a drop-in refrigerant. This would allow the testing of the refrigerant from the fundamental thermophysical properties, up to the practical cycle analysis.

Nomenclature

AAD_P	Absolute Average Deviation in Pressure
AHRI	Air Conditioning Heating & Refrigeration Institute
AT	Antoine
CC	Clausius – Clapeyron
CFC	ChloroFluoroCarbon
CO_2	CarbonDioxide
COP	Coefficient of Performance [-]
$\dot{E}$ / X	Exergy [W]
EB	Energy Balance [-]
$\dot{E}_D$ / $X_{destruction}$	Exergy Destruction [W]
EER	Energy Efficiency Ratio [BTU/Wh]
EOS	Equation of State
EU	European Union
f	Fugacity [kPa]
GWP	Global Warming Potential
h	Enthalpy [kJ/kg]
HCFC	HydroChloroFluoroCarbon
HFC	HydroFluoroCarbon
HFO	HydroFluoroOlefin
HVAC&R	Heating Ventilation Air Conditioning and Refrigeration
MBWR	Modified – Benedict – Web – Rubin
MVC	Mechanical Vapor Compression
ODP	Ozone Depletion Potential
P	Pressure [kPa]
PFC	PerFluoroCarbon
PR	Peng – Robinson
PT	Pressure Temperature
Q / q	Heat [J] / Mass Specific Heat [J/kg]
T	Temperature [K]
T_{avg}	Average Temperature

U	Expanded Uncertainty
u_c	Combined Uncertainty
UN	United Nations
UV	Ultra Violet
v	Specific Molar Volume [m^3/k.mol]
W / w	Work [J] / Mass Specific Heat [J/kg]
WAG	Wagner
η_{Ex}	Exergetic Efficiency [-]

Superscripts

L	Liquid
V	Vapor

Subscripts

avg	Average
C	Critical Point
CH	Chilled Water
Comp	Compressor
Cond	Condenser
CV	Control Volume
CW	Cooling Water
e	Exit
Evap	Evaporator
Exp	Experimental
Exp	Expansion
f	flow
H	High Temperature
HP	Heat Pump
i	Inlet
In/in	Input
L	Low Temperature
Net	Net (Input - Output)
o	Outlet
R	Refrigeration

Greek Letters

ε	Minimum Deviation / Error $1X10^{-11}$
η	Efficiency [-]
ϱ	Density [kg/m^3]
ω	Acentric Factor [-]

References

[1] M. STRAUSS, "12 Theories of How We Became Human, and Why They're All Wrong," *National Geographic*, Sep-2015. [Online]. Available: https://news.nationalgeographic.com/2015/09/150911-how-we-became-human-theories-evolution-science/. [Accessed: 30-Jul-2019].

[2] "Periods - Timeline," *Timeline Index*. [Online]. Available: http://www.timelineindex.com/content/select/612/44,1573,612. [Accessed: 30-Jul-2019].

[3] T. Hatton, "Quantifying the impact of smoke pollution on health in the 19th century," *VOX*, 2017. [Online]. Available: https://voxeu.org/article/smoke-pollution-and-health-19th-century. [Accessed: 30-Jul-2019].

[4] "Global Warming," *NASA*, 03-Jun-2010. [Online]. Available: https://earthobservatory.nasa.gov/features/GlobalWarming/page2.php. [Accessed: 30-Jul-2019].

[5] "Carbon Dioxide | Vital Signs – Climate Change: Vital Signs of the Planet," *NASA*. [Online]. Available: https://climate.nasa.gov/vital-signs/carbon-dioxide/. [Accessed: 30-Jul-2019].

[6] H. Riebeek, "The Carbon cycle," *NASA*, 2011. [Online]. Available: https://earthobservatory.nasa.gov/features/CarbonCycle.

[7] "Graphic: The relentless rise of carbon dioxide – Climate Change: Vital Signs of the Planet," *NASA*. [Online]. Available: https://climate.nasa.gov/climate_resources/24/graphic-the-relentless-rise-of-carbon-dioxide/. [Accessed: 30-Jul-2019].

[8] "World Population Prospects - Population Division - United Nations," *United Nations*. [Online]. Available: https://population.un.org/wpp/DataQuery/. [Accessed: 30-Jul-2019].

[9] J. Varrasi, "Global Cooling : The History of Air Conditioning," *ASME*, 2012. [Online]. Available: https://www.asme.org/engineering-topics/articles/technology-and-society/global-cooling-the-history-of-air-conditioning.

[10] United Nations Environmental Programme, "UN Environment: Programme Performance Report," 2019.

[11] "Heating and cooling | Energy," *European Commission*. [Online]. Available: https://ec.europa.eu/energy/en/topics/energy-efficiency/heating-and-cooling. [Accessed: 30-Jul-2019].

[12] Y. A. Cengel, M. A. Boles, and M. Kanoglu, *Thermodynamics: An Engineering Approach*, Ninth Edit. McGraw-Hill Education.

[13] "COPs, EERs, and SEERs," *Power Knot*. [Online]. Available: http://www.powerknot.com/2011/03/01/cops-eers-and-seers/. [Accessed: 30-Jul-2019].

[14] "Chiller Application Guide - Fundamentals of Water and Air Cooled Chillers," 2014.

[15] "What Is A Ton of Refrigeration? – Power Knot," *Power Knot*. [Online]. Available: http://www.powerknot.com/2010/06/06/what-is-a-ton-of-refrigeration/. [Accessed: 30-Jul-2019].

[16] "Image: Mini Split Type Air Conditioner," *Mitchell Heating DC*. [Online]. Available: http://www.mitchellheatingdc.com/wp-content/uploads/2018/04/minisplit.png. [Accessed: 30-Jul-2019].

[17] "Image: Chiller," *Daikin*. [Online]. Available: https://www.daikin.com.vn/medias/images/product/ca1733b0-b89c-11e7-b5cb-0f837dcb396a.png. [Accessed: 30-Jul-2019].

[18] "Image: Absoprtion Chiller," *York*. [Online]. Available: http://www.york.com/-/media/york/absorption-chillers/yhaucej-multi-energy.png?la=en&hash=820EE2C78A349C02D6152D8BDBE658990D54E00B. [Accessed: 30-Jul-2019].

[19] "Image: District Cooling System." [Online]. Available: https://s3.amazonaws.com/user-media.venngage.com/468990-058216e7380e3aef0e86babe6bebc6f4.gif. [Accessed: 30-Jul-2019].

[20] "Image: Refrigerator," *IKEA*. [Online]. Available: https://www.ikea.com/PIAimages/0530525_PE646733_S5.JPG. [Accessed: 30-Jul-2019].

[21] "Image: Cooling Cabinet." [Online]. Available: http://s3-us-west-2.amazonaws.com/static.trip-n-travel.com/wp-content/uploads/2016/05/27150952/3106008069_db9655d014_o-800x600.jpg. [Accessed: 30-Jul-2019].

[22] J. M. Calm, "The next generation of refrigerants – Historical review, considerations, and outlook," *Int. J. Refrig.*, vol. 31, no. 7, pp. 1123–1133, Nov. 2008.

[23] J. Thomas Midgley and A. L. Henne, "Organic fluorides as refrigerants," *Ind. Eng. Chem.*, vol. 22, no. 5, pp. 542–545, 1930.

[24] "History of Chlorofluorocarbons," 1987.

[25] M. J. Molina and F. S. Rowland, "Stratospheric sink of chlorofluoromrthanes: Chlorine atom-catalyzed destruction of ozone," *Nature*, vol. 249, no. 6, p. 810, 1974.

[26] Institute for Governance & Sustainable Development, "Scientists Confirm Ozone Layer Healing Thanks to Montreal Protocol," *CCACO*, 2018. [Online]. Available: https://ccacoalition.org/en/news/scientists-confirm-ozone-layer-healing-thanks-montreal-protocol. [Accessed: 30-Jul-2019].

[27] R. Samson, "NASA Study: First Direct Proof of Ozone Hole Recovery Due to Chemicals Ban," *NASA*, 2018. [Online]. Available: https://www.nasa.gov/feature/goddard/2018/nasa-study-first-direct-proof-of-ozone-hole-recovery-due-to-chemicals-ban. [Accessed: 30-Jul-2019].

[28] "Climate change evidence: How do we know?," 2019. [Online]. Available: https://climate.nasa.gov/evidence.

[29] "All about the ozone and the ozone layer," *UN Environment*. [Online]. Available: https://ozone.unep.org/ozone-and-you. [Accessed: 30-Jul-2019].

[30] "Handbook for the Vienna Convention for the Protection of the Ozone Layer (1985)," 2018.

[31] "Handbook for the Montreal Protocol on Substances that Deplete the Ozone Layer," 2019.

[32] C. Nunez, "What is global warming, explained," *National Geographic*, 2019. [Online]. Available: https://www.nationalgeographic.com/environment/global-warming/global-warming-overview/. [Accessed: 30-Jul-2019].

[33] UN Secretary General, "Statement by the Secretary-General on the IPCC Special Report Global Warming of 1.5 ºC," *UN*, 2018. [Online]. Available: https://www.un.org/sg/en/content/sg/statement/2018-10-08/statement-secretary-general-ipcc-special-report-global-warming-15-ºc. [Accessed: 30-Jul-2019].

[34] "About Montreal Protocol," *UN Environment*. [Online]. Available: https://www.unenvironment.org/ozonaction/who-we-are/about-montreal-protocol. [Accessed: 16-Mar-2019].

[35] "NASA Ozone Watch: Latest status of ozone," *NASA | Goddard Space Flight Center*, 2019. [Online]. Available: https://ozonewatch.gsfc.nasa.gov/. [Accessed: 30-Jul-2019].

[36] "What is the Kyoto Protocol?," *UNFCCC*. [Online]. Available: https://unfccc.int/kyoto_protocol. [Accessed: 30-Jul-2019].

[37] "PARIS AGREEMENT," 2015.

[38] "The Paris Agreement," *UNFCCC*, 2018. [Online]. Available: https://unfccc.int/process-and-meetings/the-paris-agreement/the-paris-agreement. [Accessed: 30-Jul-2019].

[39] "Nationally Determined Contributions (NDCs)," *UNFCCC*. [Online]. Available: https://unfccc.int/process-and-meetings/the-paris-agreement/nationally-

determined-contributions-ndcs. [Accessed: 30-Jul-2019].

[40] F. Leone, "Kigali Amendment Enters into Force, Bringing Promise of Reduced Global Warming | News | SDG Knowledge Hub," *IISD*, 2019. [Online]. Available: https://sdg.iisd.org/news/kigali-amendment-enters-into-force-bringing-promise-of-reduced-global-warming/. [Accessed: 30-Jul-2019].

[41] "The Montreal Protocol evolves to fight climate change," *UNIDO*. [Online]. Available: https://www.unido.org/our-focus/safeguarding-environment/implementation-multilateral-environmental-agreements/montreal-protocol/montreal-protocol-evolves-fight-climate-change. [Accessed: 30-Jul-2019].

[42] "EU legislation to control F-gases," *European Commission*. [Online]. Available: https://ec.europa.eu/clima/policies/f-gas/legislation_en. [Accessed: 16-Mar-2019].

[43] THE EUROPEAN PARLIAMENT AND THE COUNCIL OF THE EUROPEAN UNION, *DIRECTIVE 2006/40/EC OF THE EUROPEAN PARLIAMENT AND OF THE COUNCIL*. 2006.

[44] "EU MAC Directive," *Linde Gas*. [Online]. Available: http://www.linde-gas.com/en/products_and_supply/refrigerants/environment_and_legislation/global_warming_legislation_hfc_control/eu_mac_directive/index.html. [Accessed: 30-Jul-2019].

[45] *Regulation (EU) No 517/2014 of the European Parliament and of the Council of 16 April 2014 on fluorinated greenhouse gases and repealing Regulation (EC) No 842/2006 Text with EEA relevance*. .

[46] H. Kasahara, "Current status of Japan 's legislation on F-gases and RACHP using Low-GWP Refrigerants," 2018.

[47] A. Meno, "Laws and Regulation for Fluorocarbons in Japan," 2015.

[48] "Natural Refrigerant Equipment in Japan | Revised F-Gas Law in Japan," *Ministry of Environment Japan*. [Online]. Available: http://www.env.go.jp/earth/ozone/hiyasu-waza/eng/revised_f-gas_law_in_japan.html. [Accessed: 30-Jul-2019].

[49] "Montreal Protocol on Substances that Deplete the Ozone Layer," 1987.

[50] "The Kigali Amendment (2016): The amendment to the Montreal Protocol agreed by the Twenty-Eighth Meeting of the Parties (Kigali, 10-15 October 2016) |," *UNEP Ozone Secretariat*. [Online]. Available: https://ozone.unep.org/en/handbook-montreal-protocol-substances-deplete-ozone-layer/41453. [Accessed: 17-Mar-2019].

[51] "About Montreal Protocol | Ozonaction," *UN Environment*. [Online]. Available: https://www.unenvironment.org/ozonaction/who-we-are/about-montreal-protocol. [Accessed: 30-Jul-2019].

[52] Danfoss, “Refrigerant options now and in the future,” no. August, 2012.

[53] “Revised F-Gas Law in Japan,” *Ministry of Environment Government of Japan*. [Online]. Available: http://www.env.go.jp/earth/ozone/hiyasu-waza/eng/revised_f-gas_law_in_japan.html. [Accessed: 16-Mar-2019].

[54] “Refrigeration, Air Conditioning and Heat Pumps Technical Options Committee |Assessment Report,” 2018.

[55] J. M. Calm and P. A. Domanski, “R22 REPLACEMENT STATUS,” *EcoLibrium*, vol. 3, no. November, pp. 18–24, 2004.

[56] “R22 and Halon Critical Use Phase-out.” [Online]. Available: https://www.epa.ie/air/airenforcement/ozone/r22andhaloncriticalusephase-out/. [Accessed: 30-Jul-2019].

[57] “Residential Air Conditioning and the Phaseout of HCFC-22: What You Need to Know.”

[58] “EU F-gas Regulation: Ready for the future HVAC-R Market,” 2012.

[59] “AHRI Standard 551/591 (SI),” 2018.

[60] “Air conditioning use emerges as one of the key drivers of global electricity-demand growth,” *IEA*, 2018. [Online]. Available: https://www.iea.org/newsroom/news/2018/may/air-conditioning-use-emerges-as-one-of-the-key-drivers-of-global-electricity-dema.html. [Accessed: 30-Jul-2019].

[61] Y. Xu, D. Zaelke, G. J. M. Velders, and V. Ramanathan, “The role of HFCs in mitigating 21st century climate change,” *Atmos. Chem. Phys*, vol. 13, pp. 6083–6089, 2013.

[62] J. M. Belman-Flores, J. M. Barroso-Maldonado, A. P. Rodríguez-Muñoz, and G. Camacho-Vázquez, “Enhancements in domestic refrigeration, approaching a sustainable refrigerator – A review,” *Renew. Sustain. Energy Rev.*, vol. 51, pp. 955–968, Nov. 2015.

[63] A. Mota-Babiloni, J. Navarro-Esbrí, Á. Barragán-Cervera, F. Molés, B. Peris, and G. Verdú, “Commercial refrigeration – An overview of current status,” *Int. J. Refrig.*, vol. 57, pp. 186–196, Sep. 2015.

[64] N. Nethaji, T. Mohideen, and M. Nethaji, “Energy conservation in room air conditioner unit by recovering cold energy from condensate,” *Int. J. Refrig.*, vol. 104, pp. 95–102, Aug. 2019.

[65] Z. Zhang, J. Wang, X. Feng, L. Chang, Y. Chen, and X. Wang, “The solutions to electric vehicle air conditioning systems: A review,” *Renew. Sustain. Energy Rev.*, vol. 91, pp. 443–463, Aug. 2018.

[66] G. Fekadu and S. Subudhi, “Renewable energy for liquid desiccants air conditioning system: A review,” *Renew. Sustain. Energy Rev.*, vol. 93, pp. 364–379, Oct. 2018.

[67] R. Jakobs and H. Kruse, “The use of non-azeotropic refrigerant mixtures in heat pumps for energy saving,” *Int. J. Refrig.*, vol. 2, no. 1, pp. 29–32, Jan. 1979.

[68] M. . McLinden and R. Radermacher, “Methods for comparing the performance of pure and mixed refrigerants in the vapour compression cycle,” *Int. J. Refrig.*, vol. 10, no. 6, pp. 318–325, Nov. 1987.

[69] G. Lorentzen, “Ammonia: an excellent alternative,” *Int. J. Refrig.*, vol. 11, no. 4, pp. 248–252, Jul. 1988.

[70] Adrian Bejan and A. Bejan, “Theory of heat transfer-irreversible refrigeration plants,” *Int. J. Heat Mass Transf.*, vol. 32, no. 9, pp. 1631–1639, Sep. 1989.

[71] A. Henatsch and P. Zeller, “Cold air refrigeration machine with mechanical, thermal and material regeneration,” *Int. J. Refrig.*, vol. 15, no. 1, pp. 16–30, Jan. 1992.

[72] G. Lorentzen and J. Pettersen, “A new, efficient and environmentally benign system for car air-conditioning,” *Int. J. Refrig.*, vol. 16, no. 1, pp. 4–12, Jan. 1993.

[73] N. E. Wijeysundera, “Analysis of the ideal absorption cycle with external heat-transfer irreversibilities,” *Energy*, vol. 20, no. 2, pp. 123–130, Feb. 1995.

[74] K. C. Ng, H. T. Chua, W. Ong, S. S. Lee, and J. M. Gordon, “Diagnostics and optimization of reciprocating chillers: theory and experiment,” *Appl. Therm. Eng.*, vol. 17, no. 3, pp. 263–276, Mar. 1997.

[75] L. Chen, C. Wu, and F. Sun, “Steady flow combined refrigeration cycle performance with heat leak,” *Appl. Therm. Eng.*, vol. 17, no. 7, pp. 639–645, Jul. 1997.

[76] S. B. Riffat, C. F. Afonso, A. C. Oliveira, and D. A. Reay, “Natural refrigerants for refrigeration and air-conditioning systems,” *Appl. Therm. Eng.*, vol. 17, no. 1, pp. 33–42, Jan. 1997.

[77] R. Ayala, C. L. Heard, and F. A. Holland, “Ammonia/lithium nitrate absorption/compression refrigeration cycle. Part I. Simulation,” *Appl. Therm. Eng.*, vol. 17, no. 3, pp. 223–233, Mar. 1997.

[78] Y.-M. Chen and C.-Y. Sun, “Experimental study of the performance characteristics of a steam-ejector refrigeration system,” *Exp. Therm. Fluid Sci.*, vol. 15, no. 4, pp. 384–394, Nov. 1997.

[79] F. Meunier, F. Poyelle, and M. D. LeVan, “Second-law analysis of adsorptive refrigeration cycles: The role of thermal coupling entropy production,” *Appl. Therm. Eng.*, vol. 17, no. 1, pp. 43–55, Jan. 1997.

[80] L. Chen, C. Wu, and F. Sun, “Cooling load versus COP characteristics for an irreversible air refrigeration cycle,” *Energy Convers. Manag.*, vol. 39, no. 1–2, pp. 117–125, Jan. 1998.

[81] L. Chen, F. Sun, N. Ni, and C. Wu, “Optimal configuration of a class of two-heat-

reservoir refrigeration cycles," *Energy Convers. Manag.*, vol. 39, no. 8, pp. 767–773, Jun. 1998.

[82] R. Tozer and R. W. James, "Heat powered refrigeration cycles," *Appl. Therm. Eng.*, vol. 18, no. 9–10, pp. 731–743, Sep. 1998.

[83] S. Wu and I. W. Eames, "A novel absorption–recompression refrigeration cycle," *Appl. Therm. Eng.*, vol. 18, no. 11, pp. 1149–1157, Nov. 1998.

[84] H. Fukui, K. Sanechika, and M. Ikeda, "Novel refrigeration lubricants for use with HFC refrigerants," *Tribol. Int.*, vol. 33, no. 10, pp. 707–713, Oct. 2000.

[85] S. Göktun and H. Yavuz, "Performance of irreversible combined cycles for cryogenic refrigeration," *Energy Convers. Manag.*, vol. 41, no. 5, pp. 449–459, Mar. 2000.

[86] Y. . Chang, M. . Kim, and S. . Ro, "Performance and heat transfer characteristics of hydrocarbon refrigerants in a heat pump system," *Int. J. Refrig.*, vol. 23, no. 3, pp. 232–242, May 2000.

[87] T. F. Qu, R. Z. Wang, and W. Wang, "Study on heat and mass recovery in adsorption refrigeration cycles," *Appl. Therm. Eng.*, vol. 21, no. 4, pp. 439–452, Mar. 2001.

[88] A. Sözen, "Effect of heat exchangers on performance of absorption refrigeration systems," *Energy Convers. Manag.*, vol. 42, no. 14, pp. 1699–1716, Sep. 2001.

[89] Y. . Lee and C. . Su, "Experimental studies of isobutane (R600a) as the refrigerant in domestic refrigeration system," *Appl. Therm. Eng.*, vol. 22, no. 5, pp. 507–519, Apr. 2002.

[90] F. Yu, K. Chan, and H. Chu, "Efficiency Improvements of Air-Cooled Chillers Equipped With High Static Condenser Fans Efficiency Improvements of Air-Cooled Chillers Equipped with High Static Condenser Fans," *Int. Refrig. Air Cond.*

[91] "Risk Assessment of Mildly Flammable Refrigerants 2012 Progress Report," 2013.

[92] Y. Ma, Z. Liu, and H. Tian, "A review of transcritical carbon dioxide heat pump and refrigeration cycles," *Energy*, vol. 55, no. 2011, pp. 156–172, 2013.

[93] C. Kondou, F. Mishima, and S. Koyama, "Condensation and evaporation of R32/R1234ze(E) and R744/R32/R1234ze(E) flow in horizontal microfin tubes," *Sci. Technol. Built Environ.*, vol. 21, no. 5, pp. 564–577, Jul. 2015.

[94] F. W. Yu, K. T. Chan, R. K. Y. Sit, and J. Yang, "Performance Evaluation of Oil-free Chillers for Building Energy Performance Improvement," *Procedia Eng.*, vol. 121, pp. 975–983, Jan. 2015.

[95] H. Cho and C. Park, "Experimental investigation of performance and exergy analysis of automotive air conditioning systems using refrigerant R1234yf at various compressor speeds," *Appl. Therm. Eng.*, vol. 101, pp. 30–37, May 2016.

[96] Z. He *et al.*, "Study on the performance of compact adsorption chiller with vapor valves," *Appl. Therm. Eng.*, vol. 126, pp. 37–42, Nov. 2017.

[97] A. E. Kabeel, Y. A. F. El-Samadony, and M. H. Khiera, "Performance evaluation of energy efficient evaporatively air-cooled chiller," *Appl. Therm. Eng.*, vol. 122, pp. 204–213, Jul. 2017.

[98] Z. Meng, H. Zhang, M. Lei, Y. Qin, and J. Qiu, "Performance of low GWP R1234yf/R134a mixture as a replacement for R134a in automotive air conditioning systems," *Int. J. Heat Mass Transf.*, vol. 116, pp. 362–370, Jan. 2018.

[99] F. Afshari, O. Comakli, S. Karagoz, and H. G. Zavaragh, "A thermodynamic comparison between heat pump and refrigeration device using several refrigerants," *Energy Build.*, vol. 168, pp. 272–283, Jun. 2018.

[100] M. Olbricht, F. Lonardi, and A. Luke, "Performance improvement of absorption chillers by means of additives – A numerical study," *Sol. Energy*, vol. 166, pp. 138–145, May 2018.

[101] F. W. Yu and W. T. Ho, "Multivariate diagnosis analysis for chiller system for improving energy performance," *J. Build. Eng.*, vol. 20, pp. 317–326, Nov. 2018.

[102] S. Salehi, M. Yari, and M. A. Rosen, "Exergoeconomic comparison of solar-assisted absorption heat pumps, solar heaters and gas boiler systems for district heating in Sarein Town, Iran," *Appl. Therm. Eng.*, vol. 153, pp. 409–425, May 2019.

[103] G. Kosmadakis and P. Neofytou, "Investigating the effect of nanorefrigerants on a heat pump performance and cost-effectiveness," *Therm. Sci. Eng. Prog.*, vol. 13, p. 100371, Oct. 2019.

[104] P. Byrne and R. Ghoubali, "Exergy analysis of heat pumps for simultaneous heating and cooling," *Appl. Therm. Eng.*, vol. 149, pp. 414–424, Feb. 2019.

[105] D. Mikielewicz and J. Wajs, "Performance of the very high-temperature heat pump with low GWP working fluids," *Energy*, vol. 182, pp. 460–470, Sep. 2019.

[106] M. Pitarch, E. Hervas-Blasco, E. Navarro-Peris, and J. M. Corberán, "Exergy analysis on a heat pump working between a heat sink and a heat source of finite heat capacity rate," *Int. J. Refrig.*, vol. 99, pp. 337–350, Mar. 2019.

[107] F. W. Yu and W. T. Ho, "Analysis of chiller system performance with different component combinations," *Appl. Therm. Eng.*, vol. 154, pp. 699–710, May 2019.

[108] *REGULATION (EU) No 517/2014 OF THE EUROPEAN PARLIAMENT AND OF THE COUNCIL*. 2014.

[109] C. Gabrielii and L. Vamling, "Drop-in replacement of R22 in heat pumps used for district heating — influence of equipment and property limitations," *Int. J. Refrig.*, vol. 24, no. 7, pp. 660–675, Jul. 2001.

[110] K. Mani and V. Selladurai, "Experimental analysis of a new refrigerant mixture as

drop-in replacement for CFC12 and HFC134a," *Int. J. Therm. Sci.*, vol. 47, no. 11, pp. 1490–1495, Nov. 2008.

[111] D. J. Cleland, R. W. Keedwell, and S. R. Adams, "Use of hydrocarbons as drop-in replacements for HCFC-22 in on-farm milk cooling equipment," *Int. J. Refrig.*, vol. 32, no. 6, pp. 1403–1411, Sep. 2009.

[112] R. Llopis, E. Torrella, R. Cabello, and D. Sánchez, "HCFC-22 replacement with drop-in and retrofit HFC refrigerants in a two-stage refrigeration plant for low temperature," *Int. J. Refrig.*, vol. 35, no. 4, pp. 810–816, Jun. 2012.

[113] J. Navarro-Esbrí, J. M. Mendoza-Miranda, A. Mota-Babiloni, A. Barragán-Cervera, and J. M. Belman-Flores, "Experimental analysis of R1234yf as a drop-in replacement for R134a in a vapor compression system," *Int. J. Refrig.*, vol. 36, no. 3, pp. 870–880, May 2013.

[114] R. Cabello, E. Torrella, R. Llopis, D. Sánchez, and J. A. Larumbe, "Energy influence of the IHX with R22 drop-in and long-term substitutes in refrigeration plants," *Appl. Therm. Eng.*, vol. 50, no. 1, pp. 260–267, Jan. 2013.

[115] A. Mota-Babiloni, J. Navarro-Esbrí, Á. Barragán, F. Molés, and B. Peris, "Drop-in energy performance evaluation of R1234yf and R1234ze(E) in a vapor compression system as R134a replacements," *Appl. Therm. Eng.*, vol. 71, no. 1, pp. 259–265, Oct. 2014.

[116] Z. Janković, J. Sieres Atienza, and J. A. Martínez Suárez, "Thermodynamic and heat transfer analyses for R1234yf and R1234ze(E) as drop-in replacements for R134a in a small power refrigerating system," *Appl. Therm. Eng.*, vol. 80, pp. 42–54, Apr. 2015.

[117] M. El-Morsi, "Energy and exergy analysis of LPG (liquefied petroleum gas) as a drop in replacement for R134a in domestic refrigerators," *Energy*, vol. 86, pp. 344–353, Jun. 2015.

[118] A. Mota-Babiloni, J. Navarro-Esbrí, Á. Barragán-Cervera, F. Molés, and B. Peris, "Experimental study of an R1234ze(E)/R134a mixture (R450A) as R134a replacement," *Int. J. Refrig.*, vol. 51, pp. 52–58, Mar. 2015.

[119] C. Aprea, A. Greco, A. Maiorino, C. Masselli, and A. Metallo, "HFO1234ze as Drop-in Replacement for R134a in Domestic Refrigerators: An Environmental Impact Analysis," *Energy Procedia*, vol. 101, pp. 964–971, Nov. 2016.

[120] C. Aprea, A. Greco, and A. Maiorino, "An experimental investigation on the substitution of HFC134a with HFO1234YF in a domestic refrigerator," *Appl. Therm. Eng.*, vol. 106, pp. 959–967, Aug. 2016.

[121] P. Makhnatch, A. Mota-Babiloni, and R. Khodabandeh, "Experimental study of R450A drop-in performance in an R134a small capacity refrigeration unit," *Int. J. Refrig.*, vol. 84, pp. 26–35, Dec. 2017.

[122] R. Cabello, D. Sánchez, R. Llopis, J. Catalán, L. Nebot-Andrés, and E. Torrella, "Energy evaluation of R152a as drop in replacement for R134a in cascade refrigeration plants," *Appl. Therm. Eng.*, vol. 110, pp. 972–984, Jan. 2017.

[123] Y. Fang, S. Croquer, S. Poncet, Z. Aidoun, and Y. Bartosiewicz, "Drop-in replacement in a R134 ejector refrigeration cycle by HFO refrigerants," *Int. J. Refrig.*, vol. 77, pp. 87–98, May 2017.

[124] R. Llopis, D. Sánchez, R. Cabello, L. Nebot-Andrés, and J. Catalán-Gil, "R-407H as drop-in of R-404A. Experimental analysis in a low temperature direct expansion commercial refrigeration system," *Int. J. Refrig.*, vol. 80, pp. 11–23, Aug. 2017.

[125] C. Aprea, A. Greco, and A. Maiorino, "Comparative performance analysis of HFO1234ze/HFC134a binary mixtures working as a drop-in of HFC134a in a domestic refrigerator," *Int. J. Refrig.*, vol. 82, pp. 71–82, Oct. 2017.

[126] J. M. Mendoza-Miranda *et al.*, "Variable speed liquid chiller drop-in modeling for predicting energy performance of R1234yf as low-GWP refrigerant," *Int. J. Refrig.*, vol. 93, pp. 144–158, Sep. 2018.

[127] J. Garcia, T. Ali, W. M. Duarte, A. Khosravi, and L. Machado, "Comparison of transient response of an evaporator model for water refrigeration system working with R1234yf as a drop-in replacement for R134a," *Int. J. Refrig.*, vol. 91, pp. 211–222, Jul. 2018.

[128] A. Mota-Babiloni, J. Haro-Ortuño, J. Navarro-Esbrí, and Á. Barragán-Cervera, "Experimental drop-in replacement of R404A for warm countries using the low GWP mixtures R454C and R455A," *Int. J. Refrig.*, vol. 91, pp. 136–145, Jul. 2018.

[129] C. Aprea, A. Greco, and A. Maiorino, "HFOs and their binary mixtures with HFC134a working as drop-in refrigerant in a household refrigerator: Energy analysis and environmental impact assessment," *Appl. Therm. Eng.*, vol. 141, pp. 226–233, Aug. 2018.

[130] C. Aprea, A. Greco, A. Maiorino, and C. Masselli, "The drop-in of HFC134a with HFO1234ze in a household refrigerator," *Int. J. Therm. Sci.*, vol. 127, pp. 117–125, May 2018.

[131] V. H. Rangel-Hernández, J. M. Belman-Flores, D. A. Rodríguez-Valderrama, D. Pardo-Cely, A. P. Rodríguez-Muñoz, and J. J. Ramírez-Minguela, "Exergoeconomic performance comparison of R1234yf as a drop-in replacement for R134a in a domestic refrigerator," *Int. J. Refrig.*, vol. 100, pp. 113–123, Apr. 2019.

[132] R. E. Cawley, "Patent Application Publication (10) Pub. No.: US 2003/0057396 A1 (43)," US 2003/0057396 A1, 2003.

[133] M. W. Spatz and S. F. Yana Motta, "An evaluation of options for replacing HCFC-22 in medium temperature refrigeration systems," *Int. J. Refrig.*, vol. 27, no. 5, pp.

475–483, Aug. 2004.

[134] W. Chen, “A comparative study on the performance and environmental characteristics of R410A and R22 residential air conditioners,” *Appl. Therm. Eng.*, vol. 28, no. 1, pp. 1–7, Jan. 2008.

[135] S. Koyama, N. Takata, and S. Fukuda, “Drop-in Experiments on Heat Pump Cycle Using HFO-1234ze(E) and Its Mixtures with HFC-32,” *Int. Refrig. Air Cond. Conf.* , pp. 1–7, 2010.

[136] S. Taira, T. Yamakawa, A. Nakai, and R. Yajima, “EXAMINATION REGARDING AIR-CONDITIONERS AND HEAT PUMPS, USING THE NEXT GENERATION REFRIGERANTS Shigeharu,” in *10th IEA Heat Pump Conference 2011*, 2011, pp. 1–8.

[137] H. Pham and R. Rajendran, “R32 And HFOs As Low-GWP Refrigerants For Air Conditioning,” 2012, pp. 1–10.

[138] K. Schultz and S. Kujak, “TEST REPORT #1: System Drop-in Test of R-410A Alternative Fluids in a 5-RT Air-Cooled Water Chiller (Cooling Mode),” 2012.

[139] L. Cremaschi, X. Wu, A. Biswas, and P. Deokar, “Experimental study of compressor operating characteristics and performance when using refrigerants R32, R1234yf, and two new low GWP developmental refrigerants as drop-in replacements for R410A,” *8th Int. Conf. Compressors their Syst.*, pp. 57–66, Jan. 2013.

[140] X. Xu, Y. Hwang, and R. Radermacher, “Performance comparison of R410A and R32 in vapor injection cycles,” *Int. J. Refrig.*, vol. 36, no. 3, pp. 892–903, 2013.

[141] B. Bella, N. Kaemmer, R. Brignoli, and C. Zilio, “Energy Efficiency of a Chiller Using R410A or R32,” in *International Refrigeration and Air Conditioning Conference*, 2014, vol. Paper 1453, pp. 1–10.

[142] S. Fukuda, C. Kondou, N. Takata, and S. Koyama, “Low GWP refrigerants R1234ze(E) and R1234ze(Z) for high temperature heat pumps,” *Int. J. Refrig.*, vol. 40, pp. 161–173, Apr. 2014.

[143] Q. Tian *et al.*, “An experimental investigation of refrigerant mixture R32/R290 as drop-in replacement for HFC410A in household air conditioners,” *Int. J. Refrig.*, vol. 57, pp. 216–228, Sep. 2015.

[144] S. Fukuda, H. Kojima, C. Kondou, N. Takata, and S. Koyama, “Comparative assessment on irreversible losses in heat pumps using R744/R32/R1234yf and R744/R32/R1234ze(E),” *Sci. Technol. Built Environ.*, vol. 22, no. 8, pp. 1118–1127, Nov. 2016.

[145] S. Fukuda, “Experimental Assessment on Performance of a Heat Pump Cycle Using R32 / R1234yf and R744 /,” 2016.

[146] J. K. Vaghela, “Comparative Evaluation of an Automobile Air - Conditioning System Using R134a and Its Alternative Refrigerants,” *Energy Procedia*, vol. 109, pp. 153–160, Mar. 2017.

[147] A. Mota-Babiloni, J. Navarro-Esbrí, P. Makhnatch, and F. Molés, “Refrigerant R32 as lower GWP working fluid in residential air conditioning systems in Europe and the USA,” *Renew. Sustain. Energy Rev.*, vol. 80, pp. 1031–1042, Dec. 2017.

[148] J. Qiu, H. Zhang, J. Sheng, and Z. Wu, “Experimental investigation of L41b as replacement for R410A in a residential air-source heat pump water heater,” *Energy Build.*, vol. 199, pp. 190–196, Sep. 2019.

[149] “Natural Refrigerant Equipment in Japan | Revised F-Gas Law in Japan.” [Online]. Available: http://www.env.go.jp/earth/ozone/hiyasu-waza/eng/revised_f-gas_law_in_japan.html. [Accessed: 16-Mar-2019].

[150] “LabVIEW - National Instruments,” *National Instruments*. [Online]. Available: http://www.ni.com/en-us/shop/labview.html. [Accessed: 31-Jul-2019].

[151] “Wolfram Mathematica: Modern Technical Computing,” *WOLFRAM*. [Online]. Available: http://www.wolfram.com/mathematica/. [Accessed: 31-Jul-2019].

[152] H. W. Coleman and W. G. Steele, *Experimental Validation, and Uncertainty Analysis for Engineers*, Third Edit. John Wiley & Sons, Inc., 1394.

[153] “Genetron ® 410A.”

[154] “REFPROP 10,” *NIST*. [Online]. Available: http://doi.wiley.com/10.1002/aic.16074. [Accessed: 31-Jul-2019].

[155] “R32 Instructions for Use and Handling.”

[156] “Risk Assessment of Mildly Flammable Refrigerants,” 2017.

[157] “Classification of refrigerants.”

[158] K. Thu *et al.*, “Experimental investigation of a mechanical vapour compression chiller at elevated chilled water temperatures,” *Appl. Therm. Eng.*, vol. 123, pp. 226–233, 2017.

[159] S. O. Andersen, N. J. Sherman, S. Carvalho, and M. Gonzalez, “The global search and commercialization of alternatives and substitutes for ozone-depleting substances,” *Comptes Rendus Geosci.*, vol. 350, no. 7, pp. 410–424, Nov. 2018.

[160] J. S. Brown, “Introduction to hydrofluoro-olefin alternatives for high global warming potential hydrofluorocarbon refrigerants Introduction to hydrofluoro-olefin alternatives for high global warming potential hydrofluorocarbon refrigerants,” *HVAC&R Res.*, vol. 19, no. 6, pp. 693–704, 2013.

[161] M. O. McLinden, J. S. Brown, R. Brignoli, A. F. Kazakov, and P. A. Domanski, “Limited options for low-global-warming-potential refrigerants,” *Nat. Commun.*,

vol. 8, p. 14476, Feb. 2017.

[162] I. H. Bell, P. A. Domanski, M. O. McLinden, and G. T. Linteris, “The hunt for nonflammable refrigerant blends to replace R-134a,” *Int. J. Refrig.*, vol. 104, pp. 484–495, Aug. 2019.

[163] Y. L. Yagupolskii *et al.*, “Alternative synthetic routes to hydrofluoroolefins,” *J. Fluor. Chem.*, vol. 179, pp. 134–141, Nov. 2015.

[164] C. B. Rivela, C. M. Tovar, M. A. Teruel, I. Barnes, P. Wiesen, and M. B. Blanco, “CFCs replacements: Reactivity and atmospheric lifetimes of a series of Hydrofluoroolefins towards OH radicals and Cl atoms,” *Chem. Phys. Lett.*, vol. 714, pp. 190–196, Jan. 2019.

[165] J. S. Brown, C. Zilio, and A. Cavallini, “Thermodynamic properties of eight fluorinated olefins,” *Int. J. Refrig.*, vol. 33, no. 2, pp. 235–241, Mar. 2010.

[166] J. Steven Brown, “HFOs New, low global warming potential refrigerants,” *ASHRAE J.*, vol. 51, no. 8, pp. 22–29, 2009.

[167] “HFOs | Linde Gas.” [Online]. Available: http://www.linde-gas.com/en/products_and_supply/refrigerants/hfo_refrigerants/index.html. [Accessed: 31-Jul-2019].

[168] R. Radermacher and Y. Hwang, *Vapor compression heat pumps with refrigerant mixtures*. 2005.

[169] “Chapter 30: Thermophysical Properties of Refrigerants,” 2009.

[170] J. E. Lane, “Correction terms for calculating surface tension from capillary rise,” *J. Colloid Interface Sci.*, vol. 42, no. 1, pp. 145–149, 1973.

[171] R. De Santis, F. Gironi, and L. Marrelli, “Vapor-Liquid Equilibrium from a Hard-Sphere Equation of State,” *Ind. Eng. Chem. Fundam.*, vol. 15, no. 3, pp. 183–189, 1976.

[172] N. Kagawa, M. Uematsu, and K. Watanabe, “A Thermodynamic Surface of State for Refrigerant 22 + Refrigerant 114 System and an Application to Cycle Analysis,” *Fluid Phase Equilib.*, vol. 80, pp. 19–31, 1992.

[173] Z. Y. Zhao, J. M. Yin, and L. C. Tan, “Measurements of PVT properties and vapor pressure for HFC152a,” *Fluid Phase Equilib.*, vol. 80, pp. 191–202, Nov. 1992.

[174] G. Giuliani, S. Kumar, and F. Polonara, “A constant volume apparatus for vapour pressure and gas phase P-ν-T measurements: validation with data for R22 and R134a,” *Fluid Phase Equilib.*, vol. 109, no. 2, pp. 265–279, 1995.

[175] M. Nagel and K. Bier, “Vapour-liquid equilibrium of ternary mixtures of the refrigerants R125, R143a and R134a,” *Int. J. Refrig.*, vol. 19, no. 4, pp. 264–271, 1996.

[176] J. Wilhelm and E. Vogel, “Gas-phase viscosity of the alternative refrigerant R134a at low densities,” *Fluid Phase Equilib.*, vol. 125, no. 1–2, pp. 257–266, 1996.

[177] Y. Higashi and T. Ikeda, “Critical parameters for 1,1,1-trifluoroethane (R-143a),” *Fluid Phase Equilib.*, vol. 125, no. 1–2, pp. 139–147, 1996.

[178] C. Piao and M. Noguchi, “An equation of state for pentafluoroethane (HFC-125),” *Fluid Phase Equilib.*, vol. 125, no. 1–2, pp. 45–54, 1996.

[179] M. H. Barley, J. D. Morrison, A. O’Donnel, I. B. Parker, S. Petherbridge, and R. W. Wheelhouse, “Vapour-liquid equilibrium data for binary mixtures of some new refrigerants,” *Fluid Phase Equilib.*, vol. 140, no. 1–2, pp. 183–206, 1997.

[180] G. A. Iglesias-Silva and K. R. Hall, “A saturated liquid density equation for refrigerants,” *Fluid Phase Equilib.*, vol. 131, no. 1–2, pp. 97–105, 1997.

[181] R. Heide, “The surface tension of HFC refrigerants and mixtures,” *Int. J. Refrig.*, vol. 20, no. 7, pp. 496–503, 1997.

[182] J. Y. Shin, M. S. Kim, and S. T. Ro, “Experimental study on forced convective boiling heat transfer of pure refrigerants and refrigerant mixtures in a horizontal tube Etude exp6rimentale sur le transfert de chaleur lors de l ’ 6bullition en convection forc6e de corps purs et de m61anges frigo,” vol. 20, no. 4, pp. 267–275, 1997.

[183] K. Srinivasan and L. R. Oellrich, “Saturation properties of the refrigerant 143A,” *Int. J. Refrig.*, vol. 20, no. 5, pp. 332–338, 1997.

[184] S. Ioannidis and D. E. Knox, “Vapor-liquid equilibrium predictions of refrigerant mixtures from a cubic equation of state with a GE-EoS mixing rule,” *Fluid Phase Equilib.*, vol. 140, no. 1–2, pp. 17–35, 1997.

[185] T. Rachidi, A. Bernatchou, M. Charia, and H. Loutfi, “New fluids as substitute refrigerants for R12,” *Sol. Energy Mater. Sol. Cells*, vol. 46, no. 4, pp. 333–347, 1997.

[186] M. O. Al-Shafe’i and K. Mečárik, “A modified Carnahan-Starling-de Santis equation of state to compute thermodynamic properties of refrigerants,” *Int. J. Refrig.*, vol. 20, no. 1, pp. 38–48, 1997.

[187] L. J. Van Poolen, C. D. Holcomb, and V. G. Niesen, “Critical temperature and density from liquid-vapor coexistence data: application to refrigerants R32, R124, and R152a,” *Fluid Phase Equilib.*, vol. 129, no. 1–2, pp. 105–111, Mar. 1997.

[188] M. O. McLinden, E. W. Lemmon, and R. T. Jacobsen, “Thermodynamic properties for the alternative refrigerants,” *Int. J. Refrig.*, vol. 21, no. 4, pp. 322–338, 1998.

[189] S. Bobbo and R. Camporese, “Vapour liquid equilibrium measurements and correlations of the refrigerant mixture,” *J. Chem. Thermodyn.*, vol. 30, pp. 1041–1046, 1998.

[190] K. Satoh, H. Nishiumi, and T. Kasatani, “Vapor pressure of CH3OCHF2 synthesized from HCFC22,” *Fluid Phase Equilib.*, vol. 144, no. 1–2, pp. 211–216, 1998.

[191] H. L. Wilson and W. V. Wilding, “Pressure–volume–temperature behavior of binary mixtures of hydrogen fluoride with HCFC-22, HFC-32 and HFC-134a,” *Fluid Phase Equilib.*, vol. 150–151, pp. 323–332, 1998.

[192] G. Di Nicola, G. Giuliani, G. Passerini, F. Polonara, and R. Stryjek, “Vapor-Liquid-Equilibrium (VLE) properties of R-32 + R-134a system derived from isochoric measurements,” *Fluid Phase Equilib.*, vol. 153, no. 1, pp. 143–165, 1998.

[193] S. B. Kiselev, “Cubic crossover equation of state,” *Fluid Phase Equilib.*, vol. 147, no. 1–2, pp. 7–23, 1998.

[194] J. Lee, J. Lee, and H. Kim, “Vapor–liquid equilibria for HFC-32 containing systems,” *Fluid Phase Equilib.*, vol. 150–151, pp. 297–302, 1998.

[195] H.-L. Zhang, S. Tada, H. Sato, and K. Watanabe, “PVTx properties in the gas phase for binary R-125/143a system,” *Fluid Phase Equilib.*, vol. 150–151, pp. 333–341, 1998.

[196] S. B. Kiselev, R. A. Perkins, and M. L. Huber, “Transport properties of refrigerants R32 , R125 , R134a , and R125 + R32 mixtures in and beyond the critical region $ Â te Â s de transport des frigorige Proprie Â langes de R125 + R32 dans et au-dela Á la re Â gion critique des me,” vol. 22, pp. 7–9, 1999.

[197] J. Li, R. Tillner-Roth, H. Sato, and K. Watanabe, “Equation of state for hydrofluorocarbon refrigerant mixtures of HFC-125/143a, HFC-125/134a, HFC-134a/143a and HFC-125/134a/143a,” *Fluid Phase Equilib.*, vol. 161, no. 2, pp. 225–239, 1999.

[198] G. Di Nicola, G. Giuliani, F. Polonara, and R. Stryjek, “PVTx measurements for N2O + CH3F, N2O + CH2F2, and N2O + CHF3 binary systems,” *Fluid Phase Equilib.*, vol. 230, no. 1–2, pp. 81–89, 2005.

[199] G. Di Nicola, G. Giuliani, F. Polonara, and R. Stryjek, “Second and third virial coefficients for the R41+N2O system,” *Fluid Phase Equilib.*, vol. 228–229, pp. 373–379, Feb. 2005.

[200] A. Sözen, E. Arcakliog˘lu, and M. Özalp, “Formulation based on artificial neural network of thermodynamic properties of ozone friendly refrigerant/absorbent couples,” *Appl. Therm. Eng.*, vol. 25, no. 11–12, pp. 1808–1820, Aug. 2005.

[201] Q. Chen, R. H. Hong, and G. M. Chen, “Measurements of gas phase PVTx properties for the ternary HFC-161/125/32 system,” *Fluid Phase Equilib.*, vol. 249, no. 1–2, pp. 92–96, 2006.

[202] Q. Chen, R. H. Hong, and G. M. Chen, “PVTx properties in the gas phase for binary HFC-161/125 system,” *Fluid Phase Equilib.*, vol. 240, no. 1, pp. 63–66, 2006.

[203] Q. Chen, R. hua Hong, and G. ming Chen, “An experimental study of PVTx properties in the gas phase for binary mixtures of HFC-161 and HFC-32,” *Fluid Phase Equilib.*, vol. 243, no. 1–2, pp. 156–160, 2006.

[204] R. Hong, Q. Chen, and G. Chen, “Gas phase PVTx properties for binary mixtures of HFC-161 and HFC-143a,” *Fluid Phase Equilib.*, vol. 259, no. 2, pp. 153–156, Oct. 2007.

[205] A. Sözen, M. Özalp, and E. Arcaklioğlu, “Calculation for the thermodynamic properties of an alternative refrigerant (R508b) using artificial neural network,” *Appl. Therm. Eng.*, vol. 27, no. 2–3, pp. 551–559, 2007.

[206] K. Tanaka and Y. Higashi, “Measurements of the surface tension for R290, R600a and R290/R600a mixture,” *Int. J. Refrig.*, vol. 30, no. 8, pp. 1368–1373, 2007.

[207] R. Akasaka, Y. Higashi, K. Tanaka, Y. Kayukawa, and K. Fujii, “Vapor-liquid equilibrium measurements and correlations for the binary mixture of difluoromethane + isobutane and the ternary mixture of propane + isobutane + difluoromethane,” *Fluid Phase Equilib.*, vol. 261, no. 1–2, pp. 286–291, 2007.

[208] Q. Chen, R. H. Hong, and G. M. Chen, “PVTx measurements in the gas phase for binary mixtures of HFC-161-and HFC-227ea,” *Fluid Phase Equilib.*, vol. 269, no. 1–2, pp. 113–116, 2008.

[209] N. G. Polikhronidi, I. M. Abdulagatov, R. G. Batyrova, and G. V. Stepanov, “PVT measurements of water-ammonia refrigerant mixture in the critical and supercritical regions,” *Int. J. Refrig.*, vol. 32, no. 8, pp. 1897–1913, 2009.

[210] K. Tanaka and Y. Higashi, “Thermodynamic properties of HFO-1234yf (2,3,3,3-tetrafluoropropene),” *Int. J. Refrig.*, 2010.

[211] R. Akasaka, K. Tanaka, and Y. Higashi, “Thermodynamic property modeling for 2,3,3,3-tetrafluoropropene (HFO-1234yf),” *Int. J. Refrig.*, vol. 33, no. 1, pp. 52–60, Jan. 2010.

[212] Q. Chen, Y. Tong, R. Hong, and G. Chen, “Gas phase PVTx properties for binary mixtures of HFC-161 and HFC-134a,” *Fluid Phase Equilib.*, vol. 304, no. 1–2, pp. 61–63, 2011.

[213] A. J. Tan, “Energy consumption and greenhouse gas emissions from commercial and manufacturing sectors Specific studies on HVAC equipment and dairy processing,” vol. 1509601, p. 76, 2012.

[214] G. Di Nicola, A. Arteconi, G. Nardini, and R. Stryjek, “Solid-liquid equilibria measurements of the carbon dioxide+2,3,3,3-tetrafluoroprop-1-ene and carbon dioxide+trans-1,3,3,3-tetrafluoropropene mixtures,” *Fluid Phase Equilib.*, 2013.

[215] R. Akasaka, “Thermodynamic property models for the difluoromethane (R-32)+trans-1,3,3,3-tetrafluoropropene (R-1234ze(E)) and difluoromethane+2,3,3,3-tetrafluoropropene (R-1234yf) mixtures,” *Fluid Phase Equilib.*, 2013.

[216] R. Akasaka, K. Tanaka, and Y. Higashi, “Measurements of saturated densities and critical parameters for the binary mixture of 2,3,3,3-tetrafluoropropene (R-1234yf) + difluoromethane (R-32),” *Int. J. Refrig.*, vol. 36, no. 4, pp. 1341–1346, Jun. 2013.

[217] R. Akasaka, Y. Higashi, A. Miyara, and S. Koyama, “A fundamental equation of state for cis-1,3,3,3-tetrafluoropropene (R-1234ze(Z)),” *Int. J. Refrig.*, vol. 44, pp. 168–176, Aug. 2014.

[218] Y. Qi, H. Zhang, Y. Liu, W. Wu, X. Chen, and X. Yang, “PVTx properties in the gas phase for binary R290/R134a system,” *J. Chem. Thermodyn.*, vol. 70, pp. 111–121, 2014.

[219] M. K. Vollmer, S. Reimann, M. Hill, and D. Brunner, “First observations of the fourth generation synthetic halocarbons HFC-1234yf, HFC-1234ze(E), and HCFC-1233zd(E) in the atmosphere,” *Environ. Sci. Technol.*, vol. 49, no. 5, pp. 2703–2708, 2015.

[220] Q. Chen, H. Qi, S. Zhang, R. Hong, and G. Chen, “An experimental study of PVTx properties in the gas phase for binary mixtures of HFO-1234yf and HFC-134a,” *Fluid Phase Equilib.*, vol. 385, pp. 25–28, 2015.

[221] R. Akasaka, Y. Higashi, Y. Yamada, and T. Shibanuma, “Thermodynamic properties of 1,1,1,2-tetrafluoroethane (R-134a) + 2,3,3,3-tetrafluoropropene (R-1234yf) mixtures: Measurements of the critical parameters and a mixture model based on the multi-fluid approximation,” *Int. J. Refrig.*, vol. 58, pp. 146–153, Oct. 2015.

[222] Y. Higashi, S. Hayasaka, C. Shirai, and R. Akasaka, “Measurements of PρT properties, vapor pressures, saturated densities, and critical parameters for R 1234ze(Z) and R 245fa,” *Int. J. Refrig.*, vol. 52, pp. 100–108, Apr. 2015.

[223] C. Kondou, R. Nagata, N. Nii, S. Koyama, and Y. Higashi, “Surface tension of low GWP refrigerants R1243zf, R1234ze(Z), and R1233zd(E),” *Int. J. Refrig.*, vol. 53, pp. 80–89, May 2015.

[224] N. Abas, A. R. Kalair, N. Khan, A. Haider, Z. Saleem, and M. S. Saleem, “Natural and synthetic refrigerants, global warming: A review,” *Renew. Sustain. Energy Rev.*, vol. 90, no. February, pp. 557–569, 2018.

[225] S. Bobbo, G. Di Nicola, C. Zilio, J. S. Brown, and L. Fedele, “Low GWP halocarbon refrigerants: A review of thermophysical properties,” *Int. J. Refrig.*, vol. 90, pp. 181–201, Jun. 2018.

[226] S. Khosharay, M. Pierantozzi, and G. Di Nicola, “Modeling investigation on the viscosity of pure refrigerants and their liquid mixtures by using the Patel–Teja viscosity equation of state,” *Int. J. Refrig.*, vol. 85, pp. 255–267, 2018.

[227] G. Di Nicola, G. Coccia, M. Pierantozzi, and S. Tomassetti, “Vapor-liquid

equilibrium of binary systems containing low GWP refrigerants with cubic equations of state," *Energy Procedia*, vol. 148, pp. 1246–1253, 2018.

[228] G. Di Nicola, G. Coccia, M. Pierantozzi, and S. Tomassetti, "Equations for the surface tension of low GWP halogenated alkene refrigerants and their blends," *Int. J. Refrig.*, vol. 86, pp. 410–421, Feb. 2018.

[229] Y. Higashi and N. Sakoda, "Measurements of PvT Properties, Saturated Densities, and Critical Parameters for 3,3,3-Trifluoropropene (HFO1243zf)," *J. Chem. Eng. Data*, vol. 63, no. 10, pp. 3818–3822, 2018.

[230] M. Pierantozzi and G. Di Nicola, "Surface tension correlation of carboxylic acids from liquid viscosity data," *Fluid Phase Equilib.*, vol. 482, pp. 118–125, 2019.

[231] "Advantages of AC resistance thermometry bridges | CTR6500."

[232] "AC resistance thermometry bridge Model CTR6500."

[233] "Digiquartz ® Pressure Instrumentation | Model 735."

[234] J. S. Brown, "Introduction to hydrofluoro-olefin alternatives for high global warming potential hydrofluorocarbon refrigerants Introduction to hydrofluoro-olefin alternatives for high global warming potential hydrofluorocarbon refrigerants," *HVAC&R Res.*, vol. 19, pp. 693–704, 2013.

[235] A. Kazakov, M. O. Mclinden, and M. Frenkel, "Computational Design of New Refrigerant Fluids Based on Environmental, Safety, and Thermodynamic Characteristics †."

[236] M. Fukushima and A. Kawaguchi, "Working medium for heat cycle, composition for heat cycle system, and heat cycle system," WO2015186558A1, 2015.

[237] M. Fukushima, "Working medium for heat cycle, composition for heat cycle system, and heat cycle system," WO2015186557A1, 2015.

[238] "A Brief Guide to Types of Isomerism in Organic Chemistry | Compound Interest," *CompoundChem*. [Online]. Available: https://www.compoundchem.com/2014/05/22/typesofisomerism/. [Accessed: 31-Jul-2019].

[239] "1,2-Difluoroethylene," *US National Library of Medicine | PubChem*. [Online]. Available: https://pubchem.ncbi.nlm.nih.gov/compound/1_2-Difluoroethylene. [Accessed: 31-Jul-2019].

[240] "(Z)-1,2-Difluoroethylene," *US National Library of Medicine | PubChem*. [Online]. Available: http://doi.wiley.com/10.1002/chem.200400223. [Accessed: 31-Jul-2019].

[241] "XP1203S - Overview - METTLER TOLEDO." [Online]. Available: https://www.mt.com/vn/en/home/phased_out_products/Laboratory_Weighing/Precision_Balances/XP_Precision_Balances/XP_1203_S.html. [Accessed: 31-Jul-

2019].

[242] “Turbo Molecular Pumping System YTP series Ver.B |,” *ULVAC*. [Online]. Available: https://www.ulvac.co.jp/products_e/components/ytpb. [Accessed: 31-Jul-2019].

[243] “Ionization Vacuum Gauge | TL3.”

[244] “ITS-90 Platinum Resistance Thermometer NSR Series,” *Netsushin*. [Online]. Available: https://netsushin.co.jp/en/product6.html. [Accessed: 31-Jul-2019].

[245] “Absolute Pressure Transducers Series 3000 & 4000.”

[246] “Snoop Liquid Leak Detector,” *Swagelok*. [Online]. Available: https://www.swagelok.co.jp/en/product/Leak-Detectors-Lubricants-Sealants/Snoop-Liquid-Leak-Detector. [Accessed: 31-Jul-2019].

[247] “AEROFLEX® (HT) SHEET – Insulation,” *NMC*. [Online]. Available: https://nmc-insulation.com/product/aeroflex-ht-sheet/. [Accessed: 31-Jul-2019].

[248] S. I. Sandler, *Chemical, Biochemical, and Engineering Thermodynamics*. 2006.

[249] O. L. I. Brown, “The Clausius-Clapeyron equation,” *J. Chem. Educ.*, vol. 28, no. 8, p. 428, 2009.

[250] J. Wisniak, “Historical development of the vapor pressure equation from Dalton to Antoine,” *J. Phase Equilibria*, vol. 22, no. 6, pp. 622–630, 2001.

[251] D. Roizard, “Antoine Equation Denis.”

[252] G. W. Thomson, “The antoine equation for vapor-pressure data,” *Chem. Rev.*, vol. 38, no. 1, pp. 1–39, 1946.

[253] H. Sato, “Currently Reliable Property Values And Simple Equation For Pure Hydrofluorocarbons,” in *International Refrigeration and Air Conditioning Conference*, 2002.

[254] P. A. Domanski, R. Brignoli, J. S. Brown, A. F. Kazakov, and M. O. McLinden, “Low-GWP refrigerants for medium and high-pressure applications,” *Int. J. Refrig.*, vol. 84, pp. 198–209, Dec. 2017.

[255] G. Di Nicola, F. Polonara, and G. Santori, “Saturated pressure measurements of 2,3,3,3-tetrafluoroprop-1-ene (HFO-1234yf),” *J. Chem. Eng. Data*, vol. 55, no. 1, pp. 201–204, 2010.

[256] L. Fedele, S. Bobbo, F. Groppo, J. S. Brown, and C. Zilio, “Saturated pressure measurements of 2,3,3,3-tetrafluoroprop-1-ene (R1234yf) for reduced temperatures ranging from 0.67 to 0.93,” *J. Chem. Eng. Data*, vol. 56, no. 5, pp. 2608–2612, 2011.

[257] J. S. Brown, F. Polonara, G. Di Nicola, L. Fedele, S. Bobbo, and C. Zilio, “Vapor Pressure of Hydrofluoroolefins: Critical Review of Experimental Data and Models,” *Int. Refrig. Air Cond. Conf. Purdue*, 2012.

[258] E. W. Lemmon and A. R. H. Goodwin, “Critical Properties and Vapor Pressure Equation for Alkanes CnH2n2 : Normal Alkanes With n,” *MPa J. Phys. Chem. Ref. Data*, vol. 29, p. 1509, 2000.

[259] S. L. Outcalt and M. O. McLinden, “A Modified Benedict–Webb–Rubin Equation of State for the Thermodynamic Preoperties of R125a (1,-difluoroethane),” *J. Phys. Chem.*, vol. 25, no. 2, 1996.

[260] D.-Y. Peng and D. B. Robinson, “A New Two-Constant Equation of State,” *Ind. Eng. Chem. Fundam. Eng. Chem. Fundam.*, vol. 15, no. 1, pp. 11–18, 1976.

[261] J. S. Brown, G. Coccia, G. Di Nicola, M. Pierantozzi, and F. Polonara, “Vapor Phase PvTx Measurements of Binary Blends of 2,3,3,3-Tetrafluoroprop-1-ene + Propane and cis-1,2,3,3,3-Pentafluoroprop-1-ene + Propane,” *J. Chem. Eng. Data*, 2016.

[262] G. Di Nicola, F. Polonara, and R. Stryjek, “P-V-T-x and VLE Properties of Difluoromethane (R32) + 1,1,1,2,3,3-Hexafluoropropane (R236ea) and Pentafluoroethane (R125) + R236ea Systems Derived from Isochoric Measurements,” pp. 359–366, 2001.

[263] “Gap Fillers vs. Thermal Pads | LORD Corp.” [Online]. Available: https://www.lord.com/products-and-solutions/electronic-materials/thermal-management-materials/gap-fillers-vs-thermal-pads. [Accessed: 02-Aug-2019].

[264] “Honeywell FP5000 pressure transducer.” [Online]. Available: https://sensing.honeywell.com/lp/fp5000/?utm_source=google_ads&utm_medium=cpc&utm_campaign=19_03_FP5000_pressure_transducer&gclid=CjwKCAjwm4rqBRBUEiwAwaWjjLwsk-ELmIJImpCe279yX9HqALgFKskMzf5-C4KIo7gR-DU07oVibBoCw04QAvD_BwE. [Accessed: 02-Aug-2019].

Appendix

Table 1. Standard Rating Conditions

Operating Category	Conditions	Cooling Mode Evaporator[2]			Cooling Mode Heat Rejection Heat Exchanger											
					Tower (Water Conditions)[3]			Heat/Recovery (Water Conditions)[4]		Evaporatively-cooled Entering Temperature[5]		Air-cooled (AC) Entering Temperature[6, 8]		Without Condenser			
														Air-cooled Refrigerant Temp.		Water & Evaporatively Cooled Refrigerant Temp.	
		Entering Temp. °C	Leaving Temp. °C	Flow Rate L/(s·kW)	Entering Temp. °C	Leaving Temp. °C	Flow Rate L/(s·kW)	Entering Temp. °C	Leaving Temp. °C	Dry-Bulb °C	Wet-Bulb °C	Dry-Bulb °C	Wet-Bulb °C	SDT[11] °C	LIQ[12] °C	SDT[11] °C	LIQ[12] °C
All Cooling	Std	12.00	7.00	(0.0478)[9]	30.00	35.00	Note - 10	--	--	35.00	24.00	35.0	--	52.0	41.0	41.00	37.00
AC Heat Pump High Heating[7]	Low	--	40.00	Note - 1	--	--	--	--	--	--	--	8.00	6.00	--	--	--	--
	Medium	--	50.00	Note - 1	--	--	--	--	--	--	--	8.00	6.00	--	--	--	--
	High	--	60.00	Note - 1	--	--	--	--	--	--	--	8.00	6.00	--	--	--	--
AC Heat Pump Low Heating[7]	Low	--	40.00	Note - 1	--	--	--	--	--	--	--	-8.00	-9.00	--	--	--	--
	Medium	--	50.00	Note - 1	--	--	--	--	--	--	--	-8.00	-9.00	--	--	--	--
	High	--	60.00	Note - 1	--	--	--	--	--	--	--	-8.00	-9.00	--	--	--	--
Water Cooled Heating	Low	12.00	7.00	(0.0478)[9]	--	--	--	35.00	40.00	--	--	--	--	--	--	--	--
	Medium	12.00	7.00	(0.0478)[9]	--	--	--	42.00	50.00	--	--	--	--	--	--	--	--
	High	12.00	7.00	(0.0478)[9]	--	--	--	50.00	60.00	--	--	--	--	--	--	--	--
	Boost	24.00	19.00	(0.0478)[9]	--	--	--	50.00	60.00	--	--	--	--	--	--	--	--
Heat Recovery	Low	12.00	7.00	(0.0478)[9]	24.00	--	Note - 10	35.00	40.00	4.00	3.00	4.00	3.00	--	--	--	--
	Medium	12.00	7.00	(0.0478)[9]	24.00	--	Note - 10	42.00	50.00	4.00	3.00	4.00	3.00	--	--	--	--
	Hot Water 1	12.00	7.00	(0.0478)[9]	24.00		Note - 10										
	Hot Water 2	12.00	7.00	(0.0478)[9]	24.00	--	Note - 10	50.00	60.00	4.00	3.00	4.00	3.00	--	--	--	--

Notes:

1. The water flow rate used for the heating tests of reverse cycle air to water heat pumps shall be the flow rate determined during the cooling test., as determined by Note 9.
2. The rating fouling factor allowance for the cooling mode evaporator or the heating condenser for AC reversible cycles shall be R_{fou} = 0.0180 m²·K/kW.
3. The rating fouling factor allowance for tower heat exchangers shall be R_{fou} = 0.0440 m²·K/kW.
4. The rating fouling factor allowance for heating and heat recovery heat exchangers shall be R_{fou} = 0.0180 m²·K/kW for closed loop and R_{fou} = 0.0440 m²·K/kW for open loop systems.
5. Evaporatively cooled condensers shall be rated with a fouling factor allowance of zero, R_{fou} = 0.000 m²·K/kW.
6. Air-Cooled Condensers shall be rated with a fouling factor allowance of zero, R_{fou} = 0.000 m²·K/kW.
7. A reversible cycle is assumed where the cooling mode evaporator becomes the condenser circuit in the heating mode.
8. Air-cooled & evaporatively-cooled unit ratings are at standard atmposheric conditions (sea level). Measure test data will be corrected to atmospheric pressure of 101.33 kPa per Appendix F.
9. Rated water flow is determined by the water temperatures at the rated capacity. The normalized flow rate shown, per unit of evaporator capacity, is for reference only at Standard Rating Conditions.
10. Rated water flow is determined by the water temperatures at the rated capacity and rated efficiency.
11. Saturated Discharge Temperature (SDT).
12. Liquid Refrigerant Temperature (LIQ).

ANSI/AHRI STANDARD 551/591 (SI)-2014

Figure A. 1 The AHRI Standard 551/591 (SI) Table 1 for the standard rating conditions for testing different chillers

Table 3. Part-load Conditions for Rating		
	IPLV.SI[5]	NPLV.SI
Evaporator (All Types)		
All loads LWT, °C[2]	7.0 0	Selected LWT
Flow Rate (L/s per kW)[3]	Per Table 1	Per Table 1, Note 10[3]
$R_{fouling}$, m^2·K/kW	0.018	As Specified
Water-cooled Condenser[1, 2]		
100% load EWT, °C	30.00	Selected EWT
75% load EWT, °C	24.50	Note[4]
50% load EWT, °C	19.00	Note[4]
25% load EWT , °C	19.00	Note[4]
Flow rate, L/s per kW[3]	Note[3]	Selected flow rate
$R_{fouling}$ m^2·K/kW	0.044	As Specified
Air-cooled Condenser[1, 6]		
100% load EDB, °C	35.0	No Rating Requirements (NPLV.SI not applicable)
75% load EDB, °C	27.0	
50% load EDB, °C	19.0	
25% load EDB, °C	13.0	
$R_{fouling}$, m^2·K/kW	0.0	
Evaporatively-cooled Condenser[1, 6]		
100% load EWB, °C	24.00	No Rating Requirements (NPLV.SI not applicable)
75% load EWB, °C	20.50	
50% load EWB, °C	17.00	
25% load EWB, °C	13.50	
$R_{fouling}$, m^2·K/kW	0.0	
Air-cooled Without Condenser		
100% load SDT, °C	52.00	No Rating Requirements (NPLV.SI not applicable)
75% load SDT, °C	42.00	
50% load SDT, °C	32.00	
25% load SDT, °C	22.00	
$R_{fouling}$, m^2·K/kW	0.0	
Water-cooled or Evaporatively-cooled Without Condenser		
100% load SDT, °C	41.00	No Rating Requirements (NPLV.SI not applicable)
75% load SDT, °C	35.50	
50% load SDT, °C	30.00	
25% load SDT, °C	24.50	
$R_{fouling}$, m^2·K/kW	0.0	

Notes:

1. If the unit manufacturer's recommended minimum temperatures are greater than those specified in Table 3, then those may be used in lieu of the specified temperatures. If head pressure control is active below the rating temperature then tests should be run at a temperature above which head pressure control is activated.
2. Correct for Fouling Factor Allowance by using the calculation method described in Section C3.3.4.
3. The flow rates are to be held constant at full-load values for all part-load conditions as per Table 1.
4. For part-load entering condenser water temperatures, the temperature should vary linearly from the selected EWT at 100% load to 19.0°C at 50% loads, and fixed at 19.0°C for 50% to 0% loads.
5. Reference Equations 10 through 14 for calculation of temperatures at any point that is not listed.
   - 5.1 - Entering air dry-bulb temperature (EDB).
   - 5.2 - Entering water temperature (EWT).
   - 5.3 - Entering air wet-bulb temperature (EWB).
   - 5.4 - Compressor Saturated discharge temperature (SDT for air-cooled).
   - 5.5 - Compressor Saturated discharge temperature (SDT for water-cooled or evaporatively-cooled).
6. Air-cooled and evaporatively-cooled unit ratings are at standard atmospheric condition (sea level). Measured data shall be corrected to standard atmospheric pressure of 101.33 kPa per Appendix F.

Figure A. 2 AHRI Standard 551/591 (SI) Table 3 for Part-load condition rating

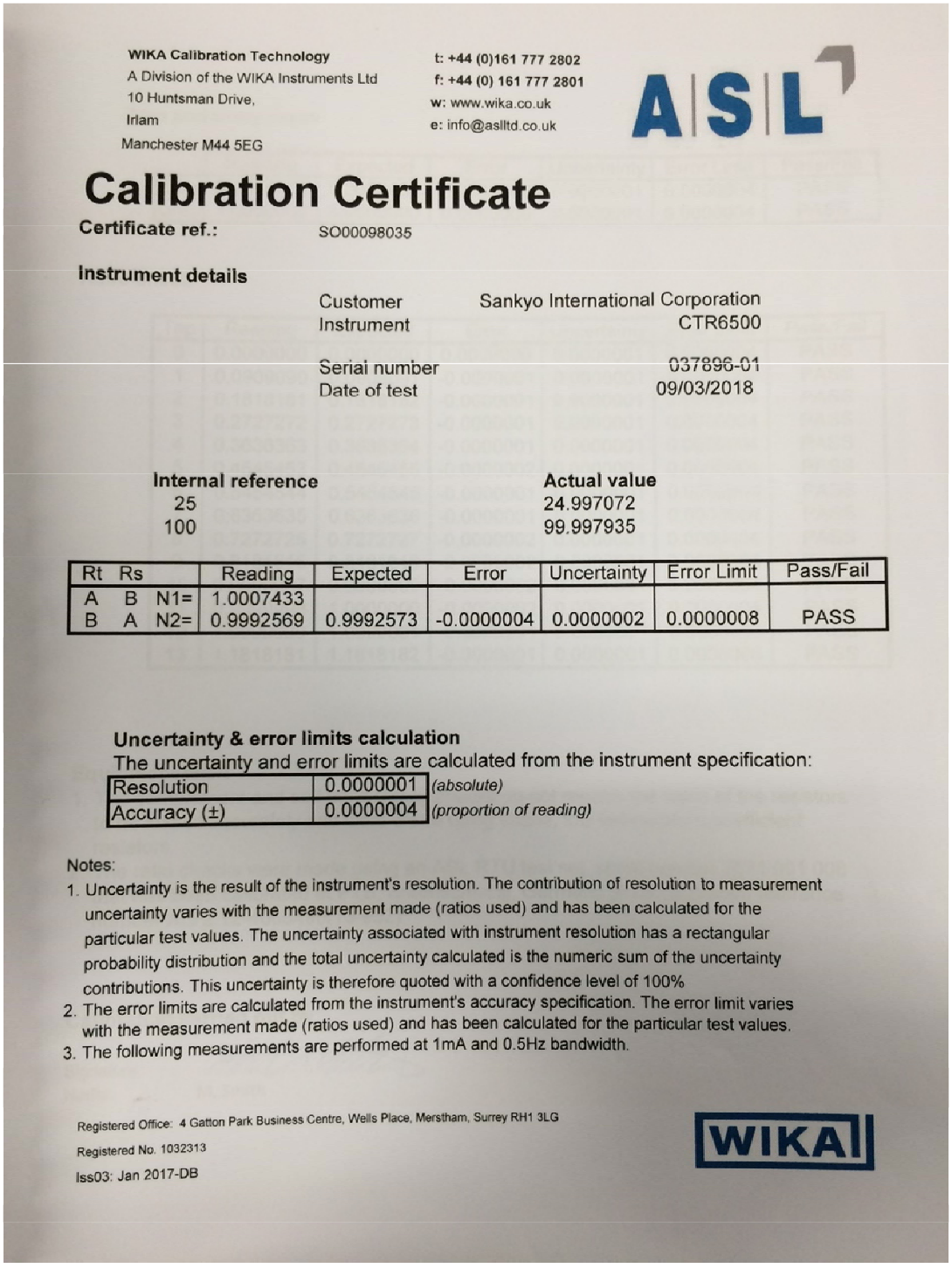

WIKA Calibration Technology
A Division of the WIKA Instruments Ltd
10 Huntsman Drive,
Irlam
Manchester M44 5EG

t: +44 (0)161 777 2802
f: +44 (0) 161 777 2801
w: www.wika.co.uk
e: info@asllltd.co.uk

ASL

Calibration Certificate

Certificate ref.: SO00098035

Instrument details

Customer	Sankyo International Corporation
Instrument	CTR6500
Serial number	037896-01
Date of test	09/03/2018

Internal reference	Actual value
25	24.997072
100	99.997935

Rt	Rs		Reading	Expected	Error	Uncertainty	Error Limit	Pass/Fail
A	B	N1=	1.0007433					
B	A	N2=	0.9992569	0.9992573	-0.0000004	0.0000002	0.0000008	PASS

Uncertainty & error limits calculation

The uncertainty and error limits are calculated from the instrument specification:

Resolution	0.0000001	*(absolute)*
Accuracy (±)	0.0000004	*(proportion of reading)*

Notes:

1. Uncertainty is the result of the instrument's resolution. The contribution of resolution to measurement uncertainty varies with the measurement made (ratios used) and has been calculated for the particular test values. The uncertainty associated with instrument resolution has a rectangular probability distribution and the total uncertainty calculated is the numeric sum of the uncertainty contributions. This uncertainty is therefore quoted with a confidence level of 100%
2. The error limits are calculated from the instrument's accuracy specification. The error limit varies with the measurement made (ratios used) and has been calculated for the particular test values.
3. The following measurements are performed at 1mA and 0.5Hz bandwidth.

Registered Office: 4 Gatton Park Business Centre, Wells Place, Merstham, Surrey RH1 3LG
Registered No. 1032313
Iss03: Jan 2017-DB

WIKA

Figure A. 3 Calibration Certificate for the Platinum Resistance Thermometer

Temperature (K)	± TE_{xp} Uncertainty (K)	± Perc. TE_{xp} Uncertainty (%)
290.06	0.0222	0.0076
259.75	0.0182	0.0070
250.18	0.0180	0.0072
255.17	0.0177	0.0070
255.17	0.0179	0.0070
255.17	0.0178	0.0070
255.15	0.0179	0.0070
250.07	0.0183	0.0073
250.07	0.0260	0.0104
250.06	0.0189	0.0075
255.16	0.0178	0.0070
255.18	0.0178	0.0070
255.14	0.0187	0.0073

Table A. 1 The experimental temperature uncertainties after the removal of the anomalies

Pressure (kPa)	± P_{Exp} Uncertainty (K)	± Perc. P_{Exp} Uncertainty (%)
1340.52	1.04	0.08
527.18	1.04	0.20
373.22	1.04	0.28
448.45	1.04	0.23
448.56	1.07	0.24
448.38	1.04	0.23
448.03	1.04	0.23
372.01	1.04	0.28
371.96	1.04	0.28
371.96	1.04	0.28
447.86	1.04	0.23
447.74	1.04	0.23
447.66	1.04	0.23

Table A. 2 The experimental pressure uncertainties after the removal of the anomalies

T_{Eexp}	P_{Eexp}	P_{CC}	ΔP (kPa)	ΔP. Perc (%)
290.06	1340.52	1336.96	3.56	0.27
259.75	527.18	526.03	1.15	0.22
250.18	373.22	373.81	-0.59	-0.16
255.17	448.45	448.13	0.32	0.07
255.17	448.56	448.13	0.43	0.10
255.17	448.38	448.13	0.25	0.06
255.15	448.03	447.79	0.24	0.05
250.07	372.01	372.23	-0.22	-0.06
250.07	371.96	372.30	-0.34	-0.09
250.06	371.96	372.14	-0.18	-0.05
255.16	447.86	447.92	-0.06	-0.01
255.18	447.74	448.24	-0.50	-0.11
255.14	447.66	447.66	0.00	0.00
259.96	530.99	529.69	1.31	0.25
305.00	1979.93	1978.05	1.88	0.09
310.00	2236.15	2236.15	0.00	0.00
315.00	2515.32	2518.10	-2.77	-0.11
320.00	2820.85	2825.09	-4.24	-0.15
325.00	3151.87	3158.32	-6.45	-0.20
330.00	3512.69	3518.94	-6.25	-0.18
335.00	3905.23	3908.10	-2.86	-0.07
340.00	4332.87	4326.92	5.94	0.14
345.00	4797.88	4776.52	21.36	0.45
348.72	5174.46	5131.62	42.84	0.83

Table A. 3 The pressure calculations and the errors in fitting for the CC equation with the removal of anomalies

T_{Eexp}	P_{Eexp}	P_{AT}	ΔP (kPa)	ΔP. Perc (%)
290.06	1340.52	1338.42	2.10	0.16
259.75	527.18	526.21	0.97	0.18
250.18	373.22	373.63	-0.41	-0.11
255.17	448.45	448.13	0.32	0.07
255.17	448.56	448.13	0.43	0.10
255.17	448.38	448.13	0.25	0.06
255.15	448.03	447.79	0.24	0.05
250.07	372.01	372.06	-0.04	-0.01
250.07	371.96	372.12	-0.16	-0.04
250.06	371.96	371.96	0.00	0.00
255.16	447.86	447.92	-0.06	-0.01
255.18	447.74	448.24	-0.50	-0.11
255.14	447.66	447.66	0.00	0.00
259.96	530.99	529.88	1.11	0.21
305.00	1979.93	1979.56	0.38	0.02
310.00	2236.15	2237.44	-1.29	-0.06
315.00	2515.32	2519.01	-3.69	-0.15
320.00	2820.85	2825.44	-4.59	-0.16
325.00	3151.87	3157.87	-6.00	-0.19
330.00	3512.69	3517.43	-4.74	-0.14
335.00	3905.23	3905.23	0.00	0.00
340.00	4332.87	4322.36	10.50	0.24
345.00	4797.88	4769.88	28.00	0.58
348.72	5174.46	5123.16	51.30	0.99

Table A. 4 The pressure calculations and the errors in fitting for the AT equation with the removal of anomalies

T_{Eexp}	P_{Eexp}	P_{WAG}	ΔP (kPa)	ΔP. Perc (%)
290.06	1340.52	1341.21	-0.69	-0.05
259.75	527.18	526.92	0.26	0.05
250.18	373.22	373.48	-0.26	-0.07
255.17	448.45	448.39	0.07	0.01
255.17	448.56	448.38	0.18	0.04
255.17	448.38	448.38	0.00	0.00
255.15	448.03	448.04	-0.01	0.00
250.07	372.01	371.89	0.12	0.03
250.07	371.96	371.96	0.00	0.00
250.06	371.96	371.80	0.16	0.04
255.16	447.86	448.17	-0.31	-0.07
255.18	447.74	448.50	-0.75	-0.17
255.14	447.66	447.91	-0.25	-0.06
259.96	530.99	530.61	0.38	0.07
305.00	1979.93	1979.65	0.28	0.01
310.00	2236.15	2235.95	0.20	0.01
315.00	2515.32	2515.84	-0.52	-0.02
320.00	2820.85	2820.85	0.00	0.00
325.00	3151.87	3152.67	-0.80	-0.03
330.00	3512.69	3513.32	-0.64	-0.02
335.00	3905.23	3905.23	0.00	0.00
340.00	4332.87	4331.57	1.29	0.03
345.00	4797.88	4797.02	0.86	0.02
348.72	5174.46	5174.46	0.00	0.00

Table A. 5 The pressure calculations and the errors in fitting for the WAG equation with the removal of anomalies

T_{Eexp}	P_{Eexp}	P_{MBWR}	ΔP (kPa)	ΔP. Perc (%)
290.06	1340.52	1342.45	-1.93	-0.14
259.75	527.18	527.06	0.12	0.02
250.18	373.22	373.48	-0.26	-0.07
255.17	448.45	448.39	0.06	0.01
255.17	448.56	448.38	0.18	0.04
255.17	448.38	448.39	0.00	0.00
255.15	448.03	448.04	-0.01	0.00
250.07	372.01	371.89	0.12	0.03
250.07	371.96	371.96	0.00	0.00
250.06	371.96	371.80	0.16	0.04
255.16	447.86	448.17	-0.31	-0.07
255.18	447.74	448.50	-0.75	-0.17
255.14	447.66	447.91	-0.25	-0.06
259.96	530.99	530.76	0.24	0.04
305.00	1979.93	1979.93	0.00	0.00
310.00	2236.15	2235.79	0.36	0.02
315.00	2515.32	2515.31	0.01	0.00
320.00	2820.85	2820.10	0.75	0.03
325.00	3151.87	3151.94	-0.07	0.00
330.00	3512.69	3512.87	-0.18	-0.01
335.00	3905.23	3905.26	-0.02	0.00
340.00	4332.87	4332.11	0.76	0.02
345.00	4797.88	4797.67	0.21	0.00
348.72	5174.46	5174.46	0.00	0.00

Table A. 6 The pressure calculations and the errors in fitting for the MBWR equation with the removal of anomalies